T2R2 東京科学大学 リサーチリポジトリ
Science Tokyo Research Repository

論文 / 著書情報
Article / Book Information

題目(和文)	
Title(English)	Study on Dynamic Behavior of Superparamagnetic Iron Oxide Nanoparticles Modified with Citric Acid under Physiological Conditions
著者(和文)	MULIAWANWibias
Author(English)	Wibias Muliawan
出典(和文)	学位:博士(工学), 学位授与機関:東京工業大学, 報告番号:甲第12905号, 授与年月日:2024年9月20日, 学位の種別:課程博士, 審査員:北本 仁孝,柘植 丈治,曽根 正人,和田 裕之,岡田 智
Citation(English)	Degree:Doctor (Engineering), Conferring organization: Tokyo Institute of Technology, Report number:甲第12905号, Conferred date:2024/9/20, Degree Type:Course doctor, Examiner:,,,,
学位種別(和文)	博士論文
Type(English)	Doctoral Thesis

Powered by T2R2 (Science Tokyo Research Repository)

Study on Dynamic Behavior of Superparamagnetic Iron Oxide Nanoparticles Modified with Citric Acid under Physiological Conditions

Wibias Muliawan

Doctoral Dissertation

submitted to the
Department of Materials Science and Engineering School of Materials and Chemical Technology Tokyo Institute of Technology

in partial fulfillment of the requirements for the degree of
Doctor of Engineering
Human-Centered Science and Biomedical Engineering Major
August 2024

Supervised by Professor: Yoshitaka Kitamoto

Table of Contents

Chapter 1 – General Introduction

1.1 Introduction

Nanotechnology, a field that manipulates matter at the nanoscale to create new materials and devices, has a rich history dating back to the 4th century, with the Lycurgus Cup as an early example of nanoparticle use. [1] However, it wasn't until the late 20th century that nanotechnology truly began to flourish, following Richard Feynman's famous 1959 speech, "There's Plenty of Room at the Bottom," and the subsequent development of tools like the scanning tunneling microscope in the 1980s.[2,3] This period marked a significant shift, enabling scientists to directly observe and manipulate atoms and molecules. The allure of nanotechnology lies in its potential to revolutionize a myriad of sectors, from medicine and electronics to energy and environmental protection, by leveraging the unique properties of materials at the nanoscale, such as increased reactivity, strength, and electrical characteristics.[4-8]

The applications of nanotechnology are vast and varied, touching nearly every aspect of our daily lives. Medicine offers targeted drug delivery systems that reduce side effects and improve treatment efficacy.[9-13] In electronics, nanotechnology has been instrumental in creating smaller, more efficient devices, leading to faster computers and more compact memory storage.[14-19] Environmental applications include nanomaterials for water purification and energy conversion, significantly impacting renewable energy technologies and pollution control.[20-26] Moreover, nanotechnology plays a critical role in developing advanced materials with enhanced properties, such as increased mechanical strength,[27] lighter weight,[28] and improved thermal performance,[29] finding applications in industries ranging from aerospace to sports equipment.[30,31]

Before the advent of nanotechnology, biosensors were limited by the materials and technologies

available, often resulting in devices with lower sensitivity and specificity.[32,33] Traditional biosensors relied on bulkier materials that could not provide the same level of interaction with analytes as nanomaterials do.[34] The emergence of nanotechnology in biosensing has dramatically transformed the field, introducing materials with high surface area-to-volume ratios, unique optical properties, and enhanced electrical conductivity.[35-38] These advancements have led to the development of biosensors with significantly improved performance, capable of detecting biomolecules at much lower concentrations, with greater accuracy, and over broader ranges of conditions. Nanotechnology has enabled the creation of compact, portable biosensors that can be used for rapid, on-site analysis in environmental monitoring, medical diagnostics, and food safety.

Analytes in biosensors can range from ions and small molecules to proteins and nucleic acids, each requiring specific strategies for effective detection [39-42)]. The binding of nanoparticles to these analytes is crucial for the functionality of nanotechnology-enhanced biosensors.[43-45] This binding can be achieved through various mechanisms, including covalent bonding,[46,47] where a stable, permanent linkage is formed between the nanoparticle and the analyte; ionic bonding, [48,49] which relies on the electrostatic attraction between charged entities; and click chemistry,[50-52] a newer approach that enables the rapid, selective synthesis of substances by joining small units together. Each of these binding strategies offers different advantages, such as the strength and stability of covalent bonds, the versatility and reversibility of ionic bonds, and the efficiency and specificity of click chemistry reactions.[53-55] Through these methods, nanoparticles can be precisely and effectively linked to analytes, significantly enhancing the sensitivity and selectivity of biosensors.

The integration of nanotechnology into the field of biosensing represents a monumental leap forward, offering unprecedented levels of sensitivity, specificity, and versatility. As research and development in nanotechnology continue to advance, the potential applications of nanotechnology-enhanced biosensors will expand, further revolutionizing our ability to detect and analyze biological and chemical substances. This ongoing evolution underscores the transformative impact of nanotechnology on biosensing and

many other fields, promising a future where the limits of detection and analysis continue to be pushed ever further.

1.2 Sensing Label and Method

Sensing labels are the cornerstone of biosensing technologies, playing an instrumental role in detecting and quantifying biological markers across many applications. Engineered to interact with analytes—essential substances within samples specifically—these labels are crucial for the precise identification and quantification of biological entities [56,57]. Selecting an appropriate sensing label is critical, profoundly influencing the biosensor's sensitivity, specificity, and overall operational efficiency. Enzymes, antibodies, aptamers, and nanomaterials are among the typical labels, each offering distinct advantages. Enzymes are lauded for their specific catalytic action and signal amplification capabilities, while antibodies offer unparalleled specificity towards target antigens.[58-60]

At the core of biosensing technology lies the intricate interaction between the sensing label and the analyte, which induces a measurable physical alteration directly correlated with the analyte's concentration. This crucial interaction can manifest in detectable changes, such as optical, electrochemical, or thermal shifts. The specific nature of these changes is meticulously designed to align with the biosensor's architecture and the unique characteristics of the sensing label employed.

The advent of nanotechnology has heralded the introduction of an innovative category of sensing labels, namely nanoparticles, distinguished by their exceptional physical and chemical attributes. This distinction is attributed to their diminutive size and expansive surface area-to-volume ratio. Among the plethora of nanoparticles being rigorously investigated for their biosensor labeling capabilities are magnetic nanoparticles, quantum dots, and gold nanoparticles. Each of these nanoparticles offers unique properties, making them invaluable in biosensing. In the ensuing discussions, I delve into the nuances of various types of biosensor labels, specifically focusing on those based on electrochemical, optical (photo), and magnetic principles, outlining their distinctive features and applications in the biosensing landscape.

Electrochemical biosensors utilizing nanoparticles harness specific detection mechanisms, where the interaction between nanoparticles and target analytes induces measurable changes in electrical properties, such as current, voltage, or impedance. [61-65] Nanoparticles commonly employed in electrochemical biosensors include conductive polymers,[66-68] carbon nanotubes (CNTs),[69-74] and metal nanoparticles like gold and platinum, [75-80] which facilitate electron transfer processes enhancing the sensor's sensitivity and specificity. These nanoparticles offer significant advantages, including low detection limits, high surface area for immobilization of recognition elements, and the capability for miniaturization and integration into portable devices. However, they also come with disadvantages, such as potential environmental and health risks associated with nanoparticle disposal and the need for precise control over nanoparticle synthesis to ensure uniformity and reproducibility in sensor performance.

Optical biosensors utilize nanoparticles to achieve susceptible and specific detection of biological analytes through mechanisms such as fluorescence or surface plasmon resonance. [81-84] Gold nanoparticles and quantum dots are prime examples used in these systems, owing to their strong optical properties and the ability to modify their surface for specific analyte recognition.[85-90] The detection mechanism often involves changes in the optical signal, such as shifts in fluorescence intensity or wavelength, when nanoparticles interact with the target analyte, allowing for quantitative analysis. While optical nanoparticle biosensors offer the advantages of rapid detection and high sensitivity, they also face challenges. These include the potential for photobleaching, where the fluorescent signal fades over time, and quenching effects that can reduce signal clarity. Additionally, the synthesis and functionalization processes for these nanoparticles can be complex and expensive, limiting their accessibility and increasing the overall cost of the biosensing method.

Building upon our discussion of electrochemical and optical biosensors, I delve into the realm of magnetic biosensors, which harness the capabilities of magnetic nanoparticles to achieve highly sensitive and specific detection of biological analytes. Utilizing materials such as superparamagnetic iron oxide nanoparticles (SPIONs) and magnetic quantum dots, these biosensors employ the distinct magnetic

properties of these nanoparticles to facilitate direct detection of target analytes without reliance on optical visibility. The underlying detection mechanism in magnetic biosensing predominantly involves the observation of modifications in magnetic field strength or magnetic resonance signatures induced by the interaction between magnetic nanoparticles and the target analyte. [91-95] Such interactions may manifest as quantifiable alterations in the magnetic signal, including variations in signal amplitude or phase shifts, thereby enabling accurate determination of analyte concentrations. Magnetic biosensors present several advantages, including their capability to penetrate deep tissues unimpeded by biological matter and their immunity to photobleaching and quenching phenomena, which are common pitfalls of optical biosensing methods. Nonetheless, they are not without challenges. The requirement for an advanced magnetic field detection apparatus and the intricate process of synthesizing and functionalizing magnetic nanoparticles with precise specificity and stability present considerable hurdles. These factors can influence the scalability and economic viability of magnetic biosensing platforms. Consequently, while magnetic biosensors hold significant promise for the future of biomolecule detection, addressing these challenges will be pivotal in fully realizing their potential and integrating them into widespread practical applications.

1.3 Magnetic Sensing Method

Magnetic sensing offers a compelling alternative to optical and radiation-based sensing techniques, especially in biomedical applications, where the sample matrix's complexity can significantly impact detection methods' efficacy. Optical techniques, which rely on light transmittance, face challenges in environments like bodily fluids, where turbidity can scatter or absorb light signals, complicating detection. Radiation sensing, while capable of penetrating the body, poses health risks due to exposure, necessitating specialized facilities and personnel, thus limiting its practicality and safety for routine use.

In contrast, magnetic sensing techniques stand out for their ability to transmit through the body harmlessly, leveraging the non-invasive nature of magnetic fields. This method does not alter or damage cellular structures, making it ideal for biomedical applications. The stable magnetic signal from labels

within the body can be detected and measured relatively easily, bypassing the limitations of optical and radiation methods.

Several magnetic detection techniques have been developed, each with its unique application and mechanism of action:

I. Magnetic Sensing. Magnetic sensing, as a pivotal technique in detecting magnetic labels within biological samples, utilizes sophisticated magnetic field sensors, such as the Hall effect and magnetoresistive sensors, to discern subtle changes in magnetic field strength. [96-99] These sensors operate on the principle that when introduced to a sample, magnetic labels measurably alter the local magnetic field. Hall effect sensors leverage the Hall effect, where a voltage difference is generated across an electrical conductor transverse to an electric current in the conductor and a magnetic field perpendicular to the current. Magnetoresistive sensors, on the other hand, detect changes in resistance that occur in response to a magnetic field. These variations in voltage or resistance directly correlate with the presence and concentration of magnetic labels in the sample, allowing for precise quantification and localization.

II. Magnetic Particle Detection. Magnetic Particle Detection is a sophisticated technique that employs specialized instruments like magnetic susceptometers or magnetometers to directly assess the magnetic properties of particles that have been tagged with magnetic labels. [100,101] This method hinges on the principle that when subjected to an external magnetic field, magnetic labels measurably alter their magnetic state. The susceptometers or magnetometers used are highly sensitive to these changes, enabling them to detect even minute variations in the magnetic behavior of the labeled particles. This technique provides a detailed quantitative analysis of the labeled particles in a sample by measuring parameters such as magnetic susceptibility, remanence, and coercivity.

III. Magnetic Resonance Imaging (MRI). Magnetic Resonance Imaging (MRI) is a sophisticated diagnostic tool that utilizes the magnetic properties of atoms within the body, often enhanced by the introduction of magnetically labeled particles, to generate detailed images of tissues and biological structures. [102-104] This technique hinges on the alignment of the nuclear spins of atoms, mainly hydrogen,

in response to a strong external magnetic field. When these aligned atoms are exposed to radiofrequency pulses, they emit signals as they return to their original alignment. The presence of magnetically labeled particles can alter the local magnetic field, affecting the relaxation times of nearby hydrogen atoms. These variations in signal intensity are captured and converted into high-resolution images by the MRI scanner, providing unparalleled insights into the body's internal structures and the distribution of labeled particles. This ability to visualize soft tissues with exceptional clarity makes MRI an invaluable tool in diagnosing a wide range of physiological conditions, from brain tumors to heart diseases, by offering a non-invasive, detailed view of the body's internal workings without ionizing radiation.

IV. Magnetophoresis. Magnetophoresis, a sophisticated technique within magnetic sensing, operates by applying magnetic forces to control and segregate labeled magnetic particles suspended in a fluid medium.[105] This method exploits the principle that magnetic particles will move in response to a magnetic field gradient, with their velocity and direction depending on the strength and orientation of the applied magnetic field and the magnetic properties and size of the particles themselves. By carefully modulating these magnetic forces, magnetophoresis enables the precise manipulation of particles, guiding their movement toward specific locations or through predefined paths. This controlled movement effectively separates particles from a complex mixture or their concentration in particular areas, making it possible to detect and analyze the labeled entities based on their spatial distribution or accumulation. Such a technique is invaluable in various applications, including targeted drug delivery, biomolecular separation, and the enrichment of sample components for enhanced detection sensitivity in biosensing platforms.

V. Magnetic Particle Spectroscopy (MPS). Magnetic Particle Spectroscopy (MPS) is a sophisticated technique that probes the behavior of magnetically labeled particles when subjected to alternating magnetic fields.[106-109] In this process, the labeled particles are exposed to a magnetic field that changes direction at varying frequencies, causing the magnetic moments of the particles to realign with the field's direction. This realignment is not instantaneous; the particles' magnetic moments lag behind the changing

field, creating a phase shift and generating higher harmonics of the original frequency in the magnetic signal. By analyzing these harmonics and phase shifts, MPS can provide detailed information about the magnetic properties of the particles, including their size, concentration, and distribution within a biological sample. This makes MPS a powerful tool for the non-invasive detection and quantification of magnetic particles, offering potential applications in medical diagnostics, therapeutic monitoring, and targeted drug delivery systems.

VI. Superconducting Quantum Interference Device (SQUID) Detection. The Superconducting Quantum Interference Device (SQUID) detection mechanism is one of the most sensitive methods for measuring extremely weak magnetic fields, such as those generated by magnetic labels in biosensors.[110] SQUID sensors operate on superconductivity and quantum interference principles, employing two superconducting loops connected by Josephson junctions. When exposed to a magnetic field, the current flowing through these loops is modulated, resulting in quantifiable changes in voltage that directly correlate with the strength of the magnetic field. This allows SQUIDs to detect minute changes in magnetic fields with unparalleled precision. The ability of SQUID sensors to identify these subtle variations makes them exceptionally useful in biomedical applications, where they can pinpoint the presence of magnetically labeled particles, even in the complex and noisy background of biological samples. Their high sensitivity and specificity enable the detailed analysis and imaging of biological structures and functions, contributing significantly to medical diagnostics and research advancements.

VII. Magnetic Relaxation. Magnetic relaxation sensing involves observing changes in the relaxation times of magnetic labels when subjected to an external magnetic field.[102] This technique is predicated on the principle that when placed in a magnetic field, magnetic nanoparticles will align with that field. Once the external field is removed, the particles return to their initial random orientation, characterized by a specific relaxation time. The relaxation time is influenced by several factors, including the nanoparticles' size, shape, and magnetic properties, as well as their environment and concentration. By measuring how quickly or slowly the magnetic labels return to equilibrium after removing the magnetic field, magnetic

relaxation sensing can deduce the concentration of labeled particles in a sample. This is because the relaxation times vary depending on the interactions between the particles and their distribution within the medium, providing valuable information about the characteristics of the labeled particles and their surrounding environment. This method is advantageous in biosensing applications, allowing for detecting and quantifying target molecules or cells in complex biological matrices without the need for direct visualization or labeling with optical or radioactive markers.

Each of these techniques leverages magnetic sensing's unique advantages, offering noninvasive, highly sensitive, and specific detection methods suitable for a wide range of biomedical applications, from diagnostics to therapeutic monitoring. This highlights magnetic sensing's transformative potential in medical science.

1.4 Magnetic Nanoparticles

1.4.1 Overview

In the landscape of magnetic nanoparticles, a diverse array of types exists, each characterized by distinct magnetic behaviors. Among these, superparamagnetic, ferromagnetic, and paramagnetic nanoparticles are the most prevalent, with their differences in characteristics fundamentally explained by the Stoner-Wohlfarth model.[111,112] This model provides a theoretical framework for understanding the magnetic properties of nanoparticles, mainly focusing on their response to external magnetic fields and their magnetic anisotropy energy barriers, which dictate their magnetic orientation stability.

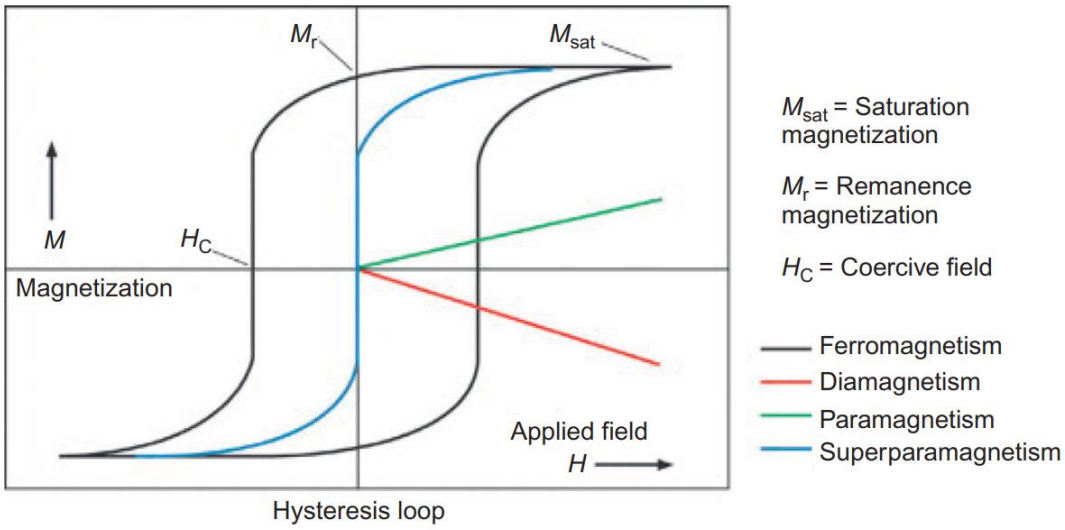

Figure 1 The hysteresis loops generated by the Stoner–Wohlfarth model are utilized to distinguish between ferromagnetic, paramagnetic, and superparamagnetic nanoparticles. [113]

Ferromagnetic nanoparticles are characterized by their ability to retain a significant amount of magnetization even after removing the external magnetic field, known as remanent magnetization. While useful in specific applications, this trait leads to a tendency for these particles to aggregate, which depends on the magnetic field and particle magnetic moment, reducing their performance in biomedical applications due to the induced dipole-dipole attractions.[114,115] Conversely, paramagnetic nanoparticles exhibit magnetization only in an external magnetic field and do not retain magnetization once the field is removed. While this behavior minimizes aggregation, the drawback lies in the necessity for a large

magnetic field to induce a sufficient level of magnetization for detection purposes, necessitating larger coils and thereby increasing the complexity and size of the detection apparatus.

Superparamagnetic nanoparticles, particularly those exemplified by superparamagnetic iron oxide nanoparticles (SPIONs), offer a middle ground that combines the advantages of both ferro- and paramagnetic materials without their respective drawbacks. When subjected to an external magnetic field, these nanoparticles become magnetized, similar to ferromagnetic particles, but crucially, they do not retain any magnetization upon removal of the field, effectively eliminating the risk of aggregation due to remanent magnetization. This property renders them ideal for biosensing applications, as it facilitates ease of handling and precise control over particle behavior in biological matrices.

The absence of remanent magnetization in superparamagnetic nanoparticles significantly enhances their utility as magnetic labels in biosensing. [116] This characteristic ensures that superparamagnetic nanoparticles remain dispersed and mobile in solution, improving the sensitivity and specificity of detection by allowing for a more homogeneous and dynamic interaction with target analytes. Moreover, the need for only minimal external magnetic fields to magnetize these particles simplifies the design and operation of the biosensing platform, making it more efficient and cost-effective. In contrast, the aggregation tendency of ferromagnetic nanoparticles and the high magnetic field requirements for paramagnetic nanoparticle magnetization present substantial challenges, making superparamagnetic nanoparticles (SPIONs) a more favorable choice for magnetic labeling in biosensing applications.

1.4.2. Synthesis Route of SPIONs

Iron oxide nanoparticles (IONPs) have captured the scientific world's attention for over four decades, remaining among the most extensively studied and applied nanomaterials. The significant interest in IONPs stems from their unique physicochemical and magnetic properties, such as superparamagnetic, high coercivity, low Curie temperature, and notable magnetic susceptibility.[112,113] These features render IONPs highly adaptable, facilitating their incorporation into diverse applications ranging from multi-terabit data storage [117] and catalysis [118,119] to targeted drug delivery [120], magnetic hyperthermia [121-123],

MRI contrast enhancement [124], biosensing [125], bioseparation [126], thermoablation [127], and the creation of intelligent materials.[128] The effectiveness and functionality of IONPs are intimately connected to their size, shape, and morphological characteristics, thereby emphasizing the ongoing need to refine synthesis methods to achieve precise control over these fundamental aspects. [129,130]

Various synthesis techniques are available for crafting IONPs, each presenting distinct advantages tailored to specific application requirements. For instance, **solvothermal synthesis** [131-134] involves reacting a precursor within a solvent under elevated temperatures and pressures, enabling meticulous particle size and morphology adjustment. The **co-precipitation** method [135,136], recognized for its simplicity and efficiency, precipitates iron salts from an aqueous solution by adding a base under controlled conditions. **Thermal decomposition** [137,138] breaks down iron-containing compounds at high temperatures in the presence of organic solvents with high boiling points, producing uniform, high-quality nanoparticles. **Hydrothermal** synthesis,[139] a water-based variant of solvothermal synthesis, is celebrated for its environmental friendliness and capability to govern nanoparticle development. **Microemulsion** techniques [140] create a specialized medium for nanoparticle synthesis, providing superior control over particle dimensions, albeit sometimes involving intricate processes. **Mechanochemical** [141] synthesis, a solvent-free, dry method, employs mechanical energy to trigger chemical reactions, making it environmentally friendly. **Electrochemical** synthesis [142], finally, utilizes electrochemical reactions to form nanoparticles, facilitating straightforward regulation of particle size and distribution.

This research primarily delves into solvothermal methods due to their notable advantages. The solvothermal approach is distinguished by its superior control over nanoparticles' crystal structure and surface attributes, which assures the fabrication of highly monodispersed nanoparticles with specific sizes and shapes. This method's precision is especially appreciated for its capacity to generate nanoparticles with precise properties essential for cutting-edge applications, demonstrating the solvothermal technique's crucial role in advancing the field of nanotechnology and broadening the scope

of possible IONP applications.

1.4.3. Strategy for High Stability of SPIONs

To enhance the high stability of superparamagnetic iron oxide nanoparticles (SPIONs) within complex biological systems, it is essential to employ strategies that involve meticulous stabilization through surface modification. These strategies are crucial for mitigating the undesired aggregation caused by the screening effects of ions, proteins, and other macromolecules prevalent in biological systems. One efficient approach uses citric acid (CA) to stabilize SPIONs by coating their surfaces to form CA-functionalized iron oxide nanoparticles. This method provides a robust colloidal solution that resists agglomeration and enhances the hydrophilicity and dispersibility of nanoparticles in aqueous solutions, thereby maintaining their functionality in water [136,143-148)].

The screening effects from ionic interactions in biological fluids can significantly agglomerate nanoparticles, impairing their functionality and limiting their application potential. [149-155] By modifying the surface of SPIONs with citric acid, the nanoparticles gain an electrostatic force that minimizes interactions with biomolecules. This electrostatic stabilization is achieved by forming a diffuse layer around each nanoparticle, as shown in Fig. 1.1.(a). The diffuse layer consists of counterions surrounding the charged nanoparticle, creating an electrostatic repulsion between particles and thus enhancing their stability in water, preventing precipitation at the bottom of the container. However, when salt is added to the solution (Fig. 1.1.(b)), the concentration of counterions increases, which screens the nanoparticles' surface charges and results in a thinner diffuse layer. This reduction in the thickness of the diffuse layer weakens the repulsive forces between nanoparticles, adversely affecting their stability. Consequently, the nanoparticles may collide more frequently and form larger clusters due to random colloidal motion. Over time, as these clusters grow, some particles may begin to precipitate. The longer the nanoparticles are exposed to counterions and the higher the salt concentration, the more pronounced this effect becomes, forming even larger clusters and ultimately causing more particles to precipitate at the bottom

of the glass, as depicted in Fig. 1.1.(c).

Moreover, the stabilization strategy involving citric acid is complemented by using other coating agents such as polyethylene glycol (PEG), dextran, or polyethyleneimine (PEI). [156-166] These substances are known to reduce the nonspecific adsorption of proteins and prevent the aggregation of nanoparticles in ionic environments, further enhancing the performance of SPIONs in clinical settings. However, the simplicity and efficacy of citric acid modification, as elaborated in recent studies, highlight its potential to offer a protective coat and enhance the magnetic responses of SPIONs. This makes citric acid a desirable option for developing next-generation medical applications where nanoparticle stability and functionality are paramount.

Including citric acid as a stabilizing agent is advantageous because it binds effectively to iron oxide surfaces, creating a stable layer that prevents clumping and preserves the nanoparticles' superparamagnetic properties. This interaction between citric acid and the nanoparticle surface is crucial for maintaining the discrete nature of nanoparticles, which is essential for achieving precise targeting capabilities in therapeutic and diagnostic applications. Additionally, the enhanced surface charge provided by citric acid modification leads to increased repulsion between individual nanoparticles, further preventing aggregation.

Given these attributes, the strategic use of citric acid fortifies the physical and chemical stability of SPIONs and opens new, promising avenues for their application in biomedicine. This approach, backed by empirical research and successful stabilization techniques, underscores the critical role of surface chemistry in developing and deploying nanoparticle-based technologies in healthcare. The ongoing exploration of citric acid and other biocompatible coatings will continue to advance our understanding and ability to engineer SPIONs optimally tailored for specific medical interventions, instilling a sense of optimism about the future of SPION applications in biomedicine.

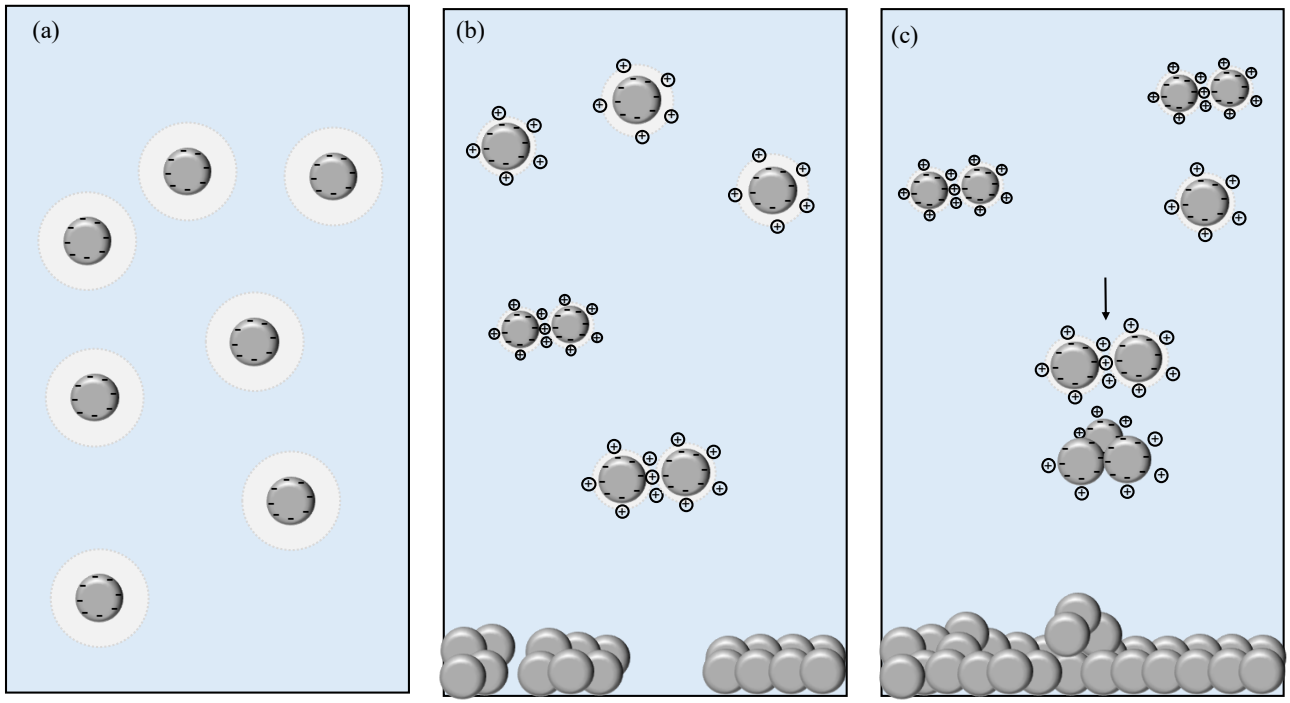

Figure 1.1. Illustration of nanoparticle stability in water and varying salt concentrations. (a) Nanoparticles dispersed in water remain stable due to electrostatic repulsion on their surfaces, resulting in a thick diffuse layer. (b) Increasing salt concentration introduces counterions, which reduce the diffuse layer's thickness and lead to the formation of larger clusters. (c) Prolonged exposure to counterions and higher salt concentrations causes further aggregation, leading to more nanoparticles precipitating at the bottom of the container.

1.5 Magnetorelaxometry

Magnetorelaxometry (MRX) is a sophisticated analytical technique pivotal in studying and applying magnetic nanoparticles, particularly SPIONs, for biosensing.[167-170] This technique exploits the unique relaxation properties of magnetic nanoparticles when the external magnetic field is removed, providing critical insights into their dynamics and interactions at the nanoscale. MRX's ability to measure the relaxation times of SPIONs under various conditions makes it an invaluable tool for detecting and quantifying biomolecular interactions, enhancing the sensitivity and specificity of biosensors.

The utility of MRX in biosensing is derived from its sensitivity to changes in the magnetic

environment of nanoparticles induced by biomolecular binding. This sensitivity is analyzed through three fundamental aspects: the relaxation of magnetic nanoparticles, the measurement of their relaxation time, and the analysis of the harmonic signals produced during these processes.[169,171-178] Each component plays A crucial role in understanding how SPIONs interact with target molecules and their subsequent detection capabilities. By examining these elements, researchers can infer the binding characteristics of biomolecules to SPIONs, facilitating the development of highly responsive biosensing platforms.

MRX is an advanced technique that is leading the way in characterizing the dynamic magnetic properties of SPIONs, especially in the context of biosensing applications. This technique revolves around the precise measurement of the relaxation processes of SPIONs after removing an external magnetic field, offering invaluable insights into their magnetic relaxation dynamics. These dynamics are crucial for developing SPION-based biosensors, where the detection and quantification of target biomolecules are achieved through changes in the magnetic response of the nanoparticles.

In biosensing, the ability to monitor and understand how SPIONs respond under varying magnetic conditions allows for the design of highly sensitive diagnostic tools. MRX exploits this principle by measuring how quickly the magnetization of SPIONs returns to equilibrium—a process governed by Neel and Brownian relaxation mechanisms. Neel relaxation involves the reorientation of the magnetic moment of each nanoparticle within its crystal lattice, primarily influenced by the particle's magnetic anisotropy and temperature. In contrast, Brownian relaxation refers to the physical rotation of the nanoparticles in response to the fluid's viscosity within which they are suspended. The interaction with biomolecules can significantly affect these processes; for example, the binding of biomolecules can alter the viscosity around the nanoparticles, affecting Brownian relaxation, or it can change the magnetic environment near the nanoparticles, influencing Neel relaxation.

1.6 Application to Biosensing Using AC Magnetorelaxometry

The importance of MRX in biosensing is underscored by its ability to differentiate between the magnetic relaxation behaviors of nanoparticles in free solution versus those bound to target molecules.

[174-175] This differentiation is critical to developing non-invasive diagnostic techniques that require minimal sample preparation and can operate under physiologically relevant conditions. This study will explore the relaxation of magnetic nanoparticles, the methodologies for accurately measuring these relaxation times, and the interpretation of dynamic magnetic susceptibility (DMS) signals generated during these processes. Through this detailed analysis, I aim to highlight the sophisticated interplay between SPION dynamics and their potential applications in medical diagnostics and other biotechnological fields. This comprehensive exploration enhances our understanding of SPION behavior under magnetic fields and paves the way for novel applications of MRX in medical technology.

Figure 1.2 shows a schematic overview of how SPIONs (Superparamagnetic Iron Oxide Nanoparticles) detect target molecules. When SPIONs are mixed with body fluids, target molecules, macromolecules, and various salts (e.g., sodium, chloride, potassium) are present. SPIONs exhibit increased hydrodynamic size upon binding to target molecules, indicating successful binding. However, interactions between SPIONs and salts and potential aggregation due to macromolecular crowding must also be considered, as these factors can also alter hydrodynamic size.

Macromolecular crowding [(176)] refers to the high concentration of macromolecules in biological environments, which can significantly influence the behavior of nanoparticles. In such crowded environments, macromolecules occupy a large volume, leading to an excluded volume effect that can promote aggregation and self-assembly of nanoparticles. This crowding effect can alter the stability and behavior of SPIONs, potentially causing changes in their hydrodynamic size that are not related to target molecule binding. The crowding effect increases the configurational entropy of the surrounding molecules, stabilizing self-assembled states and potentially causing nanoparticles to aggregate more readily.

In biosensing applications, it is common for sensing samples to undergo pre-treatment processes such as washing, filtration, or centrifugation. These steps help to remove macromolecules and other non-target entities that could interfere with the sensing process. As a result, macromolecule-SPION interactions are

generally minimized, allowing for a more accurate assessment of SPION behavior in the sample.

The remaining interactions of concern are SPION-salt and buffer-SPION interactions. Additionally, salt molecules can affect SPION stability through pH changes or screening effects. [177] The screening effect refers to reducing electrostatic repulsion between charged particles in the presence of salts. Salts can shield the charges on the surface of SPIONs, leading to decreased repulsion and potential aggregation. Changes in pH can alter the surface charge of SPIONs, influencing their stability and interactions with other molecules. For example, at specific pH levels, the surface charge of SPIONs can be neutralized, leading to reduced repulsion and an increased likelihood of aggregation. Furthermore, salt concentration variations can impact the solution's ionic strength, affecting the overall stability and dispersion of SPIONs.

These interactions and the potential for SPIONs to interact with buffer solutions can complicate the interpretation of hydrodynamic measurements. While the effects of macromolecular crowding, screening, and pH on particle stability are well-documented, there is a lack of research on the impact of different types of buffer solutions on SPION stability.

These SPION-salt interactions can lead to false positives, complicating the interpretation of hydrodynamic measurements. Therefore, a comprehensive and urgent study is needed to investigate how varying salt concentrations affect the MRX (Magnetic Relaxation) signal of SPIONs. By differentiating between signals arising from SPION-target molecule binding and those from salt-SPION interactions, I can enhance the accuracy of MRX-based biosensing. This differentiation is crucial for improving the reliability of diagnostics in complex biological environments, potentially reducing false positive results and ensuring more accurate and reliable detection of target molecules.

Understanding these nuances is not just essential for developing highly sensitive diagnostic tools, but it also holds the potential to revolutionize medical diagnostics and other biotechnological fields. The sophisticated interplay between SPION dynamics and their potential applications highlights the importance of precisely controlling the magnetic properties of SPIONs by manipulating cluster sizes and

environmental conditions.

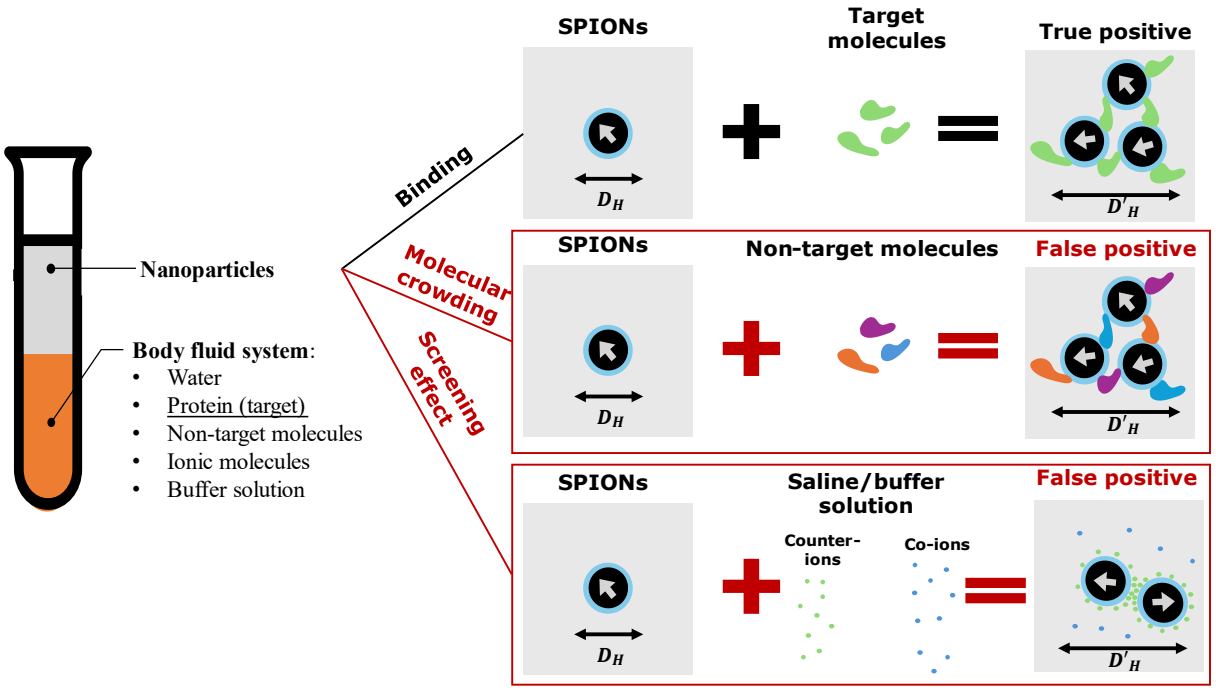

Figure 1.2. Impact of Molecular Crowding and Screening Effects on SPIONs Binding Specificity in Body Fluids. The image illustrates the interaction of superparamagnetic iron oxide nanoparticles (SPIONs) within a body fluid system containing water, target proteins, non-target molecules, ionic molecules, and a buffer solution. The left side shows a test tube with labeled layers representing the various components. The right side presents three scenarios: SPIONs binding to target molecules resulting in true positives, binding to non-target molecules leading to false positives due to molecular crowding and interaction with saline/buffer solutions also causing false positives due to screening effects. The diagrams highlight the challenge of distinguishing specific from non-specific binding in complex biological environments.

1.7 Fundamental Model of Magnetization Dynamics of Magnetic Nanoparticles

Measurement of AC magnetic susceptibility is a pivotal method used for detecting biomaterials in biosensors. Such measurements can provide critical insights into how superparamagnetic iron oxide nanoparticles (SPIONs) interact with target molecules or other substances, such as ionic solutions or

non-target molecules, which may significantly alter their dynamic behavior. Understanding these interactions is essential for developing effective biosensors and ensuring accurate detection and quantification of target biomolecules. A suitable model is typically required to interpret the data to analyze magnetization dynamics accurately.

I aim to provide a comprehensive overview of the available models commonly used to simulate how interactions between SPIONs and target molecules, as well as SPIONs and ionic solutions, alter the magnetization dynamics of SPIONs. I will divide into four fundamental models: Debye, Cole-Cole, Cole-Davidson, and Havriliak-Negami. The Debye model, which assumes that the system consists of single-size nanoparticles, is oversimplified and unrealistic in practical scenarios. Meanwhile, the other models, such as Cole-Cole, Cole-Davvidson, and Havriliak Negami, are extension versions of the Debye model that consider particle polydispersity and symmetry of the magnetization signal. The other approach I could take is using the Debye model to introduce the relaxation time distribution. Previous works have extended the Debye model by considering that SPIONs consist of nanoparticles of various sizes, thereby introducing the distribution of relaxation times. This statistical approach makes the model more realistic and better suited for interpreting the complex behaviors observed in SPION systems.

1.7.1 Debye Model

The Debye model is a fundamental approach to understanding the low-frequency magnetic dynamics of materials, particularly in the range of 0.1–10,000 Hz in low magnetic fields. Initially, the Debye model was proposed to model dielectric materials, not magnetic materials. However, over time, it has become applicable to theoretical studies of the magnetization dynamics of magnetic particles. This model primarily considers the magnetic susceptibility response of materials, where a single relaxation time characterizes the relaxation of magnetic dipoles within a medium under an alternating current (AC) field. The original theory by Debye posits that a material's static magnetic susceptibility (χ_s) The Debye model describes the behavior of a material's static magnetic susceptibility as it transitions from a static value at

low frequencies to a smaller value at high frequencies. This transition region is characterized by a characteristic relaxation time, a key parameter in the Debye model that influences the material's magnetic dynamics.

Key findings from foundational studies on the Debye model, such as those by Cole and Cole (1941), indicate that. χ_s The loss factor (the imaginary part of the dielectric constant) follows specific mathematical forms that can be represented as semicircles in a complex plane. This model assumes a simple exponential decay of magnetization, which works well for ideal, monodisperse systems where interactions between particles are negligible. However, deviations from the Debye model have been noted, especially in real-world systems where polydispersity and interactions complicate the relaxation behavior.

Mathematically, the Debye model can be written as:

$$\chi(\omega) = \chi_\infty + \left(\frac{\chi_s - \chi_\infty}{1 + i\omega\tau_{eff}}\right) \quad (1\text{-}1)$$

where $\chi(\omega)$ is the complex magnetic susceptibility as a function of angular frequency ω, χ_s is the static magnetic susceptibility, i is the imaginary unit, and τ_{eff}Is the characteristic relaxation time. In separate works τ_{eff}Is defined as an adequate relaxation time, given by:

$$\frac{1}{\tau_{eff}} = \frac{1}{\tau_N} + \frac{1}{\tau_B} \quad (1\text{-}2)$$

Neel and Brownian relaxation are two primary mechanisms that govern the magnetic relaxation dynamics of superparamagnetic iron oxide nanoparticles (SPIONs). Neel relaxation (τ_N) describes the rotation of the magnetic moment within a nanoparticle without any physical rotation of the particle itself. This type of relaxation is dominant in smaller particles where thermal energy can overcome the energy barrier separating different magnetic states. The characteristic time for Neel relaxation is given by:

$$\tau_N = \tau_0 exp\left(\frac{KV}{k_B T}\right) \quad (1\text{-}3)$$

where τ_0 is the attempt time (on the order of 10^{-9} seconds), K is the anisotropy constant, V is the volume of the nanoparticle, k_B is the Boltzmann constant, and T is the temperature. The exponential dependence on KV indicates that larger particles with higher anisotropy will have much longer Neel relaxation times.

Brownian relaxation (τ_B), on the other hand, involves the physical rotation of the entire nanoparticle in a fluid medium. This process is influenced by the surrounding medium's viscosity and the particles' hydrodynamic size. The characteristic time for Brownian relaxation is given by:

$$\tau_B = \frac{3\eta V_H}{k_B T} \tag{1-4}$$

where ηIs the viscosity of the medium, V_H Is the hydrodynamic volume of the particle, and $k_B T$Is the thermal energy. Brownian relaxation becomes significant for larger particles or in highly dense environments where the physical rotation of particles is more restricted.

Together, Néel and Brownian relaxation contribute to the overall relaxation dynamics of SPIONs, with their relative contributions depending on the size of the nanoparticles, the temperature, and the viscosity of the medium. The interplay between these two mechanisms is crucial for understanding and optimizing the performance of SPION-based biosensors and other magnetic applications. However, the ideal Debye model is too simplistic to accurately model the dynamic behavior of colloidal SPIONs in water (nanofluids). The ideal Debye model assumes that the colloidal SPIONs form a monodispersed system and neglect dipole interactions. In reality, colloidal SPIONs are polydisperse, and magnetic dipole interactions cannot be ignored in many cases. To account for the polydispersity in our system, I can use an extended version of the Debye model by introducing a relaxation time distribution. I will discuss this advanced model further in the next sub-chapter.

1.7.2 Debye Model with Distribution of Relaxation Time

In natural colloidal systems of superparamagnetic iron oxide nanoparticles (SPIONs), the dynamic magnetic susceptibility often deviates from the idealized Debye model, evidenced by asymmetric patterns in the Cole-Cole diagram. Extended models such as Cole-Cole, Cole-Davidson, and Havriliak-

Negami are used to address these deviations. These models can account for symmetric and asymmetric behaviors but often involve complex fitting techniques and parameters that may lack intuitive physical meaning. To better capture the relaxation behaviors of SPIONs, the concept of a relaxation time distribution function, $f(\tau)$, is introduced. This approach expresses the relaxation behavior as a superposition of Debye functions with different relaxation times, providing a more accurate representation of real systems. The distribution function $f(\tau)$ can be derived from dynamic light scattering (DLS) measurements, which provide hydrodynamic diameter data correlated with relaxation times. This method allows for realistic and physically interpretable modeling of SPIONs' relaxation dynamics, reflecting the actual size distribution and complex interactions within the system. Mathematically, this can be expressed as:

$$\chi(\omega) = \chi_s \int_0^\infty \frac{f(\tau)d\tau}{1+i\omega\tau_{eff}} \tag{1-5}$$

with $\int_0^\infty \mathrm{f}(\tau)\mathrm{d}\tau = 1$. If I do not carefully select appropriate functions, $f(\tau)$, I may encounter similar issues as the other available models: complexity and lack of physical interpretability. Therefore, I used the mass distribution function obtained from DLS measurements.

In conducting DLS measurements, I obtained hydrodynamic diameter data and their corresponding mass distribution. When applied to the equation above, these data sets serve as the distribution function of relaxation times. DLS measurements provide the hydrodynamic diameters of particles in the colloid, which can then be correlated with their relaxation times. The hydrodynamic diameter data and their respective populations allow us to construct a realistic distribution function that reflects the actual size distribution and dynamic behavior of SPIONs in a given environment. This method offers a more physically interpretable approach to modeling the relaxation dynamics of SPIONs, considering the inherent polydispersity and complex interactions present in real-world samples.

1.8 Effect of The Magnetic Dipole Interactions on Dynamic Behavior of SPIONs

Magnetic dipole interactions significantly influence the dynamic behavior of SPIONs [191-201]. These interactions arise when the magnetic moments of individual nanoparticles influence each other, especially when the particles are closely packed. This influence alters the overall magnetic behavior of the nanoparticle system. Dipole interactions can cause changes' relaxation dynamics of SPIONs, affecting both Néel and Brownian relaxation processes. The degree of these interactions often depends on factors such as particle concentration, size distribution, and the viscosity of the surrounding medium.

In systems where SPIONs are used for applications like magnetic hyperthermia, strong dipole interactions can reduce the specific absorption rate (SAR). This occurs because dipole interactions increase the effective anisotropy and reduce the overall magnetic susceptibility, leading to less efficient heat generation under an alternating magnetic field. Similarly, for biosensing applications, where the detection sensitivity is crucial, the dipole interactions can affect the stability and aggregation behavior of the nanoparticles, thereby influencing the signal output and reliability of the sensor.

The previous works collectively demonstrate the significant impact of interparticle interactions on the magnetic properties and dynamic behavior of SPIONs. For instance, the study by Serantes et al. [200] employs both experimental evidence and Monte Carlo simulations to show that increasing the intensity of dipolar interactions leads to decreased magnetic susceptibility and hysteresis losses, thereby reducing the heating efficiency in hyperthermia applications. Similarly, Morozov et al. [201] presented data on the initial susceptibility of magnetic fluids, highlighting that deviations from the expected behavior can be attributed to interparticle interactions, proven by increasing average cluster volume of SPIONs. They remarked that the interparticle interactions lead to cluster aggregation. Their theoretical model, which accounts for dipolar interactions, shows a non-monotonic temperature dependence of susceptibility and the formation of magnetic clusters.

1.8.1 Interparticle and Inter-cluster Magnetic Dipolar Interactions

Our study on interparticle magnetic dipolar interaction is built on a foundation of previous research. Numerous past studies have investigated the effects of dipolar magnetic interactions on magnetization dynamics, particularly for hyperthermia applications. Understanding these interactions is crucial as strong dipolar interactions can significantly reduce the specific absorption rate (SAR), impacting hyperthermia efficiency. This reduction occurs because dipole interactions increase effective anisotropy and decrease overall magnetic susceptibility, leading to less efficient heat generation under an alternating magnetic field.

For example, Serantes et al. [200] combined experimental evidence and Monte Carlo simulations to demonstrate that stronger dipolar interactions decrease magnetic susceptibility and hysteresis losses, reducing heating efficiency in hyperthermia applications. Similarly, Morozov et al. [201] provided data showing that deviations in the initial susceptibility of magnetic fluids are due to interparticle interactions, which lead to cluster aggregation. Their theoretical model, which accounts for dipolar interactions, illustrates a non-monotonic temperature dependence of susceptibility and the formation of magnetic clusters. In biosensing applications, where detection sensitivity is paramount, dipolar interactions can similarly influence nanoparticles' stability and aggregation behavior, affecting signal output and sensor reliability[202-204]. When nanoparticles aggregate, interparticle magnetic dipolar interactions may be induced[203,204]. Previous works [203,204] mention that these interparticle dipolar magnetic interactions alter relaxation behavior and suggest a change in the hydrodynamic volume due to secondary particle aggregation.

Trisnanto et al. [203] explored the interplay between dipolar magnetism and electrostatic repulsion in a polydisperse magnetic colloid by manipulating the distance between particles. By introducing ionic solutions like NaCl or PBS buffer, they observed a decrease in electrostatic repulsion, increasing the attractive forces between particles. This attraction led to a reduced interparticle distance, ultimately causing secondary particle clustering. Additionally, the study demonstrated that higher particle

concentrations enhance dipolar interparticle interactions, contributing to clustering. The study quantified secondary particle clustering through a collective time constant, τ

$$\tau = \frac{3\eta}{k_B T}\left[\sum_i \frac{\rho(V_{h,i})}{V_{h,i}}\right]^{-1} \quad (1\text{-}6)$$

derived from equation (1-6). The authors noted that a larger τ might indicate significant primary clustering. To differentiate τ originating from primary and secondary clustering, the latter shows a broader size distribution than the former, as illustrated in Figure 1.3. Figure 1.3(a) displays the imaginary part of the DMS signal. In contrast, Figure 1.3(b) shows the hydrodynamic size distributions for SPIONs at concentrations of 30 wt%, 14 wt%, and 3 wt% extracted from DMS signal in Figure 1.3 (a).

However, extracting size distribution from the DMS signal can be challenging due to the need to select appropriate models and employ complex numerical methods. This doctoral thesis proposes a more straightforward approach to indicating secondary particle clustering by measuring the spectrum's broadness. This is done by calculating the ratio between the peak frequency f_{peak} and the frequency f_{half}, where the normalized imaginary part of DMS equals 0.5 in the lower frequency region, as discussed in Chapter 3. This method is more straightforward and effective than the previous study [203].

Trisnanto and Kitamoto[204] argued that two types of Brownian relaxation mechanisms exist within the system, originating from cluster rotation and individual clusters. Their study used two SPIONs: specimen 1, representing a dispersed-particle system, and specimen 2, representing a clustered-particle system, as illustrated in Figure. 1.4 (a-b). They proposed that relaxation symmetry can be used to demonstrate the coexistence of these two Brownian relaxation mechanisms. This relaxation symmetry is obtained by plotting the real part of magnetic susceptibility (as the x-axis) against the imaginary part of magnetic susceptibility (as the y-axis). They further plotted the relaxation symmetry using Cole-Cole (CC) and Cole-Davidson (CD) models, as shown in Figure 1.4 (c-d). The CC model, an extension of the Debye model, accounts for particle size polydispersity, resulting in a symmetric graph in their approximation. In contrast, the CD model showed an asymmetric or skewed arc, represented as beta,

with values ranging from 0 to 1. Their study concluded that if beta equals 1, only particle rotation exists within the system. Conversely, if beta is between 0 and 1, it implies the coexistence of cluster and particle rotation within the system.

A full version of the DMS signal is typically required to conduct their experiment, as dealing with an asymmetric arc necessitates applying a dynamic magnetic field from a couple of Hz to millions of Hz. However, this dissertation proposes a narrower frequency range (10 to 10,000 Hz) to explain interparticle dipolar interactions, eliminating the need for a full DMS signal. The peak frequency of DMS is sufficient for the analysis.

Additionally, this dissertation introduces the concept of the coexistence of inter-cluster magnetic dipolar interactions, observable in the DMS spectra. While interparticle dipolar magnetic interactions are negligible in individually dispersed particles, they become stronger as individual particles aggregate to form a clustered-particle system. This analogy extends to individually dispersed particle and clustered-particle systems, which may aggregate under the influence of saline concentration and buffer solutions, encouraging inter-cluster magnetic dipolar interactions. Qualitative descriptions of these interactions are provided by noting changes in the DMS spectra.

1.9 Aim of This Study

This study aims to elucidate the dynamic magnetic behavior of superparamagnetic iron oxide nanoparticles (SPIONs) coated with citric acid (CA) under various physiological conditions. This research focuses on understanding the influences of interparticle and inter-cluster dipole-dipole interactions on these nanoparticles' stability and magnetic properties. By systematically varying ionic concentrations and buffer solutions, the study aims to comprehensively analyze how these factors affect the behavior of CA-coated SPIONs, which is crucial for their application in biosensing technologies. Through detailed experiments involving the measurement of hydrodynamic size, zeta potential, and dynamic magnetic susceptibility, this research offers new insights into optimizing the performance of

SPIONs in biomedical applications.

1.10 Novelty of The Present Study

This dissertation introduces a novel approach to understanding the dynamic behavior of citric acid-coated superparamagnetic iron oxide nanoparticles (CA-SPIONs) by systematically examining the effects of interparticle and inter-cluster dipole-dipole interactions under varying conditions. Unlike conventional studies that treat these factors in isolation, this research uniquely integrates cluster size and ionic concentration modulation in the suspensions. By controlling incubation times and altering ionic strengths, the study provides a comprehensive analysis of how magnetic interactions influence the behavior of CA-SPIONs.

A significant innovation of this research is the simultaneous investigation of cluster size and ionic strength. This dual focus allows a detailed examination of how interparticle and inter-cluster magnetic dipolar interactions affect the dynamic magnetic susceptibility (DMS) spectra. The results reveal distinct shifts and broadening in the DMS spectra, offering new insights into the magnetic properties of SPIONs. These findings are particularly crucial for optimizing the use of SPIONs in biomedical applications, such as biosensing and imaging, where precise control over magnetic behavior is essential.

Moreover, this dissertation addresses a fundamental limitation in existing studies by proposing a narrower frequency range (from 10 to 10,000 Hz) to explain interparticle dipolar interactions. Traditionally, a full DMS signal across a broad frequency spectrum (from a couple of Hz to millions of Hz) is required to conduct these experiments. However, this study demonstrates that the peak frequency of DMS is sufficient for the analysis, simplifying the experimental process and enhancing the practicality of the findings.

Overall, this research provides experimental evidence of nuanced magnetic interactions and offers a more practical approach to DMS analysis, paving the way for developing more precise and effective SPION-based technologies in nanomedicine. The innovations presented in this dissertation contribute significantly to the field, advancing our understanding of magnetic dipolar interactions and their

implications for applying SPIONs in various biomedical contexts.

Reference

(1) I. Freestone, N. Meeks, M. Sax, C. Higgitt, “The Lycurgus Cup – A Roman Nanotechnology,” Gold Bull., 2007;40(4):270-27

(2) R.P. Feynman, “There’s Plenty of Room at the Bottom,” Eng Sci. 1960;23(5):22-36.

(3) G. Binnig, H. Rohrer, “Scanning Tunneling Microscopy,” J Appl Phys. 1986;61(2):R1-R6.

(4) K. Balakumar, R. Rajesh, R. Kumaravel, et al., “Diverse application of green nanotechnology – A review,” Chemosphere. 2022;287(Part 1):131979.

(5) P. Ahadi, M. Azenha, H. De Sousa, A. Samagaio, “Applications of Nanomaterials in Construction with an Approach to Energy Issue,” Adv Mater Res. 2011;261-263:509-514.

(6) S. Mohapatra, P. Giri, “Green Synthesis of Nanoparticles and Their Energy Storage, Environmental, and Biomedical Applications,” Crystals. 2023;13(11):1576.

(7) J. Bae, "Applications of Nanomaterials and Nanotechnology in Energy Storage Device," Nanomaterials. 2022;12(24):4353.

(8) J.M.P.Q. Delgado, A. Öchsner, A.G. Barbosa de Lima, “Nanotechnology for Energy and Environment,” Hindawi, 2014;2014:1-14.

(9) Farooq W, Hano C, Abbasi BH, Anjum I. Emerging Applications of Nanotechnology in Healthcare Systems: Grand Challenges and Perspectives. Pharmaceuticals. 2021;14(8):707. doi:10.3390/ph14080707.

(10) Molloy K, Golombek S, Hong J, et al. Advances in nanomaterial-based targeted drug delivery systems. Frontiers. 2020. doi:10.3389/fphar.2020.580029.

(11) Nasra S, Bhatia D, Kumar A. Recent advances in nanoparticle-based drug delivery systems for rheumatoid arthritis treatment. Nanoscale Adv. 2022;4(7):3479-3494. doi:10.1039/D2NA00229A.

(12) Zhang L, Gu FX, Chan JM, Wang AZ, Langer RS, Farokhzad OC. Nanoparticles in medicine: therapeutic applications and developments. Clin Pharmacol Ther. 2008;83(5):761-769. doi:10.1038/sj.clpt.6100400.

(13) Marinelli L, Ciulla M, Ritsema JAS, van Nostrum CF, Cacciatore I, Dimmito MP, Palmerio F, Orlando G, Robuffo I, Grande R, Puca V, Di Stefano A. Preparation, Characterization, and Biological Evaluation of a Hydrophilic Peptide Loaded on PEG-PLGA Nanoparticles. Pharmaceutics. 2022 Aug 29;14(9):1821. doi: 10.3390/pharmaceutics14091821. PMID: 36145568; PMCID: PMC9506305.

(14) V. K. Sangwan, M. C. Hersam, “Nanomaterials pave the way for the next computing generation,” Nature Nanotechnol. 2022;15:517-528. doi:10.1038/d41586-022-02147-3.

(15) Lo Nigro, Raffaella, Patrick Fiorenza, Béla Pécz, and Jens Eriksson. 2022. "Nanotechnology for Electronic Materials and Devices" *Nanomaterials* 12, no. 19: 3319. https://doi.org/10.3390/nano12193319

(16) B. Yu and M. Meyyappan, “Nanotechnology: Role in emerging nanoelectronics, ” *Solid-State Electronics* **50** (4). 536-544. 2006

(17) Zhang, Z. M., C. J. Fu, and Q. Z. Zhu. "Optical and thermal radiative properties of semiconductors related to micro/nanotechnology." *Advances in Heat Transfer* 37, no. 3 (2003): 179-296.

(18) Sebastian, A., Le Gallo, M., Khaddam-Aljameh, R. and Eleftheriou, E., 2020. Memory devices and applications for in-memory computing. Nature nanotechnology, 15(7), pp.529-544.

(19) Hwang, C.G., 2003. Nanotechnology enables a new memory growth model. Proceedings of the IEEE, 91(11), pp.1765-1771.
(20) Savage, N., & Diallo, M. S. (2005). Nanomaterials and water purification: opportunities and challenges. *Journal of Nanoparticle research*, *7*, 331-342.
(21) Arora, B., & Attri, P. (2020). Carbon nanotubes (CNTs): a potential nanomaterial for water purification. *Journal of Composites Science*, *4*(3), 135.
(22) Ning, Cun-Zheng. "Semiconductor nanolasers and the size-energy-efficiency challenge: a review." *Advanced Photonics* 1, no. 1 (2019): 014002-014002.
(23) Wang, Zhong Lin, and Wenzhuo Wu. "Nanotechnology-enabled energy harvesting for self-powered micro-/nanosystems." *Angewandte Chemie International Edition* 51, no. 47 (2012): 11700-11721.
(24) Hussein, Ahmed Kadhim. "Applications of nanotechnology in renewable energies—A comprehensive overview and understanding." *Renewable and Sustainable Energy Reviews* 42 (2015): 460-476.
(25) Baruah, Sunandan, and Joydeep Dutta. "Nanotechnology applications in pollution sensing and degradation in agriculture: a review." *Environmental Chemistry Letters* 7 (2009): 191-204.
(26) Bystrzejewska-Piotrowska, Grazyna, Jerzy Golimowski, and Pawel L. Urban. "Nanoparticles: their potential toxicity, waste and environmental management." *Waste management* 29, no. 9 (2009): 2587-2595.
(27) Walmsley, Graham G., Adrian McArdle, Ruth Tevlin, Arash Momeni, David Atashroo, Michael S. Hu, Abdullah H. Feroze et al. "Nanotechnology in bone tissue engineering." *Nanomedicine: Nanotechnology, Biology and Medicine* 11, no. 5 (2015): 1253-1263.
(28) Huang, Wenwen, Shengjie Ling, Chunmei Li, Fiorenzo G. Omenetto, and David L. Kaplan. "Silkworm silk-based materials and devices generated using bio-nanotechnology." *Chemical Society Reviews* 47, no. 17 (2018): 6486-6504.
(29) Williams, Joseph D., and G. P. Peterson. "A review of thermal property enhancements of low-temperature nano-enhanced phase change materials." *Nanomaterials* 11, no. 10 (2021): 2578.
(30) Bhat, Aayush, Sejal Budholiya, Sakthivel Aravind Raj, Mohamed Thariq Hameed Sultan, David Hui, Ain Umaira Md Shah, and Syafiqah Nur Azrie Safri. "Review on nanocomposites based on aerospace applications." *Nanotechnology Reviews* 10, no. 1 (2021): 237-253.
(31) Harifi, Tina, and Majid Montazer. "Application of nanotechnology in sports clothing and flooring for enhanced sport activities, performance, efficiency and comfort: a review." *Journal of Industrial Textiles* 46, no. 5 (2017): 1147-1169.
(32) Wei H, Wang E. Nanomaterial-based biosensors for biological detection. Biosens Bioelectron. 2008;23(7):1141-1149. doi:10.1016/j.bios.2007.12.003.
(33) Turner APF. Biosensors: Sense and Sensitivity. Science. 2000;290(5495):1315-1317. doi:10.1126/science.290.5495.1315.
(34) Li L, Wang T, Zhong Y, et al. A review of nanomaterials for biosensing applications. J Mater Chem B. 2024;12:1168-1193. doi:10.1039/D3TB02648E.
(35) Si P, Razmi N, Nur O, et al. Gold nanomaterials for optical biosensing and bioimaging. Nanoscale Adv. 2021;3:2679-2698. doi:10.1039/D0NA00961J.
(36) Nikolic MV, Vidic J. Advances in Nanomaterials-Based Electrochemical Biosensors for Foodborne Pathogen Detection. Nanomaterials. 2021;11(10):2700. doi:10.3390/nano11102700.
(37) D'Souza SF. Electrochemical biosensors: perspective on functional nanomaterials for on-site analysis. Biomater Res. 2021;25:34. doi:10.1186/s40824-021-00228-1.
(38) Zhang Y, Wang X, Wang Q. Recent Developments on the Catalytic and Biosensing Applications of Porous Nanomaterials. Nanomaterials. 2022;12(7):1200. doi:10.3390/nano12071200.

(39) Jianrong, Chen, Miao Yuqing, He Nongyue, Wu Xiaohua, and Li Sijiao. "Nanotechnology and biosensors." *Biotechnology advances* 22, no. 7 (2004): 505-518.
(40) Merkoçi, Arben. "Nanoparticles-based strategies for DNA, protein and cell sensors." *Biosensors and Bioelectronics* 26, no. 4 (2010): 1164-1177.
(41) Xu, Hui, Xun Mao, Qingxiang Zeng, Shengfu Wang, Abdel-Nasser Kawde, and Guodong Liu. "Aptamer-functionalized gold nanoparticles as probes in a dry-reagent strip biosensor for protein analysis." *Analytical Chemistry* 81, no. 2 (2009): 669-675.
(42) Xian, Yuezhong, Yi Hu, Fang Liu, Yang Xian, Haiting Wang, and Litong Jin. "Glucose biosensor based on Au nanoparticles–conductive polyaniline nanocomposite." *Biosensors and Bioelectronics* 21, no. 10 (2006): 1996-2000.
(43) Zhao, Xiaoli, Yaqi Cai, Thanh Wang, Yali Shi, and Guibin Jiang. "Preparation of alkanethiolate-functionalized core/shell Fe3O4@ Au nanoparticles and its interaction with several typical target molecules." *Analytical chemistry* 80, no. 23 (2008): 9091-9096.
(44) Agasti, Sarit S., Subinoy Rana, Myoung-Hwan Park, Chae Kyu Kim, Chang-Cheng You, and Vincent M. Rotello. "Nanoparticles for detection and diagnosis." *Advanced drug delivery reviews* 62, no. 3 (2010): 316-328.
(45) Ivanov, Michael R., Heidi R. Bednar, and Amanda J. Haes. "Investigations of the mechanism of gold nanoparticle stability and surface functionalization in capillary electrophoresis." *ACS nano* 3, no. 2 (2009): 386-394.
(46) Zhang, Suxia, Nü Wang, Huijun Yu, Yaming Niu, and Changqing Sun. "Covalent attachment of glucose oxidase to an Au electrode modified with gold nanoparticles for use as glucose biosensor." *Bioelectrochemistry* 67, no. 1 (2005): 15-22.
(47) Chio, Linda, Rebecca L. Pinals, Aishwarya Murali, Natalie S. Goh, and Markita P. Landry. "Covalent surface modification effects on single-walled carbon nanotubes for targeted sensing and optical imaging." *Advanced Functional Materials* 30, no. 17 (2020): 1910556.
(48) Polavarapu, Lakshminarayana, Jorge Pérez-Juste, Qing-Hua Xu, and Luis M. Liz-Marzán. "Optical sensing of biological, chemical and ionic species through aggregation of plasmonic nanoparticles." *Journal of Materials Chemistry C* 2, no. 36 (2014): 7460-7476.
(49) Jiang, Xiaowen, Hui Jin, Yujiao Sun, and Rijun Gui. "Colorimetric and fluorometric dual-channel ratiometric determination of fungicide cymoxanil based on analyte-induced aggregation of silver nanoparticles and dually emitting carbon dots." *Microchimica Acta* 186 (2019): 1-12.
(50) Zhou, Yang, Shixing Wang, Ke Zhang, and Xingyu Jiang. "Visual detection of copper (II) by azide-and alkyne-functionalized gold nanoparticles using click chemistry." *Angew. Chem* 120, no. 39 (2008): 7564-7566.
(51) Achatz, Daniela E., Florian J. Heiligtag, Xiaohua Li, Martin Link, and Otto S. Wolfbeis. "Colloidal silica nanoparticles for use in click chemistry-based conjugations and fluorescent affinity assays." *Sensors and Actuators B: Chemical* 150, no. 1 (2010): 211-219.
(52) Chen, Yiping, Yunlei Xianyu, Jing Wu, Binfeng Yin, and Xingyu Jiang. "Click chemistry-mediated nanosensors for biochemical assays." *Theranostics* 6, no. 7 (2016): 969.
(53) Ganta D, Singh P. Applications of Click Chemistry in Biosensor Development. ACS Appl Mater Interfaces. 2022;14(19):2159-2168. doi:10.1021/acsami.1c23457.
(54) Ganesh, Venkataraman, V. Sai Sudhir, Taraknath Kundu, and Srinivasan Chandrasekaran. "10 years of click chemistry: synthesis and applications of ferrocene-derived triazoles." *Chemistry–An Asian Journal* 6, no. 10 (2011): 2670-2694.
(55) Cernat, Andreea, Mihaela Tertiș, Cecilia Cristea, and Robert Săndulescu. "Applications of click chemistry in the development of electrochemical sensors." *International Journal of Electrochemical Science* 10, no. 8 (2015): 6324-6337.

(56) Bhirde, Ashwinkumar, Jin Xie, Maggie Swierczewska, and Xiaoyuan Chen. "Nanoparticles for cell labeling." *Nanoscale* 3, no. 1 (2011): 142-153.
(57) Merkoçi, A., M. Aldavert, S. Marın, and S. Alegret. "New materials for electrochemical sensing V: Nanoparticles for DNA labeling." *TrAC Trends in Analytical Chemistry* 24, no. 4 (2005): 341-349.
(58) Rhouati, Amina, Jean-Louis Marty, and Alina Vasilescu. "Electrochemical biosensors combining aptamers and enzymatic activity: Challenges and analytical opportunities." *Electrochimica Acta* 390 (2021): 138863.
(59) Bobrinetskiy, Ivan, Marko Radovic, Francesco Rizzotto, Priya Vizzini, Stefan Jaric, Zoran Pavlovic, Vasa Radonic, Maria Vesna Nikolic, and Jasmina Vidic. "Advances in nanomaterials-based electrochemical biosensors for foodborne pathogen detection." *Nanomaterials* 11, no. 10 (2021): 2700.
(60) Song, Shiping, Lihua Wang, Jiang Li, Chunhai Fan, and Jianlong Zhao. "Aptamer-based biosensors." *TrAC Trends in Analytical Chemistry* 27, no. 2 (2008): 108-117.
(61) Ronkainen, Niina J., H. Brian Halsall, and William R. Heineman. "Electrochemical biosensors." *Chemical Society Reviews* 39, no. 5 (2010): 1747-1763.
(62) Grieshaber, Dorothee, Robert MacKenzie, Janos Vörös, and Erik Reimhult. "Electrochemical biosensors-sensor principles and architectures." *Sensors* 8, no. 3 (2008): 1400-1458.
(63) Frew, Jane E., and H. Allen O. Hill. "Electrochemical biosensors." *Analytical chemistry* 59, no. 15 (1987): 933A-944A.
(64) Zhang, S., G. Wright, and Y. Yang. "Materials and techniques for electrochemical biosensor design and construction." *Biosensors and Bioelectronics* 15, no. 5-6 (2000): 273-282.
(65) Thévenot, Daniel R., Klara Toth, Richard A. Durst, and George S. Wilson. "Electrochemical biosensors: recommended definitions and classification." *Biosensors and bioelectronics* 16, no. 1-2 (2001): 121-131.
(66) Aydemir, Nihan, Jenny Malmström, and Jadranka Travas-Sejdic. "Conducting polymer based electrochemical biosensors." *Physical Chemistry Chemical Physics* 18, no. 12 (2016): 8264-8277.
(67) Moon, Jong-Min, Neeta Thapliyal, Khalil Khadim Hussain, Rajendra N. Goyal, and Yoon-Bo Shim. "Conducting polymer-based electrochemical biosensors for neurotransmitters: A review." *Biosensors and Bioelectronics* 102 (2018): 540-552.
(68) Li, Lanlan, Ye Shi, Lijia Pan, Yi Shi, and Guihua Yu. "Rational design and applications of conducting polymer hydrogels as electrochemical biosensors." *Journal of Materials Chemistry B* 3, no. 15 (2015): 2920-2930.
(69) 69. Yang, Ning, Xianping Chen, Tianling Ren, Ping Zhang, and Daoguo Yang. "Carbon nanotube based biosensors." *Sensors and Actuators B: Chemical* 207 (2015): 690-715.
(70) Balasubramanian, Kannan, and Marko Burghard. "Biosensors based on carbon nanotubes." *Analytical and bioanalytical chemistry* 385 (2006): 452-468.
(71) Wang, Joseph. "Carbon-nanotube based electrochemical biosensors: A review." *Electroanalysis: An International Journal Devoted to Fundamental and Practical Aspects of Electroanalysis* 17, no. 1 (2005): 7-14.
(72) Zhang, Yuanyuan, Mary A. Arugula, Melinda Wales, James Wild, and Aleksandr L. Simonian. "A novel layer-by-layer assembled multi-enzyme/CNT biosensor for discriminative detection between organophosphorus and non-organophosphrus pesticides." *Biosensors and Bioelectronics* 67 (2015): 287-295.
(73) Lin, Yuehe, Fang Lu, Yi Tu, and Zhifeng Ren. "Glucose biosensors based on carbon nanotube nanoelectrode ensembles." *Nano letters* 4, no. 2 (2004): 191-195.

(74) Wang, Joseph, and Mustafa Musameh. "Carbon nanotube/teflon composite electrochemical sensors and biosensors." *Analytical chemistry* 75, no. 9 (2003): 2075-2079.
(75) Pingarrón, José M., Paloma Yanez-Sedeno, and Araceli González-Cortés. "Gold nanoparticle-based electrochemical biosensors." *Electrochimica Acta* 53, no. 19 (2008): 5848-5866.
(76) Bedford, Erin E., Jolanda Spadavecchia, Claire-Marie Pradier, and Frank X. Gu. "Surface plasmon resonance biosensors incorporating gold nanoparticles." *Macromolecular bioscience* 12, no. 6 (2012): 724-739.
(77) Aldewachi, Hasan, Tamim Chalati, M. N. Woodroofe, Neil Bricklebank, B. Sharrack, and Philip Gardiner. "Gold nanoparticle-based colorimetric biosensors." *Nanoscale* 10, no. 1 (2018): 18-33.
(78) Špringer, Tomáš, Maria Laura Ermini, Barbora Spacková, Jani Jablonku, and Jiri Homola. "Enhancing sensitivity of surface plasmon resonance biosensors by functionalized gold nanoparticles: size matters." *Analytical Chemistry* 86, no. 20 (2014): 10350-10356.
(79) Hrapovic, Sabahudin, Yali Liu, Keith B. Male, and John HT Luong. "Electrochemical biosensing platforms using platinum nanoparticles and carbon nanotubes." *Analytical chemistry* 76, no. 4 (2004): 1083-1088.
(80) Yang, Minghui, Yu Yang, Haifeng Yang, Guoli Shen, and Ruqin Yu. "Layer-by-layer self-assembled multilayer films of carbon nanotubes and platinum nanoparticles with polyelectrolyte for the fabrication of biosensors." *Biomaterials* 27, no. 2 (2006): 246-255.
(81) Borisov, Sergey M., and Otto S. Wolfbeis. "Optical biosensors." *Chemical reviews* 108, no. 2 (2008): 423-461.
(82) Chen, Chen, and Junsheng Wang. "Optical biosensors: An exhaustive and comprehensive review." *Analyst* 145, no. 5 (2020): 1605-1628.
(83) Morris, May C. *Fluorescence-based biosensors: from concepts to applications*. Vol. 113. Academic Press, 2012.
(84) Malhotra, Bansi Dhar, and Md Azahar Ali. "Nanomaterials in biosensors: Fundamentals and applications." *Nanomaterials for biosensors* (2018): 1.
(85) Huang, Xiaolin, Jibin Song, Bryant C. Yung, Xiaohua Huang, Yonghua Xiong, and Xiaoyuan Chen. "Ratiometric optical nanoprobes enable accurate molecular detection and imaging." *Chemical Society Reviews* 47, no. 8 (2018): 2873-2920.
(86) Hu, Rong, Tao Liu, Xiao-Bing Zhang, Shuang-Yan Huan, Cuichen Wu, Ting Fu, and Weihong Tan. "Multicolor fluorescent biosensor for multiplexed detection of DNA." *Analytical chemistry* 86, no. 10 (2014): 5009-5016.
(87) Stranik, O., H. M. McEvoy, C. McDonagh, and B. D. MacCraith. "Plasmonic enhancement of fluorescence for sensor applications." *Sensors and Actuators B: Chemical* 107, no. 1 (2005): 148-153.
(88) Zhang, Shen, and Hui-wang Ai. "A general strategy to red-shift green fluorescent protein-based biosensors." *Nature chemical biology* 16, no. 12 (2020): 1434-1439.
(89) Gautier, Arnaud. "Fluorescence-activating and absorption-shifting tags for advanced imaging and biosensing." *Accounts of Chemical Research* 55, no. 21 (2022): 3125-3135.
(90) Dey, Swayandipta, Mathias Dolci, and Peter Zijlstra. "Single-molecule optical biosensing: Recent advances and future challenges." *ACS Physical Chemistry Au* 3, no. 2 (2023): 143-156.
(91) Cao, Bo, Kan Wang, Hao Xu, Qi Qin, Jinchuan Yang, Wei Zheng, Qinghui Jin, and Daxiang Cui. "Development of magnetic sensor technologies for point-of-care testing: Fundamentals, methodologies and applications." *Sensors and Actuators A: Physical* 312 (2020): 112130.
(92) Haun, Jered B., Tae-Jong Yoon, Hakho Lee, and Ralph Weissleder. "Magnetic nanoparticle biosensors." *Wiley Interdisciplinary Reviews: Nanomedicine and Nanobiotechnology* 2, no. 3 (2010): 291-304.

(93) Nikitin, Petr I., Petr M. Vetoshko, and Tatiana I. Ksenevich. "New type of biosensor based on magnetic nanoparticle detection." *Journal of Magnetism and Magnetic Materials* 311, no. 1 (2007): 445-449.
(94) Chemla, Y. R., H. L. Grossman, Y. Poon, R. McDermott, R. Stevens, M. D. Alper, and J. Clarke. "Ultrasensitive magnetic biosensor for homogeneous immunoassay." *Proceedings of the National Academy of Sciences* 97, no. 26 (2000): 14268-14272.
(95) Aziz, Omar A. Abdel, Kholoud Arafa, Ahmed S. Abo Dena, and Ibrahim M. El-Sherbiny. "Superparamagnetic iron oxide nanoparticles (SPIONs): preparation and recent applications." *J. Nanotechnol. Adv. Mater* 8 (2020): 21-29.
(96) Loan, Phan Thi Kim, Dongqin Wu, Chen Ye, Xiaoqing Li, Vu Thanh Tra, Qiuping Wei, Li Fu, Aimin Yu, Lain-Jong Li, and Cheng-Te Lin. "Hall effect biosensors with ultraclean graphene film for improved sensitivity of label-free DNA detection." *Biosensors and Bioelectronics* 99 (2018): 85-91.
(97) Sandhu, Adarsh, Yoshimichi Kumagai, Adam Lapicki, Satoshi Sakamoto, Masanori Abe, and Hiroshi Handa. "High efficiency Hall effect micro-biosensor platform for detection of magnetically labeled biomolecules." *Biosensors and Bioelectronics* 22, no. 9-10 (2007): 2115-2120.
(98) Graham, Daniel L., Hugo A. Ferreira, and Paulo P. Freitas. "Magnetoresistive-based biosensors and biochips." *TRENDS in Biotechnology* 22, no. 9 (2004): 455-462.
(99) Lee, Jung-Rok, Noriyuki Sato, Daniel JB Bechstein, Sebastian J. Osterfeld, Junyi Wang, Adi Wijaya Gani, Drew A. Hall, and Shan X. Wang. "Experimental and theoretical investigation of the precise transduction mechanism in giant magnetoresistive biosensors." *Scientific reports* 6, no. 1 (2016): 18692.
(100) Wikswo, J. P., Y. P. Ma, N. G. Sepulveda, S. Tan, I. M. Thomas, and A. Lauder. "Magnetic susceptibility imaging for nondestructive evaluation (using SQUID magnetometer)." *IEEE transactions on applied superconductivity* 3, no. 1 (1993): 1995-2002.
(101) Bajpai, A., and A. Banerjee. "An automated susceptometer for the measurement of linear and nonlinear magnetic ac susceptibility." *Review of scientific instruments* 68, no. 11 (1997): 4075-4079.
(102) Haun, Jered B., Tae-Jong Yoon, Hakho Lee, and Ralph Weissleder. "Magnetic nanoparticle biosensors." *Wiley Interdisciplinary Reviews: Nanomedicine and Nanobiotechnology* 2, no. 3 (2010): 291-304.
(103) Sosnovik, David E., and Ralph Weissleder. "Emerging concepts in molecular MRI." *Current opinion in biotechnology* 18, no. 1 (2007): 4-10.
(104) Witte, Christopher, Vera Martos, Honor May Rose, Stefan Reinke, Stefan Klippel, Leif Schröder, and Christian PR Hackenberger. "Live-cell MRI with xenon hyper-CEST biosensors targeted to metabolically labeled cell-surface glycans." *Angewandte Chemie International Edition* 54, no. 9 (2015): 2806-2810.
(105) Wang, Lei, and Jianhan Lin. "Recent advances on magnetic nanobead based biosensors: From separation to detection." *TrAC Trends in Analytical Chemistry* 128 (2020): 115915.
(106) Wu, Kai, Diqing Su, Renata Saha, Jinming Liu, Vinit Kumar Chugh, and Jian-Ping Wang. "Magnetic particle spectroscopy: a short review of applications using magnetic nanoparticles." *ACS Applied Nano Materials* 3, no. 6 (2020): 4972-4989.
(107) Wu, Kai, Jinming Liu, Renata Saha, Diqing Su, Venkatramana D. Krishna, Maxim C-J. Cheeran, and Jian-Ping Wang. "Magnetic particle spectroscopy for detection of influenza A virus subtype H1N1." *ACS applied materials & interfaces* 12, no. 12 (2020): 13686-13697.
(108) Sun, Yi, Zhongzhou Du, Haochen Zhang, Haozhe Wang, Teruyoshi Sasayama, and Takashi Yoshida. "Simultaneous estimation of magnetic moment and Brownian relaxation time

distributions of magnetic nanoparticles based on magnetic particle spectroscopy for biosensing application." *Nanoscale* 15, no. 39 (2023): 16089-16102.

(109) Wu, Kai, Jinming Liu, Diqing Su, Renata Saha, and Jian-Ping Wang. "Magnetic nanoparticle relaxation dynamics-based magnetic particle spectroscopy for rapid and wash-free molecular sensing." *ACS applied materials & interfaces* 11, no. 26 (2019): 22979-22986.

(110) Clarke, John, Yong-Ho Lee, and Justin Schneiderman. "Focus on SQUIDs in biomagnetism." *Supercond. Sci. Technol* 31, no. 8 (2018): 080201.

(111) Carvell, Jeff, E. Ayieta, A. Gavrin, Ruihua Cheng, V. R. Shah, and P. Sokol. "Magnetic properties of iron nanoparticle." *Journal of Applied Physics* 107, no. 10 (2010).

(112) Stoner, E. C., and E. P. Wohlfarth. "A mechanism of magnetic hysteresis in heterogeneous alloys." *IEEE Transactions on Magnetics* 27, no. 4 (1991): 3475-3518.

(113) Chee, Chin Fei, Bey Fen Leo, and Chin Wei Lai. "Superparamagnetic iron oxide nanoparticles for drug delivery." In *Applications of nanocomposite materials in drug delivery*, pp. 861-903. Woodhead Publishing, 2018.

(114) Cronemberger, Carolina, Luis C. Sampaio, Alberto P. Guimaraes, and Pierre Molho. "Model for the growth of electrodeposited ferromagnetic aggregates under an in-plane magnetic field." *Physical Review E* 81, no. 2 (2010): 021403.

(115) Abu-Bakr, Ali F., and Andrey Yu Zubarev. "Effect of ferromagnetic nanoparticles aggregation on magnetic hyperthermia." *The European Physical Journal Special Topics* 229 (2020): 323-329.

(116) Rausch, Martin, Peter Hiestand, Carolyn A. Foster, Diana R. Baumann, Catherine Cannet, and Markus Rudin. "Predictability of FTY720 efficacy in experimental autoimmune encephalomyelitis by in vivo macrophage tracking: clinical implications for ultrasmall superparamagnetic iron oxide-enhanced magnetic resonance imaging." *Journal of Magnetic Resonance Imaging: An Official Journal of the International Society for Magnetic Resonance in Medicine* 20, no. 1 (2004): 16-24.

(117) Mandal, Madhuri, Subrata Kundu, Tapan K. Sau, S. M. Yusuf, and Tarasankar Pal. "Synthesis and characterization of superparamagnetic Ni− Pt nanoalloy." Chemistry of materials 15, no. 19 (2003): 3710-3715.

(118) Bartolome, Leian, Muhammad Imran, Kyoung G. Lee, Arvin Sangalang, and Jeong Keun Ahn. "Superparamagnetic γ-Fe 2 O 3 nanoparticles as an easily recoverable catalyst for the chemical recycling of PET." Green Chemistry 16, no. 1 (2014): 279-286.

(119) Rossi, Liane M., Fernanda P. Silva, Lucas LR Vono, Pedro K. Kiyohara, Evandro L. Duarte, Rosangela Itri, Richard Landers, and Giovanna Machado. "Superparamagnetic nanoparticle-supported palladium: a highly stable magnetically recoverable and reusable catalyst for hydrogenation reactions." Green Chemistry 9, no. 4 (2007): 379-385.

(120) Palanisamy, Sathyadevi, and Yun-Ming Wang. "Superparamagnetic iron oxide nanoparticulate system: synthesis, targeting, drug delivery and therapy in cancer." Dalton transactions 48, no. 26 (2019): 9490-9515.

(121) Laurent, Sophie, Silvio Dutz, Urs O. Häfeli, and Morteza Mahmoudi. "Magnetic fluid hyperthermia: focus on superparamagnetic iron oxide nanoparticles." Advances in colloid and interface science 166, no. 1-2 (2011): 8-23.

(122) Gangopadhyay, Palash, Sébastien Gallet, Edith Franz, André Persoons, and Thierry Verbiest. "Novel superparamagnetic core (shell) nanoparticles for magnetic targeted drug delivery and hyperthermia treatment." IEEE Transactions on magnetics 41, no. 10 (2005): 4194-4196.

(123) Quinto, Christopher A., Priya Mohindra, Sheng Tong, and Gang Bao. "Multifunctional superparamagnetic iron oxide nanoparticles for combined chemotherapy and hyperthermia cancer treatment." Nanoscale 7, no. 29 (2015): 12728-12736.
(124) Chen, Can, Jianxian Ge, Yun Gao, Lei Chen, Jiabin Cui, Jianfeng Zeng, and Mingyuan Gao. "Ultrasmall superparamagnetic iron oxide nanoparticles: A next generation contrast agent for magnetic resonance imaging." Wiley Interdisciplinary Reviews: Nanomedicine and Nanobiotechnology 14, no. 1 (2022): e1740.
(125) Masud, Mostafa Kamal, Jongbeom Na, Muhammad Younus, Md Shahriar A. Hossain, Yoshio Bando, Muhammad JA Shiddiky, and Yusuke Yamauchi. "Superparamagnetic nanoarchitectures for disease-specific biomarker detection." Chemical Society Reviews 48, no. 24 (2019): 5717-5751.
(126) Kim, Jeonghyo, Van Tan Tran, Sangjin Oh, Chang-Seok Kim, Jong Chul Hong, SungIl Kim, Young-Seon Joo et al. "Scalable solvothermal synthesis of superparamagnetic Fe3O4 nanoclusters for bioseparation and theragnostic probes." ACS Applied Materials & Interfaces 10, no. 49 (2018): 41935-41946.
(127) Kita, Eiji, Tatsuya Oda, Takeru Kayano, Suguru Sato, Makoto Minagawa, Hideto Yanagihara, Mikio Kishimoto et al. "Ferromagnetic nanoparticles for magnetic hyperthermia and thermoablation therapy." Journal of Physics D: Applied Physics 43, no. 47 (2010): 474011.
(128) Patra, Santanu, Ekta Roy, Paramita Karfa, Sunil Kumar, Rashmi Madhuri, and Prashant K. Sharma. "Dual-responsive polymer coated superparamagnetic nanoparticle for targeted drug delivery and hyperthermia treatment." ACS applied materials & interfaces 7, no. 17 (2015): 9235-9246.
(129) Chandekar, Kamlesh V., and K. Mohan Kant. "Effect of size and shape dependent anisotropy on superparamagnetic property of CoFe2O4 nanoparticles and nanoplatelets." Physica B: Condensed Matter 520 (2017): 152-163.
(130) Reyes-Ortega, Felisa, Ángel V. Delgado, and Guillermo R. Iglesias. "Modulation of the magnetic hyperthermia response using different superparamagnetic iron oxide nanoparticle morphologies." Nanomaterials 11, no. 3 (2021): 627.
(131) Li, Shichuan, Tonglai Zhang, Runze Tang, Hao Qiu, Caiqin Wang, and Zunning Zhou. "Solvothermal synthesis and characterization of monodisperse superparamagnetic iron oxide nanoparticles." Journal of Magnetism and Magnetic Materials 379 (2015): 226-231.
(132) Li, Shichuan, Tonglai Zhang, Runze Tang, Hao Qiu, Caiqin Wang, and Zunning Zhou. "Solvothermal synthesis and characterization of monodisperse superparamagnetic iron oxide nanoparticles." Journal of Magnetism and Magnetic Materials 379 (2015): 226-231.
(133) Hou, Yanglong, Junfeng Yu, and Song Gao. "Solvothermal reduction synthesis and characterization of superparamagnetic magnetite nanoparticles." Journal of Materials Chemistry 13, no. 8 (2003): 1983-1987.
(134) Xuan, Shouhu, Yi-Xiang J. Wang, Jimmy C. Yu, and Ken Cham-Fai Leung. "Tuning the grain size and particle size of superparamagnetic Fe3O4 microparticles." Chemistry of Materials 21, no. 21 (2009): 5079-5087.
(135) Pereira, Clara, André M. Pereira, Carlos Fernandes, Mariana Rocha, Ricardo Mendes, María Paz Fernández-García, Alexandra Guedes et al. "Superparamagnetic MFe2O4 (M= Fe, Co, Mn)

nanoparticles: tuning the particle size and magnetic properties through a novel one-step coprecipitation route." Chemistry of Materials 24, no. 8 (2012): 1496-1504.

(136) Dheyab, Mohammed Ali, Azlan Abdul Aziz, Mahmood S. Jameel, Osama Abu Noqta, Pegah Moradi Khaniabadi, and Baharak Mehrdel. "Simple rapid stabilization method through citric acid modification for magnetite nanoparticles." Scientific reports 10, no. 1 (2020): 10793.

(137) Patsula, Vitalii, Lucie Kosinová, Marija Lovrić, Lejla Ferhatovic Hamzić, Mariia Rabyk, Rafal Konefal, Aleksandra Paruzel et al. "Superparamagnetic Fe3O4 nanoparticles: synthesis by thermal decomposition of iron (III) glucuronate and application in magnetic resonance imaging." ACS applied materials & interfaces 8, no. 11 (2016): 7238-7247.

(138) Gao, Ruo-Rui, Yue Zhang, Wei Yu, Rui Xiong, and Jing Shi. "Superparamagnetism and spin-glass like state for the MnFe2O4 nano-particles synthesized by the thermal decomposition method." Journal of magnetism and magnetic materials 324, no. 16 (2012): 2534-2538.

(139) Zahraei, Maryam, Ahmad Monshi, Maria del Puerto Morales, Daryoush Shahbazi-Gahrouei, Mehdi Amirnasr, and Behshid Behdadfar. "Hydrothermal synthesis of fine stabilized superparamagnetic nanoparticles of Zn2+ substituted manganese ferrite." Journal of magnetism and magnetic materials 393 (2015): 429-436.

(140) Salvador, María, Gemma Gutiérrez, Sara Noriega, Amanda Moyano, María Carmen Blanco-López, and María Matos. "Microemulsion synthesis of superparamagnetic nanoparticles for bioapplications." International Journal of Molecular Sciences 22, no. 1 (2021): 427.

(141) Ding, J., W. F. Miao, P. G. McCormick, and Robert Street. "Mechanochemical synthesis of ultrafine Fe powder." Applied Physics Letters 67, no. 25 (1995): 3804-3806.

(142) Becker, J. A., R. Schäfer, R. Festag, W. Ruland, J. H. Wendorff, J. Pebler, S. A. Quaiser, W. Helbig, and M. T. Reetz. "Electrochemical growth of superparamagnetic cobalt clusters." The Journal of chemical physics 103, no. 7 (1995): 2520-2527.

(143) de Sousa, M. Elisa, Marcela B. Fernandez van Raap, Patricia C. Rivas, Pedro Mendoza Zélis, Pablo Girardin, Gustavo A. Pasquevich, Jose L. Alessandrini, Diego Muraca, and Francisco H. Sánchez. "Stability and relaxation mechanisms of citric acid coated magnetite nanoparticles for magnetic hyperthermia." The Journal of Physical Chemistry C 117, no. 10 (2013): 5436-5445.

(144) Khan, Sidra, Zaheer H. Shah, Saira Riaz, Naveed Ahmad, Shumaila Islam, M. Akram Raza, and Shahzad Naseem. "Antimicrobial activity of citric acid functionalized iron oxide nanoparticles–Superparamagnetic effect." Ceramics International 46, no. 8 (2020): 10942-10951.

(145) Noqta, Osama Abu, Bashiru Kayode Sodipo, and Azlan Abdul Aziz. "One-pot synthesis of highly magnetic and stable citrate coated superparamagnetic iron oxide nanoparticles by modified coprecipitation method." Functional Composites and Structures 2, no. 4 (2020): 045005.

(146) Kotsmar, Csaba, Ki Youl Yoon, Haiyang Yu, Seung Yup Ryoo, Joseph Barth, Stephen Shao, Masa Prodanovic et al. "Stable citrate-coated iron oxide superparamagnetic nanoclusters at high salinity." Industrial & engineering chemistry research 49, no. 24 (2010): 12435-12443.

(147) Park, Yoonjee, Ragnhild D. Whitaker, Rikkert J. Nap, Jeffrey L. Paulsen, Vidhya Mathiyazhagan, Linda H. Doerrer, Yi-Qiao Song, Martin D. Hürlimann, Igal Szleifer, and Joyce Y. Wong. "Stability of superparamagnetic iron oxide nanoparticles at different pH values: experimental and theoretical analysis." Langmuir 28, no. 15 (2012): 6246-6255.

(148) Kumar, P., S. Agnihotri, and I. Roy. "Synthesis of dox drug conjugation and citric acid stabilized superparamagnetic iron-oxide nanoparticles for drug delivery." Biochem. Physiol 5, no. 2 (2016).
(149) Oncsik, Tamas, Gregor Trefalt, Michal Borkovec, and Istvan Szilagyi. "Specific ion effects on particle aggregation induced by monovalent salts within the Hofmeister series." Langmuir 31, no. 13 (2015): 3799-3807.
(150) Szilagyi, Istvan, Tamas Szabo, Anthony Desert, Gregor Trefalt, Tamas Oncsik, and Michal Borkovec. "Particle aggregation mechanisms in ionic liquids." Physical Chemistry Chemical Physics 16, no. 20 (2014): 9515-9524.
(151) Kobayashi, Motoyoshi, Frédéric Juillerat, Paolo Galletto, Paul Bowen, and Michal Borkovec. "Aggregation and charging of colloidal silica particles: effect of particle size." Langmuir 21, no. 13 (2005): 5761-5769.
(152) Trefalt, Gregor, Istvan Szilagyi, Tamas Oncsik, Amin Sadeghpour, and Michal Borkovec. "Probing colloidal particle aggregation by light scattering." Chimia 67, no. 11 (2013): 772-772.
(153) Bouyer, Frederic, Andrea Robben, Wei Li Yu, and Michal Borkovec. "Aggregation of colloidal particles in the presence of oppositely charged polyelectrolytes: effect of surface charge heterogeneities." Langmuir 17, no. 17 (2001): 5225-5231.
(154) Zhang, Yanpu, Erol Yildirim, Hanne S. Antila, Luis D. Valenzuela, Maria Sammalkorpi, and Jodie L. Lutkenhaus. "The influence of ionic strength and mixing ratio on the colloidal stability of PDAC/PSS polyelectrolyte complexes." Soft Matter 11, no. 37 (2015): 7392-7401.
(155) Hotze, Ernest M., Tanapon Phenrat, and Gregory V. Lowry. "Nanoparticle aggregation: challenges to understanding transport and reactivity in the environment." Journal of environmental quality 39, no. 6 (2010): 1909-1924.
(156) Shrestha, Sweta, Bo Wang, and Prabir Dutta. "Nanoparticle processing: Understanding and controlling aggregation." Advances in colloid and interface science 279 (2020): 102162.
(157) Kim, Taehoon, Kangtaek Lee, Myoung-seon Gong, and Sang-Woo Joo. "Control of gold nanoparticle aggregates by manipulation of interparticle interaction." Langmuir 21, no. 21 (2005): 9524-9528.
(158) Fresnais, Jérôme, Christophe Lavelle, and J-F. Berret. "Nanoparticle aggregation controlled by desalting kinetics." The Journal of Physical Chemistry C 113, no. 37 (2009): 16371-16379.
(159) Park, Yoonjee C., Jared B. Smith, Tuan Pham, Ragnhild D. Whitaker, Christopher A. Sucato, James A. Hamilton, Elizabeth Bartolak-Suki, and Joyce Y. Wong. "Effect of PEG molecular weight on stability, T2 contrast, cytotoxicity, and cellular uptake of superparamagnetic iron oxide nanoparticles (SPIONs)." Colloids and surfaces B: Biointerfaces 119 (2014): 106-114.
(160) Mohammadi, M. Rezaa, Andrey V. Malkovskiy, Preetha Jothimuthu, Kwang-Min Kim, Mansi Parekh, Mohammed Inayathullah, Yan Zhuge, and Jayakumar Rajadas. "PEG/dextran double layer influences Fe ion release and colloidal stability of iron oxide nanoparticles." Scientific reports 8, no. 1 (2018): 4286.
(161) Viali, Wesley Renato, Eloiza da Silva Nunes, Caio Carvalho Dos Santos, Sebastião William Da Silva, Fermin Herrera Aragón, José Antonio Huamaní Coaquira, Paulo César Morais, and Miguel Jafelicci. "PEGylation of SPIONs by polycondensation reactions: a new strategy to

improve colloidal stability in biological media." Journal of nanoparticle research 15 (2013): 1-14.

(162) Cano, Manuel, Rebeca Núñez-Lozano, Rocío Lumbreras, Verena González-Rodríguez, Alberto Delgado-García, José Manuel Jiménez-Hoyuela, and Guillermo de la Cueva-Méndez. "Partial PEGylation of superparamagnetic iron oxide nanoparticles thinly coated with amine-silane as a source of ultrastable tunable nanosystems for biomedical applications." Nanoscale 9, no. 2 (2017): 812-822.

(163) Steitz, Benedikt, Heinrich Hofmann, Sarah W. Kamau, Paul O. Hassa, Michael O. Hottiger, Brigitte von Rechenberg, Magarethe Hofmann-Amtenbrink, and Alke Petri-Fink. "Characterization of PEI-coated superparamagnetic iron oxide nanoparticles for transfection: Size distribution, colloidal properties, and DNA interaction." Journal of Magnetism and Magnetic Materials 311, no. 1 (2007): 300-305.

(164) Petri-Fink, Alke, Benedikt Steitz, Andrija Finka, Jatuporn Salaklang, and Heinrich Hofmann. "Effect of cell media on polymer-coated superparamagnetic iron oxide nanoparticles (SPIONs): colloidal stability, cytotoxicity, and cellular uptake studies." European journal of pharmaceutics and biopharmaceutics 68, no. 1 (2008): 129-137.

(165) Unterweger, Harald, László Dézsi, Jasmin Matuszak, Christina Janko, Marina Poettler, Jutta Jordan, Tobias Bäuerle et al. "Dextran-coated superparamagnetic iron oxide nanoparticles for magnetic resonance imaging: Evaluation of size-dependent imaging properties, storage stability and safety." International journal of nanomedicine (2018): 1899-1915.

(166) Schemberg, Jörg, Abdelouahad El Abbassi, Annerose Lindenbauer, Li-Yu Chen, Andreas Grodrian, Xenia Nakos, Gurunath Apte et al. "Synthesis of biocompatible superparamagnetic iron oxide nanoparticles (SPION) under different microfluidic regimes." ACS Applied Materials & Interfaces 14, no. 42 (2022): 48011-48028.

(167) Dolgovskiy, Vladimir, Victor Lebedev, Simone Colombo, Antoine Weis, Benjamin Michen, Liliane Ackermann-Hirschi, and Alke Petri-Fink. "A quantitative study of particle size effects in the magnetorelaxometry of magnetic nanoparticles using atomic magnetometry." Journal of Magnetism and Magnetic Materials 379 (2015): 137-150.

(168) Eberbeck, Dietmar, Christian Bergemann, Frank Wiekhorst, Uwe Steinhoff, and Lutz Trahms. "Quantification of specific bindings of biomolecules by magnetorelaxometry." Journal of nanobiotechnology 6 (2008): 1-12.

(169) Eberbeck, Dietmar, Andrea Prieto Astalan, Karolina Petersson, Frank Wiekhorst, Christian Bergemann, Christer Johansson, Uwe Steinhoff, Heike Richter, Anatol Krozer, and L. Trahms. "AC susceptometry and magnetorelaxometry for magnetic nanoparticle based biomolecule detection." In 4th European Conference of the International Federation for Medical and Biological Engineering: ECIFMBE 2008 23–27 November 2008 Antwerp, Belgium, pp. 2317-2321. Springer Berlin Heidelberg, 2009.

(170) Sayad, Abkar, Efstratios Skafidas, and Patrick Kwan. "Magneto-impedance biosensor sensitivity: Effect and enhancement." Sensors 20, no. 18 (2020): 5213.

(171) Sun, Yi, Zhongzhou Du, Haochen Zhang, Haozhe Wang, Teruyoshi Sasayama, and Takashi Yoshida. "Simultaneous estimation of magnetic moment and Brownian relaxation time

distributions of magnetic nanoparticles based on magnetic particle spectroscopy for biosensing application." Nanoscale 15, no. 39 (2023): 16089-16102.

(172) Østerberg, Frederik Westergaard, Giovanni Rizzi, and Mikkel Fougt Hansen. "On-chip Brownian relaxation measurements of magnetic nanobeads in the time domain." Journal of Applied Physics 113, no. 23 (2013).

(173) Schrittwieser, Stefan, Frank Ludwig, Jan Dieckhoff, Katerina Soulantica, Guillaume Viau, Lise-Marie Lacroix, Sergio Mozo Lentijo et al. "Modeling and development of a biosensor based on optical relaxation measurements of hybrid nanoparticles." ACS nano 6, no. 1 (2012): 791-801.

(174) Park, Kyoungchul, Tim Harrah, Edward B. Goldberg, Robert P. Guertin, and Sameer Sonkusale. "Multiplexed sensing based on Brownian relaxation of magnetic nanoparticles using a compact AC susceptometer." Nanotechnology 22, no. 8 (2011): 085501.

(175) Yoshida, T., N. B. Othman, T. Tsubaki, J. Takamiya, and K. Enpuku. "Evaluation of harmonic signals for the detection of magnetic nanoparticles." IEEE transactions on magnetics 48, no. 11 (2012): 3788-3791.

(176) Hata, Y.; Sawada, T.; Serizawa, T. Macromolecular Crowding for Materials-Directed Controlled Self-Assembly. Journal of Materials Chemistry B 2018, 6, 6344–6359..

(177) Liu, J.; Dai, C.; Hu, Y. Aqueous Aggregation Behavior of Citric Acid Coated Magnetite Nanoparticles: Effects of Ph, Cations, Anions, and Humic Acid. *Environmental Research* **2018**, *161*, 49–60.

(178) Nikitin, Petr I., Petr M. Vetoshko, and Tatiana I. Ksenevich. "New type of biosensor based on magnetic nanoparticle detection." Journal of Magnetism and Magnetic Materials 311, no. 1 (2007): 445-449.

(179) Topping, C. V.; Blundell, S. J. A.C. Susceptibility as a Probe of Low-Frequency Magnetic Dynamics. Journal of Physics: Condensed Matter 2018, 31, 013001.

(180) Debye, P. Polar Molecules; Dover Publications: New York, 1929. R.P. Feynman, “There’s Plenty of Room at the Bottom,” Eng Sci. 1960;23(5):22-36.

(181) Ota, S.; Takemura, Y. Characterization of Néel and Brownian Relaxations Isolated from Complex Dynamics Influenced by Dipole Interactions in Magnetic Nanoparticles. The Journal of Physical Chemistry C 2019, 123, 28859–28866.

(182) Cole, K. S.; Cole, R. H. Dispersion and Absorption in Dielectrics I. Alternating Current Characteristics. The Journal of Chemical Physics 1941, 9, 341–351.

(183) Davidson, D. W.; Cole, R. H. Dielectric Relaxation in Glycerol, Propylene Glycol, and n-Propanol. The Journal of Chemical Physics 1951, 19, 1484–1490.

(184) Havriliak, S.; Negami, S. A Complex Plane Representation of Dielectric and Mechanical Relaxation Processes in Some Polymers. Polymer 1967, 8, 161–210.

(185) Grosse, C. A Program for the Fitting of Debye, Cole–Cole, Cole–Davidson, and Havriliak–Negami Dispersions to Dielectric Data. Journal of Colloid and Interface Science 2014, 419, 102–106.

(186) Garton, C. G. The Distribution of Relaxation Times in Dielectrics. Transactions of the Faraday Society 1946, 42.

(187) Dierickx, S.; Weber, A.; Ivers-Tiffée, E. How the Distribution of Relaxation Times Enhances Complex Equivalent Circuit Models for Fuel Cells. Electrochimica Acta 2020, 355, 136764.

(188) Reta, D.; Chilton, N. F. Uncertainty Estimates for Magnetic Relaxation Times and Magnetic Relaxation Parameters. Physical Chemistry Chemical Physics 2019, 21, 23567–23575.

(189) Iglesias, T. P.; Vilão, G.; Reis, J. C. An Approach to the Interpretation of Cole–Davidson and

Cole–Cole Dielectric Functions. Journal of Applied Physics 2017, 122.
(190) Chen, Y. Study on Analysis of Frequency Spectrum in Alternating Current Magnetization of Magnetic Nanoparticles for Magnetic Biosensing. dissertation, Department of Materials Science and Engineering School of Materials and Chemical Technology Tokyo Institute of Technology: Tokyo, 2023, pp. 1–121.
(191) Abu-Bakr, A. F.; Zubarev, A. Yu. On the Theory of Magnetic Hyperthermia: Clusterization of Nanoparticles. *Philosophical Transactions of the Royal Society A: Mathematical, Physical and Engineering Sciences* **2020**, *378* (2171), 20190251. DOI:10.1098/rsta.2019.0251.
(192) Dutz, S.; Mueller, R.; Zeisberger, M. Larger Single Domain Iron Oxide Nanoparticles for Magnetic Particle Imaging. *Magnetic Nanoparticles* **2010**. DOI:10.1142/9789814324687_0005.
(193) Kim, J.; Wang, J.; Kim, H.; Bae, S. Concentration-Dependent Oscillation of Specific Loss Power in Magnetic Nanofluid Hyperthermia. *Scientific Reports* **2021**, *11* (1). DOI:10.1038/s41598-020-79871-1.
(194) Li, Y.; Wang, T. X. The Role of Dipolar Interactions for the Magnetic Properties of Ferromagnetic Nanoring. *Journal of Magnetism and Magnetic Materials* **2010**, *322* (18), 2773–2776. DOI:10.1016/j.jmmm.2010.04.025.
(195) Mamiya, H. Recent Advances in Understanding Magnetic Nanoparticles in AC Magnetic Fields and Optimal Design for Targeted Hyperthermia. *Journal of Nanomaterials* **2013**, *2013*, 1–17. DOI:10.1155/2013/752973.
(196) Ota, S.; Takemura, Y. Characterization of Néel and Brownian Relaxations Isolated from Complex Dynamics Influenced by Dipole Interactions in Magnetic Nanoparticles. *The Journal of Physical Chemistry C* **2019**, *123* (47), 28859–28866. DOI:10.1021/acs.jpcc.9b06790.
(197) Urtizberea, A.; Natividad, E.; Arizaga, A.; Castro, M.; Mediano, A. Specific Absorption Rates and Magnetic Properties of Ferrofluids with Interaction Effects at Low Concentrations. *The Journal of Physical Chemistry C* **2010**, *114* (11), 4916–4922. DOI:10.1021/jp912076f.
(198) Xu, C.; Ma, Y. Q.; Hui, P. M. Equilibrium Magnetic Moment Configurations in Magnetic Nanoparticle Films: Effects of Anisotropy, Dipolar Interaction, and Zeeman Energy. *Journal of Applied Physics* **2005**, *98* (8). DOI:10.1063/1.2103413.
(199) Ovejero, J. G.; Cabrera, D.; Carrey, J.; Valdivielso, T.; Salas, G.; Teran, F. J. Effects of Inter- and Intra-Aggregate Magnetic Dipolar Interactions on the Magnetic Heating Efficiency of Iron Oxide Nanoparticles. *Physical Chemistry Chemical Physics* **2016**, *18* (16), 10954–10963. DOI:10.1039/c6cp00468g.
(200) Serantes, D.; Baldomir, D.; Martinez-Boubeta, C.; Simeonidis, K.; Angelakeris, M.; Natividad, E.; Castro, M.; Mediano, A.; Chen, D.-X.; Sanchez, A.; Balcells, LI.; Martínez, B. Influence of Dipolar Interactions on Hyperthermia Properties of Ferromagnetic Particles. *Journal of Applied Physics* **2010**, *108* (7). DOI:10.1063/1.3488881.
(201) Morozov, K. I.; Pshenichnikov, A. F.; Raikher, Yu. L.; Shliomis, M. I. Magnetic Properties of Ferrocolloids: The Effect of Interparticle Interactions. *Journal of Magnetism and Magnetic Materials* **1987**, *65* (2–3), 269–272. DOI:10.1016/0304-8853(87)90048-5.
(202) Chen, Y.; Okubo, K.; Slavakis, K.; Kitamoto, Y. Estimation of Biomolecule Amount by Analyzing Magnetic Nanoparticle Cluster Distributions from Alternating Current Magnetization Spectra for Magnetic Biosensing. Journal of Magnetism and Magnetic Materials 2023, 588, 171387. https://doi.org/10.1016/j.jmmm.2023.171387.
(203) Trisnanto, S. B.; Yasuda, K.; Kitamoto, Y. Dipolar Magnetism and Electrostatic Repulsion of Colloidal Interacting Nanoparticle System. Japanese Journal of Applied Physics 2018, 57. https://doi.org/10.7567/JJAP.57.02CC06.
(204) Trisnanto, S. B.; Kitamoto, Y. Field-Dependent Brownian Relaxation Dynamics of a Superparamagnetic Clustered-Particle Suspension. Physical Review E 2014, 90.

https://doi.org/10.1103/PhysRevE.90.032306.

Chapter 2 – Effect of Ionic Strength on the Dynamic Behavior of Citric Acid-Coated Superparamagnetic Iron Oxide Nanoparticles (CA SPIONs)

Abstract

This chapter explores the optimal working conditions for citric acid-coated superparamagnetic iron oxide nanoparticles (CA SPIONs) in various ionic environments. CA SPIONs was synthesized and subsequently exposed to NaCl and KCl to assess how different ionic strengths influence their dynamic behavior. The study delves into the magnetization dynamics and hydrodynamic size changes of CA SPIONs under varying sodium and potassium ion concentrations, employing advanced techniques such as Dynamic Light Scattering (DLS) and Dynamic Magnetic Susceptibility (DMS) measurements. Key findings reveal that a broadening effect in the DMS spectra occurs at lower ionic concentrations, while higher concentrations of sodium and potassium ions result in a notable peak shift. In contrast, 1× phosphate-buffered saline (PBS) solutions—comprising 137 mM NaCl, 2.7 mM KCl, 10 mM Na2HPO4, and 1.8 mM KH2PO4—consistently induced a broadening effect without peak shifts. Despite the ion concentrations in PBS comparable to those in the NaCl and KCl cases, the absence of peak shifts suggests that phosphate co-ions may mitigate the interactions between CA SPIONs and counter ions. The relative influence on DMS was observed in the order of K > Na > PBS. These results highlight the complex interplay between ionic strength, electrostatic interactions, and colloidal stability, providing valuable insights for the tailored application of SPIONs in biomedical and biosensing technologies.

2.1. Introduction

Iron oxide nanoparticles (IONPs) are pivotal in numerous applications, particularly biomedicine [1-3]. However, their stability in biofluidic solutions remains a significant challenge. Aggregation is expected, which can compromise their performance and functionality [4-6]. Surface modification strategies are

crucial to mitigate this issue and harness the full potential of IONPs. These approaches enhance the stability of IONPs in complex biological environments.

The stability of IONPs, a crucial aspect of their application in biofluidic solutions, can be significantly enhanced through surface modification, which often involves using inert polymers as coating agents[7-9]. These agents, by imparting electrostatic repulsion forces, play a pivotal role in preventing particle aggregation, aligning with the fundamental principles of the Derjaguin-Landau-Verwey-Overbeek (DLVO) theory. In an ideal scenario, these repulsive forces would maintain the separation of nanoparticles in a stable dispersion. However, the reality of biofluidic solutions introduces additional challenges. Counter ions in the solution, such as sodium, potassium, or proteins, can effectively screen the charged particle surface, reducing the electric double layer thickness and promoting particle aggregation [10-12].

To overcome these challenges, inert polymers are often employed as coating agents for IONPs due to their chemical neutrality and minimal reactivity. These polymers provide a stable coating on the particle surface, offering a promising solution to the stability issue. The stability they offer arises from the combination of electrostatic and steric effects. Electrostatically, the electric double layer thickness is preserved due to the chemical neutrality of the polymer, thereby preventing aggregation. Steric effects result from the bulky and neutral nature of the polymer, which hinders close approach and contact between nanoparticles [13,14].

Inert polymers come in various forms, and examples include polyethylene glycol (PEG) [15-17], polyvinyl alcohol (PVA) [18,19], and poloxamers [20]. These polymers are known for their biocompatibility and exceptional stability in biological environments. The stability they confer results from their inert nature, preventing unwanted interactions with the complex biofluidic milieu.

Inert polymers are known to enhance the stability of IONPs significantly. However, ongoing research is exploring alternative methods to improve nanoparticle stability further. This study focuses on finding

the most stable environment for SPIONs coated with non-inert polymers in a biofluidic system. I coated our nanoparticles with citric acid and mixed them with salts and a buffer solution. Our experiments showed that CA SPIONs maintained good stability even in high concentrations of sodium, potassium, and phosphate-buffered saline (PBS).

Our study explores the complex field of nanoparticle stability in biofluidic solutions, providing new insights into stability enhancement using non-inert polymers. Understanding the stability dynamics of nanoparticles is crucial, especially for biomedical applications. This research enhances our knowledge of these fundamental concepts and contributes to developing nanoparticle-based systems in various fields. I mixed CA IONPs with sodium, potassium, or phosphate saline buffer (PBS) to demonstrate the inhomogeneous neutralization process. The choice of PBS was due to its close resemblance to biofluidic solutions, making our experimental setup more relevant to real-world conditions. To understand this process better, I thoroughly characterized the nanoparticles in PBS solutions using techniques such as dynamic light scattering (DLS), zeta potential (ZP) analysis, and magnetic susceptibility measurements.

2.2. Materials and Methods

2.2.1. Synthesis and characterization of SPIONs modified with citric acid

The synthesis of bare SPIONs was conducted utilizing a solvothermal approach. Initially, a precursor solution was prepared by dissolving 1.4 gram of iron (III) acetylacetonate (14024-18-1, Sigma-Aldrich, USA) in 40 mL of tetraethylene glycol (112-60-7, Sigma-Aldrich, USA). This solution was heated to 343 K to ensure complete dissolution of the precursor. The solution was then transferred into four 10 mL stainless steel pressure vessels. These vessels were then sealed and placed in an electric furnace, where they were subjected to a temperature of 523 K for 15 hours, facilitating the solvothermal reaction. The synthesized SPIONs were subjected to a series of washing steps after the completion of the reaction process. Initially, the SPIONs were washed with acetone to remove any residual solvent, followed by centrifugation to collect the nanoparticles. This process was repeated three times, alternating between

deionized (DI) water and ethanol to ensure thorough cleaning. Finally, the bare SPIONs were redispersed in 20 mL of DI water, preparing them for further process.

The synthesized SPIONs were dispersed in an aqueous solution containing 2 grams of trisodium citrate (197-06025, Wako Chemicals, Japan) in 120 mL of deionized (DI) water. This was achieved using an ultrasonic homogenizer at 343 K to modify the surface with citric acid molecules. After surface modification, the SPIONs were washed three times with 1 mL of DI water and 3 mL of ethanol, then dispersed in 5 mL of DI water. To adjust the cluster sizes of SPIONs, the incubation time was varied, and the inter-cluster interactions were managed by carefully adding salts. Introducing the correct concentration of salts caused the SPIONs and their clusters to aggregate by reducing the electric double-layer thickness, forming larger clusters that significantly affect their magnetic and physical properties. However, it is crucial to control the salt concentration precisely, as excessive amounts can lead to undesirable precipitation of SPIONs, making them unsuitable for further applications. To meticulously control this aspect, the ionic concentration of the suspension (sodium and potassium) was systematically varied for evaluation. I mixed 80 μL of CA SPIONs with 20 μL of ionic solutions at concentrations ranging from 0 mM to 250 mM. The final concentrations of the specimens were 50 mM, 25 mM, 5 mM, 2.5 mM, and 0 mM. In addition to salt concentration, I added a buffer solution in the latter part of this chapter to make our system more complex. In this case, I mixed SPIONs with phosphate-buffered saline (PBS) containing sodium, phosphate buffer, and potassium. The presence of potassium ions was neglected due to their minimal concentration in the PBS solution. The final sodium and phosphate ions concentrations in the specimens were around 50 mM, 25 mM, 5 mM, 2.5 mM, and 0 mM.

The primary and hydrodynamic sizes of the nanoparticles were determined using transmission electron microscopy (TEM, H-8100, Hitachi High-Tech Corporation, Japan) and dynamic light scattering measurements (DLS, SZ-100-V2, HORIBA, Japan), respectively. The frequency dependence of the AC magnetization in the range of 10–10,000 Hz was analyzed using a physical property

measurement system (PPMS; Quantum Design Corp., USA) at a magnetic field strength of 0.8 kA/m at 300 K. The SPIONs concentration and volume of specimens for PPMS measurements were 3.5 mg/mL and 100 µL, respectively.

2.3. Results

2.3.1. Dependence of sodium ion's concentration on the dynamic behavior of CA SPIONs.

Figure 2.1 illustrates (a) the DMS signal of SPIONs under varying concentrations of sodium ions and (b) the hydrodynamic diameter of SPIONs from DLS measurements under similar conditions. The DMS signal reveals that the dynamic magnetization of SPIONs changes in two distinct stages. Initially, the DMS signal broadens at lower sodium ion concentrations while maintaining a constant peak frequency, as the black arrow indicates. I refer to this phenomenon as the broadening effect. Subsequently, a noticeable peak shift is observed in the DMS signal at higher sodium ion concentrations (50 mM, highlighted with a red circle).

The DLS measurements show a gradual increase in the hydrodynamic diameter of SPIONs when mixed with sodium ions. The nanoparticle's hydrodynamic size is insensitive because sodium ions are added up to a sodium concentration of 37.5 mM, where the hydrodynamic diameter grows from 30 nm in water to 45 nm. However, as the red graph indicates, the hydrodynamic diameter significantly increases at 50 mM sodium concentration to 80 nm.

By correlating the DMS signal with the DLS results, I can infer that the broadening effect is noticeable when the particle hydrodynamic size increases slightly under the influence of sodium ions. However, significant aggregation of SPIONs, evidenced by a substantial increase in hydrodynamic size, leads to a peak shift in the DMS signal. This correlation highlights the importance of broadening and peak shift phenomena in understanding the behavior of SPIONs in varying ionic environments.

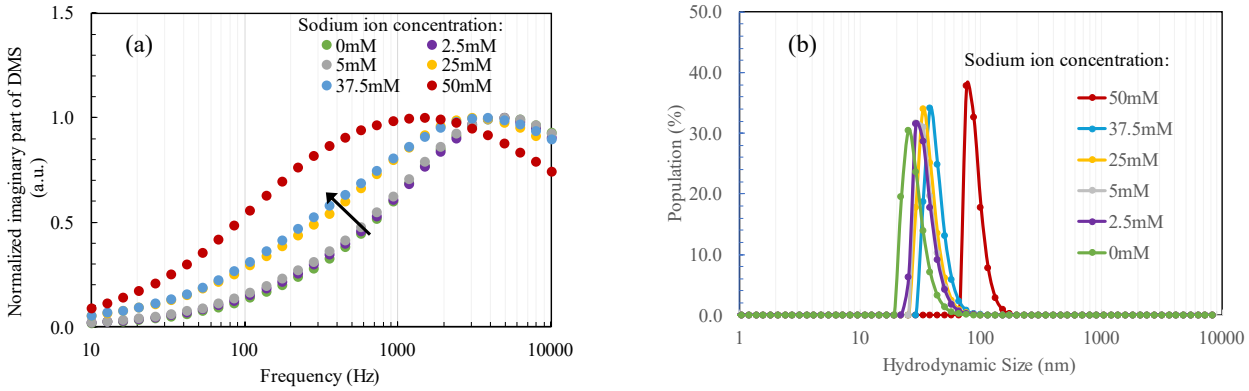

Figure 2.1. Analysis of SPION behavior under varying sodium ion concentrations. (a) DMS signal of SPIONs demonstrating broadening and peak shift phenomena at different sodium ion concentrations. (b) The hydrodynamic diameter of SPIONs measured by DLS illustrates changes in particle size with increasing sodium ion concentration.

2.3.2. Dependence of potassium ion's concentration on the dynamic behavior of CA SPIONs

Figure 2.2 presents (a) the DMS signal of SPIONs under the influence of different concentrations of potassium ions and (b) the hydrodynamic diameter of SPIONs from DLS measurements under the influence of varying concentrations of potassium ions. Our observations indicate that the DMS signal reveals the dynamic magnetization of SPIONs changes in two distinct steps. Initially, when the potassium ion concentration is relatively low, the DMS signal broadens while maintaining its peak frequency, as indicated by the black-colored arrow. I refer to this phenomenon as the broadening effect. Subsequently, a peak shift in the DMS signal is observed at higher potassium ion concentrations. Interestingly, while the peak shift in Figure 2.1(a) was noted at 50 mM for sodium ions, the peak shift for potassium ions occurs earlier, at 37.5 mM.

The hydrodynamic diameter observations from DLS measurements reveal that the particle size increases slightly with the addition of potassium ions. This trend continues until the potassium concentration reaches 37.5 mM, where the particle size increases from 30 nm in water to 50 nm at 37.5 mM. However, at 50 mM potassium concentration, the particle hydrodynamic diameter significantly increases to 100 nm, as shown by the red-colored graph.

To understand the differences between the effects of potassium ions and sodium ions on the DMS signal and DLS results, I must consider the ionic strength and its impact on the screening effect and particle stability. Potassium ions exhibit a higher ionic strength than sodium ions, significantly influencing the SPION system's electrostatic interactions. Ionic strength, a measure of the concentration of ions in solution, affects the double-layer thickness around the nanoparticles.

In solutions with higher ionic strength, the diffuse layer around the nanoparticles becomes thinner due to the increased presence of counterions that neutralize the surface charges more effectively. This reduction in the diffuse layer weakens the repulsive forces between particles, promoting closer interactions and potential aggregation. Consequently, as potassium ions are added, the stronger ionic strength leads to a more pronounced screening effect, causing the SPIONs to aggregate more readily at lower concentrations than sodium ions.

This aggregation is reflected in the DMS signal broadening at lower concentrations and the earlier onset of peak shifts. The hydrodynamic diameter's substantial increase at 50 mM potassium concentration further supports the notion that stronger ionic strength in potassium ions results in significant aggregation and larger cluster formation. Thus, the interplay between ionic strength and screening effects is crucial in determining the stability and dynamic behavior of SPIONs in different ionic environments. This understanding is essential for tailoring SPION applications in biomedical and biosensing technologies, where specific ionic conditions can dramatically impact performance and reliability.

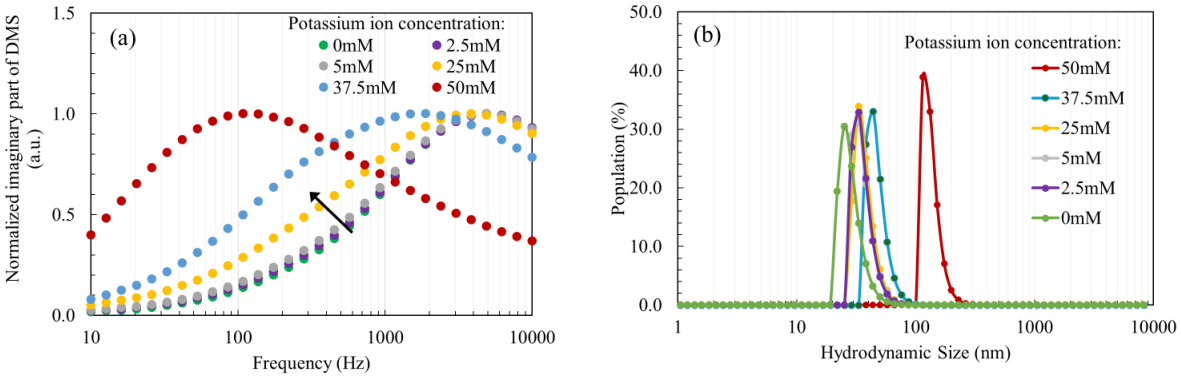

Figure 2.2. Analysis of SPION behavior under varying potassium ion concentrations. (a) DMS signal of SPIONs demonstrating broadening and peak shift phenomena at different potassium ion concentrations. (b) The hydrodynamic diameter of SPIONs measured by DLS illustrates changes in particle size with increasing potassium ion concentration.

2.3.3. Dependence PBS concentration on the dynamic behavior of CA SPIONs

As described in the previous section, sodium ions significantly impact nanoparticles, causing a broadening effect at low concentrations and a peak shift at higher concentrations. To understand how buffer solutions influence particle stability, I included a buffer solution in this part of the study. The following table, Table 2.1., lists the final concentrations of sodium and phosphate in various dilutions of PBS solutions: 0x, 0.05x, 0.1x, 0.2x, and 0.4x. For instance, a 0.1x PBS solution contains 15.7 mM sodium and 1.18 mM phosphate. This table allows readers to compare the effects of sodium ions on nanoparticle behavior with and without the buffer solution, providing insight into the mechanisms at play.

Table 2.1. Summary of sodium and phosphate concentration in PBS

PBS Solution	Sodium (mM)	Phosphate (mM)
0x PBS	0	0
0.05x PBS	7.85	0.59
0.1x PBS	15.7	1.18
0.2x PBS	31.4	2.36
0.4x PBS	62.8	4.72

Figure 2.3 illustrates (a) the DMS signal of SPIONs exposed to varying concentrations of PBS solution and (b) the hydrodynamic diameter of SPIONs measured by DLS under the same conditions. Our observations reveal that as the concentration of PBS increases, the DMS signal broadens. However, unlike the peak shifts observed with sodium and potassium ions in previous experiments, no such shifts occur when SPIONs are mixed with PBS solution. For context, a 1x PBS solution contains approximately 137 mM of sodium ions and 2.7 mM of potassium ions, while a 0.4x PBS solution corresponds to about 55 mM sodium and 1.1 mM potassium ions. Despite these ion concentrations being similar to those in earlier cases, the absence of peak shifts in the DMS signal suggests a different underlying mechanism.

The behavior of CA SPIONs in PBS differs significantly from their behavior in simpler ionic solutions, and this discrepancy can be attributed to the complex interactions between SPIONs and the anions present in PBS. In PBS, phosphate ions serve as the primary anions, whereas chloride ions are the dominant anions under the influence of NaCl or KCl. Previous studies [21] have shown that phosphate ions have a higher binding affinity for nanoparticle surfaces than chloride ions, leading to enhanced nanoparticle stability. This difference in anion interaction is crucial in understanding the distinct behaviors observed.

Phosphate ions tend to replace citric acid on the nanoparticle surfaces due to their stronger binding affinity. This ligand exchange increases the surface charge of the nanoparticles, thereby enhancing electrostatic repulsion and preventing aggregation. Additionally, phosphate ions form a dense, compact layer on the nanoparticle surface, contributing to steric stabilization. This physical barrier effectively prevents the nanoparticles from coming into close contact, reducing the likelihood of aggregation.

Consistent with this stabilizing effect, the hydrodynamic diameter measurements from DLS in Figure 2.3 show that the particle size increases only slightly across all PBS concentrations tested. Notably, all SPIONs exhibit a hydrodynamic size of approximately 40 nm, which remains unchanged even at 0.4x PBS concentration. This stability in size supports the conclusion that phosphate ions play a significant

role in maintaining the dispersion and preventing aggregation of SPIONs in PBS, in contrast to the effects observed with chloride ions in simpler buffer solutions.

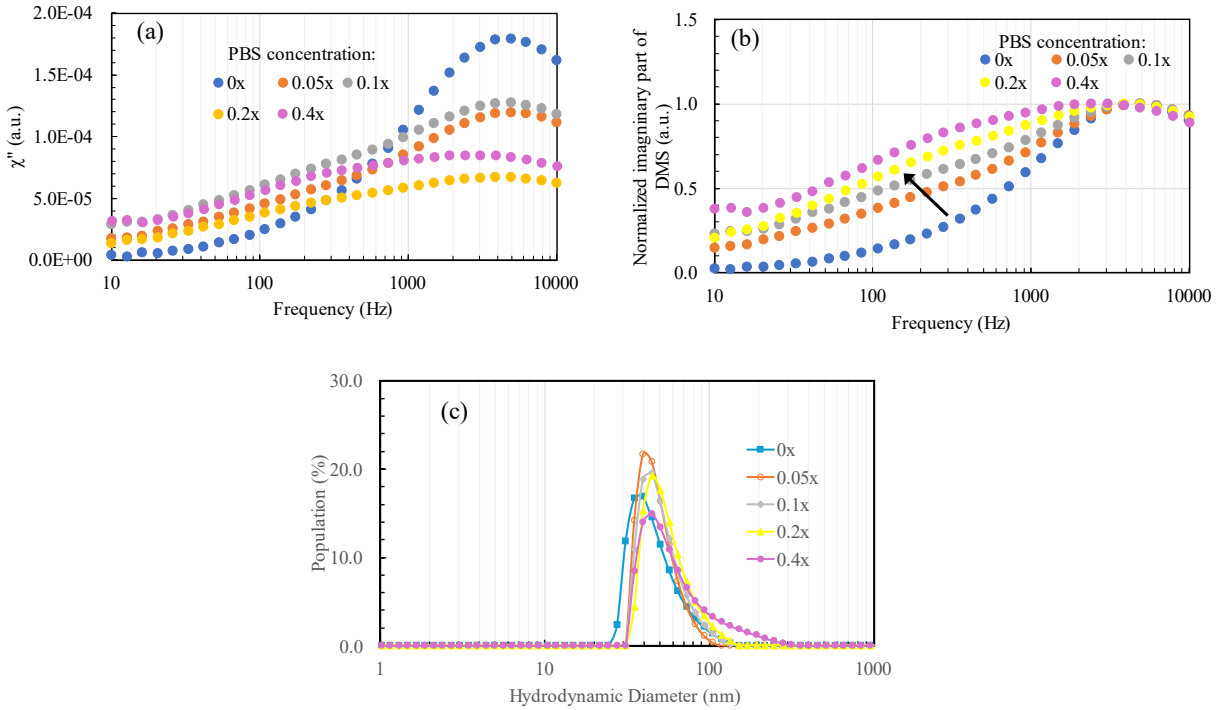

Figure 2.3. Analysis of SPION behavior under varying PBS concentration. (a) DMS signal of SPIONs and (b) normalized imaginary part of DMS signal demonstrating broadening and peak shift phenomena at different PBS concentrations. (c) The hydrodynamic diameter of SPIONs measured by DLS illustrates changes in particle size with increasing PBS concentration.

2.4. Discussion

The critical coagulation concentration (CCC) is a key parameter in colloidal chemistry that defines the minimum concentration of an electrolyte required to induce rapid aggregation of colloidal particles. The CCC can be understood through the lens of the DLVO theory, which explains the stability of colloidal systems by balancing two primary forces: van der Waals attraction and electrostatic repulsion. The total interaction energy $\boldsymbol{V_T(h)}$ between two particles as a function of their separation distance *h* is given by:

$$\boldsymbol{V_T(h) = V_A(h) + V_R(h)}$$

where $\boldsymbol{V_A(h)}$ is the van der Waals attraction and $\boldsymbol{V_R(h)}$ is the electrostatic repulsion. According to DLVO theory, colloidal particles remain stable when the electrostatic repulsion $\boldsymbol{V_R(h)}$ dominates,

preventing particles from coming too close and aggregating. Conversely, when the van der Waals attraction $\boldsymbol{V_A(h)}$ overcomes the repulsion, aggregation occurs, which is typically observed at the CCC.

The CCC, a key parameter in our study, provides a qualitative understanding of nanoparticle dispersity under varying salt concentrations. It serves as a predictive tool, helping us anticipate when and how nanoparticles will transition from a dispersed state to an aggregated state as the salt concentration increases. This knowledge empowers us with a deeper understanding of nanoparticle behavior.

The referenced study on cellulose nanocrystals (CNCs) [22] explored the impact of monovalent salts on nanoparticle stability. As shown in Figure 3 of the study, the stability ratios of CNCs decrease as the concentration of potassium chloride (KCl) increases, leading to aggregation at lower concentrations than sodium chloride (NaCl). This difference is attributed to the stronger ionic strength of potassium ions, which more effectively compresses the electrostatic double layer, reducing repulsive forces between CNC particles and causing them to aggregate at lower potassium ion concentrations. The experimental results demonstrated that the CCC for potassium ions was lower than that for sodium ions, highlighting the stronger destabilizing effect of potassium ions.

Additionally, the study examined the effect of divalent salts on nanoparticle aggregation. Figure 5 illustrates that divalent salts, such as calcium chloride ($CaCl_2$) and magnesium chloride ($MgCl_2$), cause nanoparticles to aggregate at much lower concentrations (around 10 mM) compared to monovalent salts, which typically require concentrations near 100 mM for similar effects. The stronger effect of divalent salts can be explained by their higher valence, which enhances the van der Waals attraction and reduces the electrostatic repulsion more effectively than monovalent salts. This behavior is consistent with the predictions of the DLVO theory, where the balance between van der Waals forces and electrostatic repulsion shifts towards attraction at lower electrolyte concentrations for higher valence ions.

Additionally, the study examined the effect of divalent salts on nanoparticle aggregation. Figure 5 illustrates those divalent salts, such as calcium chloride (CaCl2) and magnesium chloride (MgCl2), cause

nanoparticles to aggregate at much lower concentrations (around 10 mM) compared to monovalent salts, which typically require concentrations near 100 mM for similar effects. The stronger effect of divalent salts can be explained by their higher valence, which enhances the van der Waals attraction and reduces the electrostatic repulsion more effectively than monovalent salts. This behavior is consistent with the predictions of the DLVO theory, where the balance between van der Waals forces and electrostatic repulsion shifts towards attraction at lower electrolyte concentrations for higher valence ions.

In conclusion, understanding the CCC and the principles of DLVO theory is crucial for predicting nanoparticle stability under various ionic conditions. The study's findings provide valuable insights into how different ions and their concentrations influence nanoparticles' stability and aggregation behavior, which is essential for optimizing the design and use of nanoparticle-based systems in fields such as biomedicine and materials science. Our experimental observations further affirm these findings, particularly in demonstrating the distinct behaviors of SPIONs in potassium versus sodium solutions.

2.5. Summary

In this chapter, we investigated the effect of ionic strength on the dynamic behavior of citric acid-coated superparamagnetic iron oxide nanoparticles (CA SPIONs). By analyzing how these nanoparticles interact with sodium and potassium ions and phosphate-buffered saline (PBS), we aimed to understand how different ionic environments influence their stability and magnetization properties.

Our study revealed that the ionic strength of the solution plays a crucial role in determining the behavior of CA SPIONs. At lower concentrations of sodium and potassium ions, the nanoparticles exhibited a broadening of the dynamic magnetic susceptibility (DMS) signal without a shift in the peak frequency. This broadening effect indicates the initial stages of aggregation, where the nanoparticles begin to cluster together, yet still retain some mobility. However, as the concentration of ions increased, we observed a significant shift in the DMS peak frequency, signifying more pronounced aggregation and a reduction in the nanoparticles' ability to freely rotate in response to an external magnetic field.

Interestingly, potassium ions had a stronger effect on the CA SPIONs compared to sodium ions,

leading to a peak shift at a lower concentration. This difference is attributed to the higher ionic strength of potassium, which more effectively screens the surface charges of the nanoparticles, promoting aggregation more readily than sodium ions.

When we introduced PBS into the system, we observed a different behavior. Despite the presence of both sodium and potassium ions, the CA SPIONs did not show the same peak shift in the DMS signal as observed with individual ions. Instead, the DMS signal only broadened. This suggests that the phosphate ions in PBS play a stabilizing role, likely by forming a protective layer around the nanoparticles, which prevents them from aggregating as readily as they do in simpler ionic solutions.

Overall, this chapter highlights the complex interplay between ionic strength, nanoparticle surface chemistry, and electrostatic interactions in determining the stability and dynamic behavior of CA SPIONs. These insights are essential for optimizing the use of these nanoparticles in various biomedical and biosensing applications, where precise control over their behavior in different ionic environments is critical.

References

(1) Gupta, A. K.; Gupta, M. Synthesis and Surface Engineering of Iron Oxide Nanoparticles for Biomedical Applications. Biomaterials 2005, 26 (18), 3995–4021. DOI:10.1016/j.biomaterials.2004.10.012.

(2) Wei, H.; Hu, Y.; Wang, J.; Gao, X.; Qian, X.; Tang, M. Superparamagnetic Iron Oxide Nanoparticles: Cytotoxicity, Metabolism, and Cellular Behavior in Biomedicine Applications. International Journal of Nanomedicine 2021, Volume 16, 6097–6113. DOI:10.2147/ijn.s321984.

(3) Bustamante-Torres, M.; Romero-Fierro, D.; Estrella-Nuñez, J.; Arcentales-Vera, B.; Chichande-Proaño, E.; Bucio, E. Polymeric Composite of Magnetite Iron Oxide Nanoparticles and Their Application in Biomedicine: A Review. Polymers 2022, 14 (4), 752. DOI:10.3390/polym14040752.

(4) Vindedahl, A. M.; Strehlau, J. H.; Arnold, W. A.; Penn, R. L. Organic Matter and Iron Oxide Nanoparticles: Aggregation, Interactions, and Reactivity. Environmental Science: Nano 2016, 3 (3), 494–505. DOI:10.1039/c5en00215j.

(5) Gutiérrez, L.; de la Cueva, L.; Moros, M.; Mazarío, E.; de Bernardo, S.; de la Fuente, J. M.; Morales, M. P.; Salas, G. Aggregation Effects on the Magnetic Properties of Iron Oxide Colloids. Nanotechnology 2019, 30 (11), 112001. DOI:10.1088/1361-6528/aafbff.

(6) Guo, H.; Barnard, A. S. Naturally Occurring Iron Oxide Nanoparticles: Morphology, Surface Chemistry and Environmental Stability. J. Mater. Chem. A 2013, 1 (1), 27–42. DOI:10.1039/c2ta00523a.

(7) Berret, J.-F.; Graillot, A. Versatile Coating Platform for Metal Oxide Nanoparticles: Applications to Materials and Biological Science. Langmuir 2022, 38 (18), 5323–5338. DOI:10.1021/acs.langmuir.2c00338.

(8) Barrow, M.; Taylor, A.; Murray, P.; Rosseinsky, M. J.; Adams, D. J. Design Considerations for the Synthesis of Polymer Coated Iron Oxide Nanoparticles for Stem Cell Labelling and Tracking Using MRI. Chem. Soc. Rev. 2015, 44 (19), 6733–6748. DOI:10.1039/c5cs00331h.

(9) Kievit, F. M.; Zhang, M. Surface Engineering of Iron Oxide Nanoparticles for Targeted Cancer Therapy. Accounts of Chemical Research 2011, 44 (10), 853–862. DOI:10.1021/ar2000277.

(10) Gambinossi, F.; Mylon, S. E.; Ferri, J. K. Aggregation Kinetics and Colloidal Stability of Functionalized Nanoparticles. Advances in Colloid and Interface Science 2015, 222, 332–349. DOI:10.1016/j.cis.2014.07.015.

(11) Shrestha, S.; Wang, B.; Dutta, P. Nanoparticle Processing: Understanding and Controlling Aggregation. Advances in Colloid and Interface Science 2020, 279, 102162. DOI:10.1016/j.cis.2020.102162.

(12) Moore, T. L.; Rodriguez-Lorenzo, L.; Hirsch, V.; Balog, S.; Urban, D.; Jud, C.; Rothen-Rutishauser, B.; Lattuada, M.; Petri-Fink, A. Nanoparticle Colloidal Stability in Cell Culture Media and Impact on Cellular Interactions. Chemical Society Reviews 2015, 44 (17), 6287–6305. DOI:10.1039/c4cs00487f.

(13) Grzelczak, M.; Sánchez-Iglesias, A.; Mezerji, H. H.; Bals, S.; Pérez-Juste, J.; Liz-Marzán, L. M. Steric Hindrance Induces Crosslike Self-Assembly of Gold Nanodumbbells. *Nano Letters* **2012**, *12* (8), 4380–4384. DOI:10.1021/nl3021957.

(14) Miao, Y.; Chen, Y.; Chen, H.; Wang, X.; Zhao, Y. Using Steric Hindrance to Manipulate and Stabilize Metal Halide Perovskites for Optoelectronics. *Chemical Science* **2021**, *12* (21), 7231–7247. DOI:10.1039/d1sc01171e.

(15) García-Jimeno, S.; Estelrich, J. Ferrofluid Based on Polyethylene Glycol-Coated Iron Oxide Nanoparticles: Characterization and Properties. Colloids and Surfaces A: Physicochemical and Engineering Aspects 2013, 420, 74–81. DOI:10.1016/j.colsurfa.2012.12.022.
(16) Khandhar, A. P.; Keselman, P.; Kemp, S. J.; Ferguson, R. M.; Goodwill, P. W.; Conolly, S. M.; Krishnan, K. M. Evaluation of Peg-Coated Iron Oxide Nanoparticles as Blood Pool Tracers for Preclinical Magnetic Particle Imaging. Nanoscale 2017, 9 (3), 1299–1306. DOI:10.1039/c6nr08468k.
(17) Yue-Jian, C.; juan, T.; Fei, X.; Jia-Bi, Z.; Ning, G.; Yi-Hua, Z.; Ye, D.; Liang, G. Synthesis, Self-Assembly, and Characterization of PEG-Coated Iron Oxide Nanoparticles as Potential MRI Contrast Agent. Drug Development and Industrial Pharmacy 2010, 36 (10), 1235–1244. DOI:10.3109/03639041003710151.
(18) Mahmoudi, M.; Simchi, A.; Imani, M.; Milani, A. S.; Stroeve, P. Optimal Design and Characterization of Superparamagnetic Iron Oxide Nanoparticles Coated with Polyvinyl Alcohol for Targeted Delivery and Imaging. The Journal of Physical Chemistry B 2008, 112 (46), 14470–14481. DOI:10.1021/jp803016n.
(19) Mahmoudi, M.; Simchi, A.; Imani, M. Cytotoxicity of Uncoated and Polyvinyl Alcohol Coated Superparamagnetic Iron Oxide Nanoparticles. The Journal of Physical Chemistry C 2009, 113 (22), 9573–9580. DOI:10.1021/jp9001516.
(20) Hoang Thi, T. T.; Nguyen Tran, D.-H.; Bach, L. G.; Vu-Quang, H.; Nguyen, D. C.; Park, K. D.; Nguyen, D. H. Functional Magnetic Core-Shell System-Based Iron Oxide Nanoparticle Coated with Biocompatible Copolymer for Anticancer Drug Delivery. Pharmaceutics 2019, 11 (3), 120. DOI:10.3390/pharmaceutics11030120.
(21) Liu, J.; Dai, C.; Hu, Y. Aqueous Aggregation Behavior of Citric Acid Coated Magnetite Nanoparticles: Effects of Ph, Cations, Anions, and Humic Acid. Environmental Research 2018, 161, 49–60. DOI: 10.1016/j.envres.2017.10.045.
(22) Cao, T.; Elimelech, M. Colloidal Stability of Cellulose Nanocrystals in Aqueous Solutions Containing Monovalent, Divalent, and Trivalent Inorganic Salts. Journal of Colloid and Interface Science 2021, 584, 456–463. DOI: 10.1016/j.jcis.2020.09.117.

Chapter 3 - Effect of Interparticle and Inter-Cluster Interactions Towards Magnetization Dynamics of CA SPIONs

Abstract

The present chapter describes hydrodynamic behavior of superparamagnetic iron oxide nanoparticles modified with citric acid (CA-SPIONs) in suspensions under alternating current magnetic fields in view of interparticle and inter-cluster dipole-dipole interactions. The cluster size of the CA-SPIONs is modulated to control the interparticle interaction, and the ionic concentration of the CA-SPIONs suspension is varied to control the inter-cluster interaction. Dynamic magnetic susceptibility (DMS) measurement of the CA-SPIONs suspensions under AC magnetic fields elucidates that the interparticle interaction by the clustering and the inter-cluster interaction by the increase of the ionic concentration lead to the modulation of the frequency spectra such as their broadening in low frequency region as well as the decrease of the Brownian relaxation frequency. The DMS spectra obtained experimentally differ from spectra numerically calculated from the distribution of the hydrodynamic size of CA-SPIONs using Debye relaxation model without considering the magnetic interactions; the differences are attributed in the interparticle and inter-cluster dipole-dipole interactions. These insights contribute to a deeper understanding of SPION dynamics, facilitating the optimization of nanoparticle parameters for tailored applications in biomedical fields, which is crucial for their efficacy and precision in liquid-phase biosensing and imaging.

3.1. Introduction

Magnetic biosensing using nanoparticle labels in liquids has emerged as a superior alternative to traditional methods for the detection and quantification of biomarkers in human body fluids and cells. Its growing preference stems from the unique characteristic that biological components are largely unresponsive to magnetic fields, which significantly reduces interference from non-target substances, leading to the precise and sensitive detection of biomolecules through magnetism of magnetic nanoparticles.[1-4] Techniques such as magnetic particle spectroscopy (MPS) and dynamic magnetic susceptibility (DMS) are instrumental in this field.[5-8] MPS and DMS based on the physical rotation of superparamagnetic iron oxide nanoparticles (SPIONs) in liquids under alternating current (AC) magnetic fields (Brownian relaxation) provide valuable insights into their hydrodynamic behavior and magnetic responses.[9-11] The hydrodynamic behavior of SPIONs is influenced by the interaction with biomolecules, exhibiting the changes of the hydrodynamic volume and surrounding viscosity; the interaction modulates their magnetic properties based on Brownian relaxation. This is one of the basic principles of liquid-phase biosensing based on magnetic relaxation using SPIONs.

However, factors other than biomolecular interactions such as influences from salts in the solution can also lead to an increase in hydrodynamic size due to aggregation, potentially resulting in false-positive results. To mitigate this, researchers often employ stable coating agents like polyethylene glycol (PEG), carboxymethyl-dextran (CMD), polyethylene imine (PEI), or other polymers in ionic solutions.[12-21] The influences from magnetic interactions should be also considered to lead to the complexity in analyzing the magnetic response of SPIONs under magnetic fields. Since SPIONs are generally polydisperse including not only monodisperse ones but also clustered ones, complex magnetic interactions such as interparticle interaction and inter-cluster interaction are required to be considered.[22-24] A frequency spectrum of AC magnetic susceptibility of such SPIONs suspension is modulated particularly in a lower frequency region than the Brownian relaxation frequency of the SPIONs which

have the typical hydrodynamic size, in other words, their average hydrodynamic size in the suspension. The modulation often appears as an inflection or another peak in the lower frequency region that also appears in a similar frequency region owing to the interaction with biomolecules. Thus, detailed analyses to elucidate the influence of the magnetic interaction of SPIONs in the frequency spectrum are required to precisely detect the biomolecular interaction.[25-26]

Contrasting with conventional theories like the Debye relaxation model, which do not fully capture the dynamics of real ferrofluids under conditions of polydispersity and strong magnetic interactions, recent theoretical studies have explored the effects of clustering on dynamic magnetic susceptibility.[27-30] Ivanov et al. [28], for example, demonstrated how the formation of clusters such as chains and rings influences the magnetic properties of SPIONs. Their results show that the formation of chains extends the effective rotational time of particles, leading to a reduction in the peak frequency of the imaginary part of the AC magnetic susceptibility spectrum. As these chains transform into denser ring structures, a distinct peak appears in the higher frequency region of the spectrum, above the Brownian relaxation frequency, indicative of reorientational motions within each cluster. Although these phenomena are well-documented in theoretical and simulation studies, experimental evidence of these dynamics in clusters has been scarcely reported.

Our study investigates the effect of intracluster and inter-cluster dipole-dipole interactions on the dynamic behavior of SPIONs by tunning the two magnetic interactions. In order to observe the interparticle dipole-dipole interaction, I control the cluster size of SPIONs by changing the conditions to modify their surface with a dispersant agent, citric acid; the interparticle interaction in the clusters are controlled by changing the cluster size. Meanwhile, the inter-cluster dipole-dipole interaction is modulated by changing the ionic concentration in the colloidal suspension; the increase of the ionic concentration in the suspension modifies the inter-cluster distance owing to the control of the electric-double layer thickness on the clusters. The frequency spectra of DMS of these specimens under different

ionic concentrations show the shift of Brownian relaxation frequency and the broadening in the low-frequency region depending on the cluster size and the ionic concentration. The modulation of the spectra is discussed in view of the magnetic interparticle and inter-cluster dipole-dipole interactions.

3.2. Materials and Methods

3.2.1. Synthesis and characterization of SPIONs modified with citric acid

The synthesis of bare SPIONs was conducted utilizing a solvothermal approach. Initially, a precursor solution was prepared by dissolving 2 mmol of iron (III) acetylacetonate (14024-18-1, Sigma-Aldrich, USA) in 40 mL of tetraethylene glycol (112-60-7, Sigma-Aldrich, USA). This solution was heated to 343 K to ensure complete dissolution of the precursor. The solution was then transferred into four 10 mL stainless steel pressure vessels. These vessels were then sealed and placed in an electric furnace, where they were subjected to a temperature of 523 K for a duration of 15 hours, facilitating the solvothermal reaction.

The synthesized SPIONs were subjected to a series of washing steps after the completion of the reaction. Initially, the SPIONs were washed with acetone to remove any residual solvent, followed by centrifugation to collect the nanoparticles. This process was repeated three times, alternating between deionized (DI) water and ethanol to ensure thorough cleaning. Finally, the bare SPIONs were redispersed in 20 mL of DI water, preparing them for further process.

Following the synthesis of bare SPION, a citric acid solution was prepared for the surface modification treatment. Next, the synthesized SPIONs were dispersed in an aqueous solution of 2 g trisodium citrate (197-06025, Wako Chemicals, Japan) in 120 mL of DI water using an ultrasonic homogenizer at 343 K for surface modification with citric acid molecules. Once the surface modification process was complete, the SPIONs were washed three times with a mixture of 25 percent DI water and 75 percent ethanol by volume and subsequently dispersed in DI water (5 mL). I have changed the time between the washing process of the bare SPIONs and the start of the surface modification process to

control the cluster size of SPIONs from 0 days (immediately) to 4 days. The time is called as an incubation time t_i. Specimens with t_i of 0 days, 2 days, and 4 days are labeled as S1, S2, and S3, respectively. The increase in the incubation time of the bare SPIONs enhanced clustering; the formed clusters were not easily broken with the homogenizer.

In addition to adjusting the incubation time to tailor the cluster sizes of SPIONs, the inter-cluster interaction was effectively managed by carefully introducing salts from a phosphate-buffered saline (PBS) solution. When the appropriate concentration of salts is introduced, SPIONs and their clusters tend to aggregate owing to the reduction of the electric-double layer thickness on them, forming larger clusters which can significantly influence their magnetic and physical properties. However, it is crucial to carefully manage the salt concentration, as excessive amounts can lead to undesirable precipitation of SPIONs, rendering them unsuitable for further applications. To meticulously control this aspect, the ionic concentration of the suspension for evaluations was varied systematically. The concentrations of the specimens labeled as 0.5xPBS, 0.25xPBS, 0.125xPBS, and 0xPBS are equivalent to a half of that of PBS, 0.25 times, 0.125 times, and pure water (no ionic component), respectively.

The primary and hydrodynamic sizes of the nanoparticles were determined using transmission electron microscopy (TEM, H-8100, Hitachi High-Tech Corporation, Japan) and dynamic light scattering measurements (DLS, SZ-100-V2, HORIBA, Japan), respectively. The frequency dependence of the AC magnetization in the range of 10–10,000 Hz was analyzed using a physical property measurement system (PPMS; Quantum Design Corp., USA) at a magnetic field strength of 0.8 kA/m at 300 K. The SPIONs concentration and volume of specimens for PPMS measurements were 3.5 mg/mL and 100 µL, respectively.

3.2.2. Analysis of dynamic magnetic susceptibility spectrum for polydisperse SPIONs

When a suspension of SPIONs is polydisperse by containing several types of SPION clusters with different sizes, the imaginary part in AC magnetic susceptibility χ"(ω) corresponding to the out-of-phase response is given by [31,32]

$$\chi''(\omega) = \sum_{i=1}^{k} p_{\mathrm{d_{h,i}}}\, \chi''\left(\omega, d_{\mathrm{h,i}}\right);\ \text{with}\ \chi''\left(\omega, d_{\mathrm{h,i}}\right) = \chi_0 \frac{\omega\tau}{1+(\omega\tau)^2}\ , \qquad (1)$$

where ω is angular frequency of external magnetic field, $p_{\mathrm{d_{h,i}}}$ is the mass ratio of SPION clusters with hydrodynamic size $d_{\mathrm{h,i}}$, and $\chi''\left(\omega, d_{\mathrm{h,i}}\right)$ is the imaginary part of AC susceptibility of SPION clusters with hydrodynamic size $d_{\mathrm{h,i}}$ based on Debye relaxation model. The number of types for SPION clusters is k. χ_0 represents the magnetic susceptibility at low applied magnetic field frequencies. While acknowledging the presence of both Neel and Brownian relaxation processes, this model assumes that the dynamic magnetization of SPIONs is predominantly due to Brownian relaxation, meaning τ in eq. (1) equals to Brownian relaxation time τ_B, which is given by

$$\tau_B = \frac{\eta\pi d_h^3}{2k_B T}\ , \qquad (2)$$

where η is the fluid's dynamic viscosity, k_{B} is the Boltzmann constant, and T is the absolute temperature.

3.3. Results

3.3.1. Dependence of cluster size on incubation time.

Figure 3.1 presents TEM images, hydrodynamic size distribution by DLS, and frequency spectra of the imaginary part of AC magnetic susceptibility for SPIONs modified with citric acid (CA-SPIONs). The TEM images reveal that the primary SPION size is 17 ± 5 nm for both (a) specimen S1 (t_{i} = 0 days) and (b) specimen S3 (t_{i} = 4 days). The incubation process did not influence the primary size of SPIONs, suggesting that nanoparticle growth had completed in prior to the incubation. Furthermore, the TEM images indicated a trend towards the formation of larger nanoparticle clusters with the increase of t_{i}.

SPIONs that were not subjected to incubation formed smaller clusters, typically comprising one to five particles. In contrast, the incubation led to the formation of significantly larger clusters which contain as many as 19 SPIONs as shown in Fig. 1(b). The tendency of the increase of cluster size is likely a consequence of the inherent instability of bare SPIONs in aqueous environments.

DLS analyses supported the trend observed in the TEM images, providing quantitative evidence of the influence of the incubation on the hydrodynamic size of SPION clusters. As shown in Fig. 3.1(c), there is a clear correlation between the incubation time and the hydrodynamic size of the SPION clusters; the longer the incubation time, the larger the clusters. The mean size obtained by DLS was 25.5 nm for specimen S1, 34.9 nm for S2, and 42.1 nm for S3, indicating that this relationship underscores the significant influence of the incubation on the growth of SPION clusters.

Dynamic magnetic susceptibility (DMS) measurements clarified the influence of the incubation on SPIONs. Figure 1(d) shows a decrease of the peak frequency in the imaginary part of the DMS spectra with the increase of the incubation time. The peaks in the imaginary DMS spectra for specimen S1, S2, and S3 were observed at 10,000 Hz, 4,800 Hz, and 2,300 Hz, respectively. The peak frequency which represents Brownian relaxation frequency notably decreases with the increase of the incubation time. This trend is consistent with the equation of Brownian relaxation frequency shown in eq. (2), indicating that an increase in hydrodynamic diameter leads to a lower peak frequency. The viscosity η for specimen S1 is calculated to be 2.5 mPa·s by supposing that the hydrodynamic size d_h in the equation equals to the mean size obtained by DLS. Supposing the viscosity is the same as that S2 and S3, the Brownian frequency was calculated to be 4,100 Hz for S2 and 2,300 Hz for S3 by using the mean size by DLS; these calculated values are closely consistent with the experimentally obtained ones, suggesting that the magnetically hydrodynamic behaviors of S1, S2, and S3 are closely related to the mean size by DLS. In addition, the spectrum becomes broader with the increase of the ionic concentration.

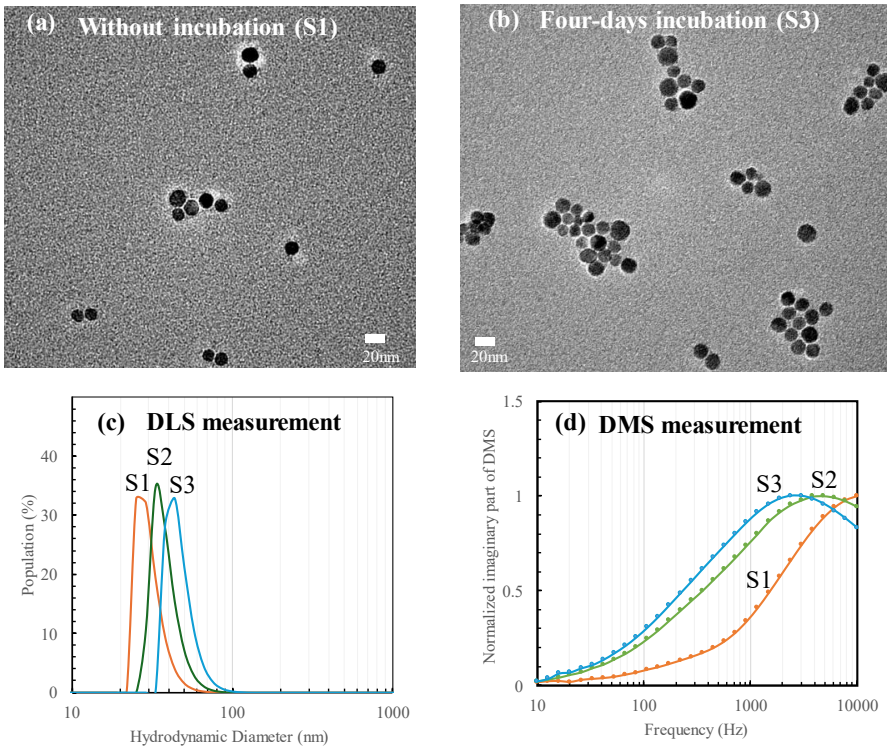

Figure. 3.1. Characterization of SPIONs modified with citric acid (CA-SPIONs) prepared by changing the incubation time t_i. (a) TEM image of CA-SPIONs for specimen S1 with t_i of 0 days, (b) TEM image of CA-SPIONs for specimen S3 with t_i of 4 days, (c) hydrodynamic size distribution obtained by DLS for specimens S1 with t_i of 0 days, S2 with t_i of 2 days, and S3 with t_i of 4 days, (d) imaginary part of DMS spectra for specimens S1, S2, and S3

3.3.2. Dependence of cluster size on ionic concentration in SPION suspension.

Table 3.1 shows the dependence of the cluster size of CA-SPIONs (specimens S1, S2, and S3) obtained by DLS on the ionic concentration in suspensions. The mean hydrodynamic size, cumulant size [33], and polydispersity index (PDI) of CA-SPIONs (specimens S1, S2, and S3) were quantitatively analyzed by changing the ionic concentration of 0xPBS, 0.125xPBS, 0.25xPBS, and 0.5xPBS in the suspension for DLS measurements. The mean size for all specimens increases with the increase of the ionic concentration as shown in Table 3.1. The cumulant size, which provides a weight-average size, in particular, reflecting a broader particle size distribution, revealed more significant changes. The ratio of the size at 0.5xPBS to that at 0xPBS for the cumulant size (1.4–1.8) is much larger than that for the mean size (1.2–1.3), indicating a substantial increase of the cluster size by the increase of the ionic

concentration. In addition, whereas PDI values exhibited slight variations at lower ionic concentrations (around 0.25 in the range of 0xPBS to 0.25xPBS), there was a significant rise in PDI in the 0.5xPBS for all the specimens, increasing up to the values higher than 0.3. This considerable increase at higher PBS concentrations indicated an increased heterogeneity in the hydrodynamic size, implying enhanced aggregation or clustering facilitated by the ionic strength of the solution.

Table 3.1. Ionic concentration dependence of DLS results for CA-SPIONs specimens S1 (t_i = 0 days), S2 (t_i = 2 days), and S3 (t_i = 4 days) in PBS solution.

Ionic concen-tration (x PBS)	Specimen S1			Specimen S2			Specimen S3		
	Mean (nm)	Cumul-ant (nm)	PDI	Mean (nm)	Cumul-ant (nm)	PDI	Mean (nm)	Cumul-ant (nm)	PDI
0	25.5	38.2	0.23	34.9	51.8	0.25	42.1	55.8	0.18
0.125	27.8	41.8	0.26	38.0	54.8	0.22	42.3	58.8	0.18
0.25	29.4	42.7	0.27	42.6	58.5	0.24	44.5	61.6	0.21
0.5	31.0	69.8	0.40	45.6	72.0	0.32	55.7	93.9	0.31

To help readers better understand the effect of sodium ions on nanoparticle stability and the resulting broadening effect, I included buffer solutions in this part of the study. The following table (Table 3.2) lists the final concentrations of sodium and phosphate in various dilutions of PBS solutions: 0x, 0.125x, 0.25x, and 0.5x. For example, a 0.125x PBS solution contains 18.375 mM sodium and 1.475 mM phosphate. This table allows readers to compare the effects of sodium ions on nanoparticle behavior with and without the buffer solution, providing valuable insights into the underlying mechanisms.

Table 3.2. Summary of sodium and phosphate concentration in PBS solution

PBS Solution	Sodium (mM)	Phosphate (mM)
0x PBS	0	0
0.125x PBS	18.375	1.475
0.25x PBS	36.75	2.95
0.5x PBS	73.5	5.9

Figures 3.2(a)-(c) present DMS spectra for (a) specimen S1, (b) S2, (c) S3 at various ionic concentrations. From spectra of the real part shown in Figs. 3.2(a)-(c), the magnetic susceptibility at a

low frequency range (10–100 Hz) which is a plateau remains relatively constant at lower salt concentrations (0x, 0.125x, and 0.25xPBS) for each specimen. However, increasing the ionic concentration to 0.5xPBS shows a discernible decrease in the real component's susceptibility.

Figures 3.2(d)-(f) show the spectra of the imaginary part normalized by the peak value for each condition to observe easily the difference in spectra, such as peak frequency and broadness. The DMS spectra of the imaginary part for all the specimens are noticeably broadened by increasing the ionic concentration, as a black-colored arrow indicates, whereas the peak frequency is not almost changed. The broadening of the spectrum for S1 with smaller clusters by the increase of the ionic concentration is the most significant among the three specimens.

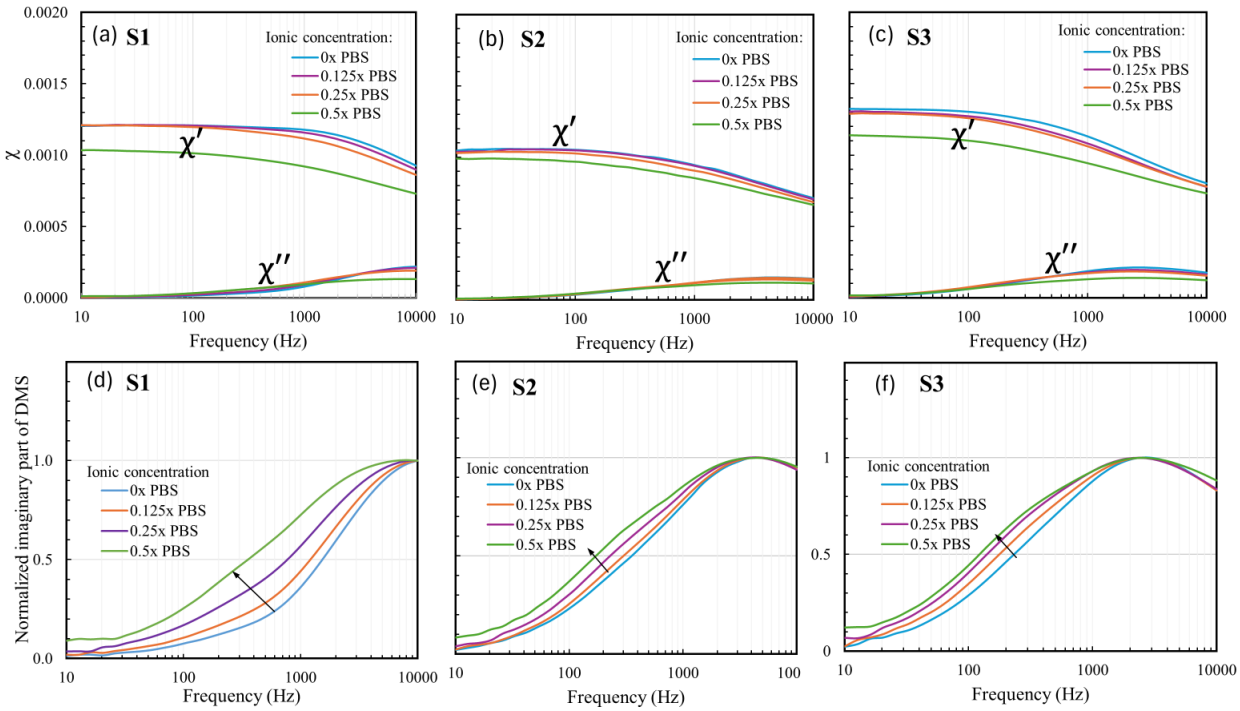

Figure. 3.2. (a-c) DMS spectra and (d-f) normalized imaginary part of the DMS spectra at various ionic concentrations. (a) and (d) for specimen S1, (b) and (e) for S2, and (c) and (f) for S3

3.4. Discussion

As shown in Figs. 3.1 and 3.2, a shift in peak frequency and an increase in broadness were observed in the imaginary part of the DMS spectra when the cluster size and ionic concentration in the suspension

were varied. Generally, a decrease in Brownian relaxation is associated with an increase in hydrodynamic size under constant viscosity, while broadness is linked to a widening of the hydrodynamic size distribution, as described by equations (1) and (2). By obtaining the hydrodynamic diameter distribution at different ionic concentrations from DLS measurements, I can calculate the DMS spectra for specimens S1–S3 using the Debye relaxation model outlined in equations (1) and (2).

The imaginary part of the DMS spectrum was numerically calculated as a superposition of spectra from 11 different cluster sizes, with hydrodynamic diameters ranging from 21.88 nm to 131.83 nm, as determined by DLS for each specimen (S1–S3) and ionic condition (0x, 0.125x, 0.25x, and 0.5xPBS) as shown in table 3.3 – 3.6. These calculations did not account for magnetic dipole-dipole interactions among individual clusters, as shown in Fig. 3.3, and the spectra were normalized similarly to Figs. 3.2(d)–(f). The results indicate that the peak frequency of the DMS spectra shifts toward a lower frequency region as cluster size (incubation time) and ionic concentration increase, though changes in broadness are not clearly observed. This finding is consistent with the hydrodynamic diameter distributions obtained by DLS, where the broadness of the distributions was similar across the 12 conditions (specimens S1–S3 and four ionic concentrations).

Experimentally, the Brownian relaxation frequency decreased as incubation time or mean hydrodynamic size increased at 0xPBS (in water), as shown in Fig. 1(d). The calculated spectra at 0xPBS exhibit a similar trend, except for changes in broadness. In the case of varying ionic concentrations, changes in the broadness of the spectra were observed experimentally, though the peak shift was not as clear, as shown in Figs. 3.2 (d)–(f). The most significant difference between the calculated and experimental spectra is the broadness. To quantify this difference, I evaluated the broadness more closely.

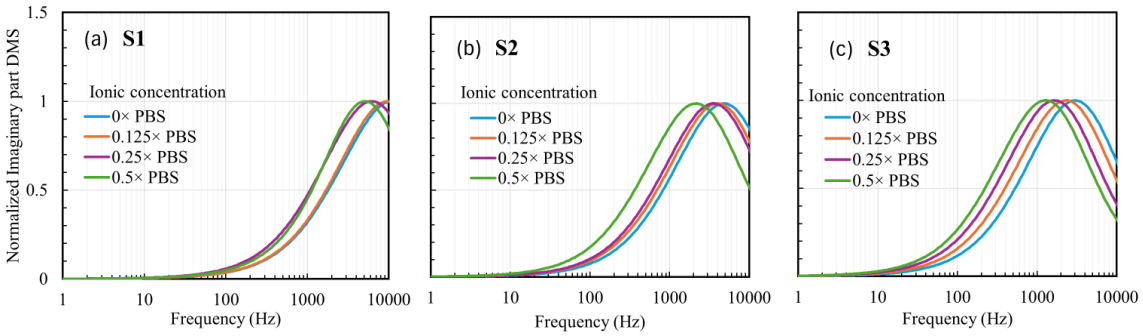

Figure. 3.3. Calculated imaginary part of DMS spectra for (a) S1, (b) S3, and (c) S3 at the ionic concentrations of 0x, 0.125x, 0.25x, and 0.5xPBS by using the distribution of hydrodynamic size obtained by DLS.

To estimate the hydrodynamic size distribution $p_{d_{h,i}}$ from the experimental DMS data, $\chi"(\omega, d_{h,i})$, equation (1) was used. It is important to note that $p_{d_{h,i}}$ in equation (1) represents the mass ratio of MNP clusters. I assume that SPIONs form a polydisperse system consisting of clusters with hydrodynamic sizes $d_{h,i}$ ranging from 21.88 nm to 131.83 nm. Each SPION cluster produces its own DMS signal, $\chi"(\omega, d_{h,i})$, which can be estimated using the Debye model, also described in equation (1). Here, χ_0 (the static magnetic susceptibility at zero frequency) is normalized to 1 for the imaginary part of DMS, ω is the angular frequency of the applied magnetic field, and $\tau_B(d_{h,i})$ is the Brownian relaxation time of the magnetic moments for different nanoparticle clusters. I can solve these equations using a regression method by employing the hydrodynamic size distribution obtained from DLS measurements. Once I obtain the size distribution for each specimen at every ionic concentration, I can then calculate and draw the normalized imaginary part of the DMS, $\chi"(\omega, d_{h,i})$ using equation (1).

Table 3.3. Size distribution of specimen S1 obtained from DLS.

p_i (%)	Diameter (nm)													
	21.88	25.12	28.84	33.11	38.02	43.65	50.12	57.54	66.07	75.86	87.1	100	114.82	131.83
water	7.22	19.92	22.62	18.85	13.38	8.57	5.10	2.85	1.51	0.00	0.00	0.00	0.00	0.00
0.125x PBS	0.39	18.61	24.77	21.52	15.32	9.63	5.50	2.89	1.38	0.00	0.00	0.00	0.00	0.00
0.25x PBS	0.00	0.00	17.36	24.52	21.88	15.80	10.03	5.80	3.09	1.51	0.00	0.00	0.00	0.00

0.5x PBS	0.00	0.00	0.00	22.67	35.46	25.70	12.16	3.64	0.37	0.00	0.00	0.00	0.00	0.00

Table 3.4. Size distribution of specimen S2 obtained from DLS.

p_i (%)	Diameter (nm)													
	21.88	25.12	28.84	33.11	38.02	43.65	50.12	57.54	66.07	75.86	87.1	100	114.82	131.83
water	0.00	0.00	6.43	20.70	23.67	19.39	13.36	8.22	4.64	2.42	1.16	0.00	0.00	0.00
0.125x PBS	0.00	0.00	0.00	16.77	24.13	21.73	15.81	10.11	5.91	3.20	1.60	0.74	0.00	0.00
0.25x PBS	0.00	0.00	0.00	11.27	22.45	22.89	17.76	11.81	7.07	3.88	1.97	0.90	0.00	0.00
0.5x PBS	0.00	0.00	0.00	0.00	7.78	20.93	23.14	18.74	12.92	8.04	4.64	2.52	1.29	0.00

Table 3.5. Size distribution of specimen S3 obtained from DLS.

p_i (%)	Diameter (nm)													
	21.88	25.12	28.84	33.11	38.02	43.65	50.12	57.54	66.07	75.86	87.1	100	114.82	131.83
water	0.00	0.00	0.00	3.32	20.08	24.62	20.60	14.24	8.72	4.84	2.45	1.11	0.00	0.00
0.125x PBS	0.00	0.00	0.00	0.00	10.81	22.08	22.80	17.87	12.02	7.29	4.06	2.09	0.99	0.00
0.25x PBS	0.00	0.00	0.00	0.00	0.00	13.71	23.67	22.77	17.00	10.93	6.32	3.33	1.59	0.67
0.5x PBS	0.00	0.00	0.00	0.00	0.00	2.39	19.65	24.46	20.59	14.39	9.00	5.21	2.84	1.47

Given the observed discrepancy, we aimed to determine how the hydrodynamic size distribution should change to accurately reflect the DMS signal presented in Figure 3.2. To achieve this, we employed a reverse engineering approach by fitting the observed DMS spectra to the modified Debye model, as outlined in Equation (1) of this chapter. This method enabled us to estimate the population percentage (pi (%)) for each cluster of SPIONs across various cluster sizes, ranging from 21.88 to 131.83 nm. The resulting size distributions for specimens S1, S2, and S3 under different PBS conditions are detailed in Tables 3.6, 3.7, and 3.8, respectively. To validate the accuracy of the estimated size distribution, we

compared the experimental DMS signal with a synthetic signal generated using the estimated size distribution and Equation (1). These comparisons are illustrated in Figure 3.4.

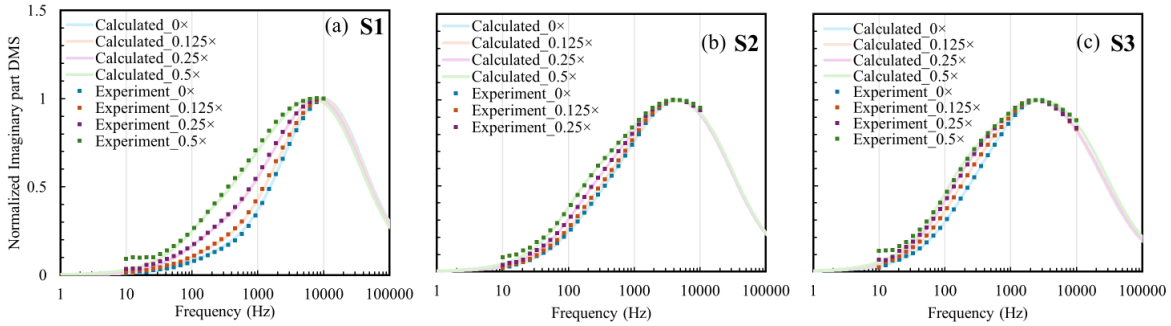

Figure. 3.4. Calculated imaginary part of DMS spectra for (a) S1, (b) S3, and (c) S3 at the ionic concentrations of 0x, 0.125x, 0.25x, and 0.5xPBS by using the distribution of hydrodynamic size obtained by DLS.

The DLS results for specimen S1 (Table 3.3) indicate that in water, the nanoparticle size distribution is heavily skewed towards smaller clusters, with 60.81% of the population within the 21.88 to 33.11 nm range. As the PBS concentration increases, the distribution shifts toward larger sizes, with the peak shifting to 38.02 nm at 0.5x PBS, suggesting the onset of aggregation. Notably, at 0.5x PBS, DLS detects no particles smaller than 33.11 nm, indicating that aggregation is substantial enough to merge smaller clusters into larger ones. In contrast, the DMS data for specimen S1 (Table 3.6) presents a broader distribution across all conditions. Even in water, DMS detects significant populations of nanoparticles across a wide range of sizes, including larger clusters up to 131.83 nm. This broader distribution persists and becomes more pronounced as PBS concentration increases. By 0.5x PBS, DMS reveals a substantial shift towards larger clusters, with notable populations even in the 87.1 to 131.83 nm range. These findings suggest that DMS is more sensitive to the formation of larger aggregates that DLS may not fully capture.

For specimen S2, DLS data (Table 3.4) shows a distribution centered around mid-sized clusters in water, with a peak at 38.02 nm. As PBS concentration increases, there is a noticeable shift towards larger clusters, with the peak size reaching 50.12 nm at 0.5x PBS. This trend indicates increasing aggregation

but with a more abrupt transition compared to S1. The DMS data for specimen S2 (Table 3.7) again displays a broader distribution than DLS. In water, the size distribution is relatively uniform across various sizes. Still, as PBS concentration increases, DMS reveals a gradual and significant shift towards larger clusters, with a peak size of 66.07 nm at 0.5x PBS. DMS also detects a considerable presence of larger aggregates, particularly in the 87.1 to 131.83 nm range, which are primarily missed by DLS. This discrepancy underscores DMS's capability to detect a broader range of particle sizes, particularly larger aggregates likely underrepresented in DLS measurements.

Specimen S3, as measured by DLS (Table 3.5), predominantly shows nanoparticles within the 38.02 to 50.12 nm range in water. As the PBS concentration increases, the peak size shifts to 57.54 nm at 0.5x PBS, indicating aggregation. However, the distribution remains relatively narrow, and DLS does not detect substantial populations of particles larger than 75.86 nm. In contrast, DMS data for specimen S3 (Table 3.8) reveals a much broader size distribution. Even in water, DMS detects significant populations across a wide range of sizes, including clusters up to 131.83 nm. With increasing PBS concentration, DMS shows a more pronounced shift towards larger clusters, with a peak size of 87.1 nm at 0.5x PBS and substantial populations in the 114.82 to 131.83 nm range.

The differences observed between the size distributions from DMS and DLS highlight the complex interactions at play in the system. The presence of an external magnetic field during DMS measurements introduces magnetic dipolar interactions that can influence the observed particle size distribution. These interactions are absent in DLS measurements, where particles are not subjected to such external forces. As a result, DMS tends to detect larger apparent sizes, particularly under higher ionic strengths, where the presence of ions from PBS solutions further alters the behavior of the nanoparticles. This suggests that the magnetic dipolar interactions are not merely a result of particle aggregation but are also influenced by the external magnetic field and the surrounding ionic environment.

Table 3.6. Size distribution of specimen S1 obtained from DMS.

p_i (%)	Diameter (nm)													
	21.88	25.12	28.84	33.11	38.02	43.65	50.12	57.54	66.07	75.86	87.1	100	114.82	131.83
water	9.91	13.47	16.54	17.44	15.36	11.37	7.09	3.43	0.80	0.46	0.32	0.59	1.42	1.83
0.125x PBS	9.07	12.35	15.21	16.17	14.57	11.36	7.89	4.81	2.34	0.83	0.46	0.90	1.62	2.44
0.25x PBS	7.84	10.66	13.11	13.95	12.76	10.50	8.26	6.25	4.34	2.75	1.79	1.59	2.21	3.96
0.5x PBS	6.77	9.14	11.12	11.68	10.66	9.19	8.17	7.39	6.31	4.89	3.46	2.48	2.83	5.92

Table 3.7. Size distribution of specimen S2 obtained from DMS.

p_i (%)	Diameter (nm)													
	21.88	25.12	28.84	33.11	38.02	43.65	50.12	57.54	66.07	75.86	87.1	100	114.82	131.83
water	5.53	7.63	9.69	11.00	11.26	10.87	10.10	8.78	6.90	5.04	3.85	3.33	3.11	2.90
0.125x PBS	5.45	7.50	9.49	10.71	10.88	10.44	9.71	8.56	6.94	5.32	4.29	3.87	3.63	3.21
0.25x PBS	5.23	7.18	9.06	10.16	10.27	9.85	9.26	8.33	6.97	5.59	4.72	4.37	4.34	4.68
0.5x PBS	5.35	7.29	9.04	9.82	9.47	8.74	8.24	7.80	7.00	5.85	4.72	4.08	4.74	7.85

Table 3.8. Size distribution of specimen S3 obtained from DMS.

p_i (%)	Diameter (nm)													
	21.88	25.12	28.84	33.11	38.02	43.65	50.12	57.54	66.07	75.86	87.1	100	114.82	131.83
water	3.93	5.48	7.13	8.54	9.61	10.49	11.01	10.59	9.10	7.08	5.35	4.27	3.76	3.66
0.125x PBS	3.88	5.40	6.97	8.23	9.06	9.68	10.05	9.77	8.67	7.15	5.82	5.02	4.85	5.43
0.25x PBS	3.95	5.45	6.95	7.99	8.51	8.88	9.22	9.17	8.43	7.18	5.90	5.16	5.54	7.66
0.5x PBS	4.41	6.02	7.51	8.30	8.34	8.24	8.38	8.42	7.91	6.80	5.46	4.65	5.64	9.92

To further understand these interactions, we must consider how they affect the dynamic magnetization of the nanoparticles, particularly in the context of their frequency-dependent behavior. The broadening of the DMS spectra, which is more pronounced under higher PBS concentrations, could be attributed to these magnetic dipolar interactions, which become more significant as the nanoparticles interact with the ions in the solution. This broadening indicates a more complex interplay between the nanoparticles' magnetic properties and their environment, which is not fully captured by DLS data alone.

Since I could not obtain AC magnetization data in the higher frequency region, I quantify the broadness of the spectrum by calculating the ratio between the peak frequency f_{peak} and the frequency f_{half} where the normalized imaginary part of DMS equal to 0.5 in the lower frequency region. The half width of the spectrum is defined as a difference between log f_{peak} and log f_{half} since the frequency axis in the spectrum is shown in a logarithmic scale. Hence, the spectrum's width is equivalent to the ratio f_{peak} / f_{half}. Figure 4 shows the ionic concentration dependence of f_{peak} / f_{half} for calculated and experimentally obtained spectra of specimens S1–S3. Figure 3.4 shows f_{peak} / f_{half}, in other words, the broadness of the calculated spectra does not depend on the incubation time and the ionic concentration; this trend is similar to that seen in Fig 3.3. In water (0xPBS), f_{peak} / f_{half} of the experimental spectrum is similar to that of the calculated spectrum for S1with the smallest cluster size. f_{peak} / f_{half} increases with the increase of the incubation time and the ionic concentration. The difference of the broadness in the DMS spectra will be attributed in interparticle and inter-cluster magnetic dipole-dipole interaction which is not considered in the calculation from DLS data.

From these points, we will explain the dependence of magnetic behavior of CA-SPIONs on the incubation time and the ionic concentration observed in Figs. 3.1 and 3.2. In specimen S1, a majority of magnetic components is probably a single SPION which is dispersed well with very weak magnetic interaction in water. Thus, the DMS spectrum experimentally obtained under 0xPBS is close to the calculated one based on Debye relaxation model without magnetic interaction. With the increase of the

incubation time, the number of particles in the cluster and its size increased as show in Fig. 3.1. The rigidity of clusters in S1–S3 suggests that the SPIONs within these clusters are not rotating freely and independently, leading to the decrease of the Brownian relaxation frequency depending on the mean hydrodynamic size. This results in predominantly independent behavior with minimal magnetic interaction, particularly in water. Under the conditions, the calculated and experimental spectra have similar broadness; the strongest electrostatic repulsion and the weakest magnetic interactions among the clusters. However, the broadness of the DMS spectra experimentally obtained is enhanced with the incubation time and the cluster size even in water, indicating that the interparticle magnetic dipole-dipole interaction appears in the cluster and modulates the spectra.

As the ionic concentration increases, the gap between theoretical predictions and experimental results widens, particularly evident in the broadening of the low-frequency region of the spectra whereas the main peak remains unchanged. This observed broadening of the particle spectrum likely arises not merely from larger hydrodynamic diameters but from complex inter-cluster magnetic interactions. An increased heterogeneity in the hydrodynamic size facilitated because of the decrease of the electric double-layer on them and the increase of inter-cluster interaction by the ionic strength of the solution is a significant reason. The inter-cluster interaction does not strongly bind clusters; the Brownian relaxation behavior of the original cluster remains with the inter-cluster magnetic interaction. Thus, the peak frequency of the spectra for S1−S3 did not change a lot although the ionic concentration was increased as shown in Figs. 3.2(d)–(f). It has been previously reported that such complex behavior from individual particles as well as cluster appears also in the magnetic particle cluster in a suspension.[34)]

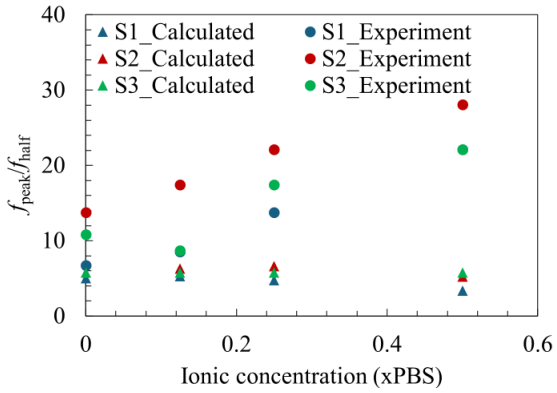

Figure. 3.4. Ionic concentration dependence of f_{peak} / f_{half} for calculated and experimentally obtained DMS spectra for CA-SPIONs of S1–S3.

3.5. Summary

In this chapter, we explored the impact of interparticle and inter-cluster interactions on the magnetization dynamics of citric acid-coated superparamagnetic iron oxide nanoparticles (CA SPIONs) under alternating current (AC) magnetic fields. By manipulating the cluster size through incubation time and modulating ionic concentrations in the suspension, we investigated how these factors influence the dynamic magnetic susceptibility (DMS) spectra of CA SPIONs.

Our results demonstrated that increasing the incubation time led to the formation of larger SPION clusters, which in turn caused a decrease in the Brownian relaxation frequency—a key indicator of how quickly nanoparticles can reorient in response to an external magnetic field. This decrease was consistent with the theoretical relationship between hydrodynamic size and Brownian relaxation frequency. Additionally, we observed that the DMS spectra broadened as both cluster size and ionic concentration increased, particularly in the low-frequency region. This broadening effect suggests that both interparticle and inter-cluster magnetic dipole-dipole interactions play a significant role in the observed magnetization behavior.

Interestingly, while the theoretical models, such as the Debye relaxation model, provided a good approximation of the peak frequency shifts in the DMS spectra, they failed to fully capture the broadening observed experimentally. This discrepancy highlights the complex nature of magnetic

interactions in polydisperse nanoparticle systems, where the external magnetic field and the surrounding ionic environment significantly influence the nanoparticles' dynamic behavior.

Overall, this chapter's findings emphasize the importance of considering both interparticle and inter-cluster interactions when analyzing SPIONs' magnetic behavior. These insights are crucial for optimizing the performance of SPION-based technologies, particularly in applications like liquid-phase biosensing, where precise control over nanoparticle behavior is essential for accurate detection and measurement.

References

(1) K. M. Koo, N. Soda, and M. Shiddiky, "Magnetic nanomaterial–based electrochemical biosensors for the detection of diverse circulating cancer biomarkers," *Current Opinion in Electrochemistry* **25**, 100645 (2021). https://doi.org/10.1016/j.coelec.2020.100645.

(2) Lin, D. Makarov, and O. Schmidt, "Magnetic sensing platform technologies for biomedical applications," *Lab Chip* **17**(11), 1884–1912 (2017). https://doi.org/10.1039/c7lc00026j.

(3) M. Masud, J. Na, M. Younus, M. S. Hossain, Y. Bando, M. Shiddiky, and Y. Yamauchi, "Superparamagnetic nanoarchitectures for disease-specific biomarker detection," *Chem. Soc. Rev.* **48**, 5717–5751 (2019). https://doi.org/ 10.1039/C9CS00174C.

(4) K.Ulbrich, K. Holá, V. Šubr, A. Bakandritsos, J. Tuček, and R. Zbořil, "Targeted drug delivery with polymers and magnetic nanoparticles: Covalent and noncovalent approaches, release control, and clinical studies,". *Chem. Rev.* **116** (9), 5338–5431. (2016). https://doi.org/10.1021/acs.chemrev.5b00589.

(5) K. Wu, J. Liu, D. Su, R. Saha, J.-P. Wang, "Magnetic nanoparticle relaxation dynamics-based magnetic particle spectroscopy for rapid and wash-free molecular sensing," *ACS Appl. Matter. Interfaces* **11**, 22979 – 22986. (2019). https://doi.org/10.1021/acsami.9b05233.

(6) K. Wu, R. Saha, D. Su, V. D. Krishna, J. Liu, M. C. J. Cheeran, J.-P. Wang, "Magnetic-nanosensor-based virus and pathogen detection strategies before and during COVID-19," *ACS Appl. Nano Mater* **3**, 10, 9560 – 9580. (2020). https://doi.org/10.1021/acsanm.0c02048.

(7) K. Enpuku, T. Tanaka, Y. Tamai, M. Matsuo, "AC susceptibility of magnetic markers in suspension for liquid phase immunoassay," *Journal of Magnetism and Magnetic Materials* **321**, 1621 – 1624. (2009). https://doi.org/ 10.1016/j.jmmm.2009.02.099.

(8) A.K. Bhuiya, T. Mitake, M. Asai, T. Ito, S. Chosakabe, T. Yoshida, K. Enpuku, A Kandori, "Liquid-phase immunoassays using Brownian relaxation of magnetic markers," *IEEE Transactions on Magnetics* **47** (10). (2011). https://doi.org/ 10.1109/TMAG.2011.2153828.

(9) K. Wu, J. Liu, D. Su, R. Saha, J.-P. Wang, "Magnetic nanoparticle relaxation dynamics-based magnetic particle spectroscopy for rapid and wash-free molecular sensing," *ACS Appl. Mater. Interfaces* **11**, 22979-22986. (2019). https://doi.org/10.1021/acsami.9b05233.

(10) A.C. Bohórquez, M. Unni, S. Belsare, A. Chiu-Lam, L. Rice, C. Pampo, D. Siemann, C. Rinaldi, "Stability and mobility of magnetic nanoparticles in biological environments determined from dynamic magnetic susceptibility measurements," *Bioconjugate Chem* **29**, 2793 – 2805. (2018). https://doi.org/10.1021/acs.bioconjchem.8b00419.

(11) A. Aires, D. Cabrera, L. C. Alonso-Pardo, A. L. Cortajarena, F.J. Teran, "Elucidation of the physicochemical properties ruling the colloidal stability of iron oxide nanoparticles under physiological conditions," *ChemNanoMat* **3**, 183-189. (2017). https://doi.org/10.1002/cnma.201600333.

(12) Y.C. Park, Y. C., J.B. Smith, R.D. Whitaker, C. A. Sucato, J.A. Hamilton, E. Bartolak-Suki, J. Y. Wong, "Effect of PEG molecular weight on stability, T2 contrast, cytotoxicity, and cellular uptake of superparamagnetic iron oxide nanoparticles (SPIONs)," *Colloids and Surfaces B: Biointerfaces* **119**, 106-114. (2014). https://doi.org/10.1016/j.colsurfb.2014.04.027.

(13) E. Amstad, et al. "Surface functionalization of single superparamagnetic iron oxide nanoparticles for targeted magnetic resonance imaging," *Small* **5** (11):1334–1342. (2009). https://doi.org/ 10.1002/smll.200801328.

(14) H. Unterweger, et al. "Dextran-coated superparamagnetic iron oxide nanoparticles for magnetic resonance imaging: evaluation of size-dependent imaging properties, storage stability and safety," *International Journal of Nanomedicine* **13**, 1899–1915. (2018). https://doi.org/10.2147/IJN.S156528.

(15) F. Yu, L. Zhang, Y. Huang, K. Sun, A. E. David, V. C. Yang, "The magnetophoretic mobility and superparamagnetism of core-shell iron oxide nanoparticles with dual targeting and imaging functionality," *Biomaterials* **31** (22) 5842-5848. (2010). https://doi.org/10.1016/j.biomaterials.2010.03.072.
(16) W. Cai and J. Wan, "Facile synthesis of superparamagnetic magnetite nanoparticles in liquid polyols," *Journal of Colloid and Interface Science* **305** (2), 366–370. (2007). https://doi.org/10.1016/j.jcis.2006.10.023.
(17) D. Maity, S. N. Kale, R. Kaul-Ghanekar, J.-M. Xue, J. Ding, "Studies of magnetite nanoparticles synthesized by thermal decomposition of iron (III) acetylacetonate in tri(ethylene glycol)," *Journal of Magnetism and Magnetic Materials* **321** (19), 3093–3098. (2009). https://doi.org/10.1016/j.jmmm.2009.05.020.
(18) R. Hachani, M. Lowdell, M. Birchall, A. Hervault, D. Mertz, S. Begin-Colin, N. T. Thanh, "Polyol synthesis, functionalization, and biocompatibility studies of superparamagnetic iron oxide nanoparticles as potential MRI contrast agents," *Nanoscale* **8**(6), 3278–3287. (2016). https://doi.org/10.1039/C5NR03867G.
(19) A. Zhu, L. Yuan, and S. Dai, "Preparation of well-dispersed superparamagnetic iron oxide nanoparticles in aqueous solution with biocompatible n-succinyl-o-carboxymethylchitosan," *The Journal of Physical Chemistry C* **112** (14), 5432–5438. (2008). https://doi.org/10.1021/jp711319a.
(20) N. Miguel-Sancho, O. Bomatí-Miguel, G. Colom, J.-P. Salvador, M.-P. Marco, J. Santamaría, "Development of stable, water-dispersible, and biofunctionalizable superparamagnetic iron oxide nanoparticles," *Chemistry of Materials* **23** (11), 2795–2802. (2011). https://doi.org/10.1021/cm1036452.
(21) E. Amstad, M. Textor, and E. Reimhult, "Stabilization and functionalization of iron oxide nanoparticles for biomedical applications," *Nanoscale* **3** (7), 2819. (2011). https://doi.org/10.1039/C1NR10173K.
(22) C. avikumar, C. "Unveiling the formation mechanism of polydisperse iron oxide nanoparticles in Coprecipitation Route," *Journal of Crystal Growth* **624**, 127419. (2023). https://doi.org/10.1016/j.jcrysgro.2023.127419.
(23) D. K. Mohapatra, P.J. Camp, and J. Philip, "Influence of size polydispersity on magnetic field tunable structures in magnetic nanofluids containing superparamagnetic nanoparticles," *Nanoscale Advances* **3** (12), 3573–3592. (2021). https://doi.org/10.1039/D1NA00131K.
(24) S. M. Dadfar, et al., "Size-isolation of superparamagnetic iron oxide nanoparticles improves MRI, MPI and hyperthermia performance," *Journal of Nanobiotechnology* **18** (1). (2020). https://doi.org/10.1186/s12951-020-0580-1.
(25) K. Park, T. Harrah, E.B. Goldberg, R.P. Guertin, S. Sonkusale. "Multiplexed sensing based on Brownian relaxation of magnetic nanoparticles using a compact AC susceptometer". *Nanotechnology* **22** (8), 085501. (2011). https://doi.org/10.1088/0957-4484/22/8/085501.
(26) T. Yoshida, T., and K. Enpuku, "Simulation and quantitative clarification of AC susceptibility of magnetic fluid in nonlinear Brownian relaxation region," *Japanese Journal of Applied Physics* **48** (12), 127002. (2009). https://doi.org/ 10.1143/JJAP.48.127002.
(27) A. O. Ivanov and P. J. Camp, "Theory of dynamic magnetic susceptibility of ferrofluids," *Physical Review E* **98**, 050602 (R). (2018). https://doi.org/10.1103/PhysRevE.98.050602.
(28) A. O. Ivanov and P. J. Camp, "Effects of interactions, structure formation, and polydispersity on the dynamic magnetic susceptibility and magnetic relaxation of ferrofluids," *Journal of Molecular Liquids* **356**, 119034. (2022). https://doi.org/10.1016/j.molliq.2022.119034.
(29) A. O. Ivanov and P. J. Camp, "How particle interactions and clustering affect the dynamic magnetic susceptibility of ferrofluids," *Journal of Magnetism and Magnetic Materials*, **586**, 171216. (2023). https://doi.org/ 10.1016/j.jmmm.2023.171216.

(30) A. Fang, “Generic theory of the dynamic magnetic response of Ferrofluids,” *Soft Matter* **16** (48), 10928–10934. (2020).
(31) Y. Chen, K. Okubo, K. Slavakis, Y. Kitamoto, “Estimation of biomolecule amount by analyzing magnetic nanoparticle cluster distributions from alternating current magnetization spectra for magnetic biosensing,” *Journal of Magnetism and Magnetic Materials* **588**, 171387. (2023). https://doi.org/10.1016/j.jmmm.2023.171387.
(32) S. B. Trisnanto and Y. Takemura, “Effective Néel relaxation time constant and intrinsic dipolar magnetism in a multicore magnetic nanoparticle system,” *Journal of Applied Physics* **130** (6). (2021). https://doi.org/10.1063/5.0058729.
(33) A.G. Mailer, P. S. Clegg, and P. N. Pusey, “Particle sizing by dynamic light scattering: Non-linear cumulant analysis,” Journal of Physics: Condensed Matter **27** (14), 145102. (2015). https://doi.org/10.1088/0953-8984/27/14/145102.
(34) S. B. Trisnanto and Y. Kitamoto, “Field-dependent Brownian relaxation dynamics of superparamagnetic clustered-particle suspension,” Phys. Rev. E **90**, 032306 (2014). https://doi.org/10.1103/PhysRevE.90.032306.

Chapter 4 – Effect of Buffer Solution Towards Dynamic Magnetization of CA SPIONs

Abstract

This chapter investigates the impact of HEPES buffer solutions on the dynamic magnetization properties of citric acid-coated superparamagnetic iron oxide nanoparticles (CA SPIONs). The study compares the effects of HEPES buffer on the nanoparticles' stability and magnetic behavior with those of PBS solution, as explored in previous chapters. Using dynamic magnetic susceptibility (DMS) measurements, the findings reveal that high concentrations of HEPES buffer promote particle aggregation and cause significant peak shifts in the DMS signal, attributed to the zwitterionic nature of HEPES. However, the concentration of HEPES required to significantly modulate the DMS spectra is much higher than standard concentrations typically used. Additionally, experiments with quasi-stable CA SPIONs in HEPES buffer showed only slight modulation of the DMS signal, indicating minimal impact under these conditions. In contrast, even small amounts of PBS produced noticeable changes in the DMS spectra. These contrasting results underscore the critical role of buffer composition in influencing nanoparticle behavior and highlight the importance of selecting appropriate buffers to optimize the performance of SPIONs in biosensing and biomedical applications. Understanding these interactions is essential for enhancing the efficiency and reliability of SPION-based technologies across various conditions.

4.1. Introduction

Superparamagnetic iron oxide nanoparticles (SPIONs) have garnered significant attention in biosensing due to their unique magnetic properties and biocompatibility [1,2]. These nanoparticles, typically composed of magnetite (Fe_3O_4) or maghemite (γ-Fe_2O_3), exhibit superparamagnetism at

nanoscale sizes, making them highly responsive to external magnetic fields without retaining residual magnetism. This characteristic is particularly advantageous for biosensing applications, where SPIONs can be functionalized with specific biomolecules to target and detect analytes with high sensitivity and specificity [3-6]. The applications of SPIONs in biosensing span various domains, including medical diagnostics, environmental monitoring, and food safety, highlighting their versatility and potential impact on multiple sectors.

SPIONs encounter a complex milieu in biological fluids comprising proteins, DNA, RNA, buffer solutions, and various ionic species [7,8]. The interaction of SPIONs with these components is critical for their performance in biosensing applications. Ideally, SPIONs are designed to bind selectively to target molecules, such as specific proteins. However, nonspecific interactions with other biomolecules can alter the nanoparticles' hydrodynamic behavior. These changes can manifest as variations in hydrodynamic size or magnetic susceptibility signals, potentially leading to false-positive results. Such unintended interactions underscore the necessity for careful optimization and characterization of SPION-based biosensors to ensure accurate and reliable detection.

The human body contains several buffer systems that maintain pH homeostasis, each with distinct mechanisms and components [9-13]. The phosphate buffer system, for example, operates in the renal and intracellular fluid compartments, buffering changes in pH through the reversible conversion of dihydrogen phosphate (H_2PO^{4-}) and hydrogen phosphate (HPO_4^{2-}). The protein buffer system leverages the amphoteric nature of proteins, particularly hemoglobin, to bind or release hydrogen ions (H+), thus stabilizing pH levels in blood and tissues. The bicarbonate buffer is crucial in the extracellular fluid, balancing pH by interconverting bicarbonate (HCO^{3-}) and carbonic acid (H_2CO_3). Similarly, the hemoglobin buffer system in red blood cells regulates pH through hemoglobin's ability to bind CO_2 and H^+. These buffer systems collectively play a vital role in maintaining physiological pH, ensuring proper cellular function and metabolic processes.

This chapter investigates the interactions between SPIONs and various buffer solutions, focusing on the HEPES buffer. Previous studies in our research have utilized phosphate-buffered saline (PBS) to evaluate SPION stability and performance. Buffer solutions enhance nanoparticle stability by maintaining a stable pH environment, which is crucial since SPIONs are susceptible to pH fluctuations. However, buffers may also induce particle aggregation due to their ionic content, which can screen the particle surface charges and reduce repulsive forces between nanoparticles. By exploring these interactions, I seek to understand buffer solutions' dual role in stabilizing and potentially aggregating SPIONs, thereby providing insights into optimizing SPION-based biosensors for practical applications.

In conclusion, this chapter aims to elucidate the intricate interplay between buffer systems and SPIONs, providing insights into how these interactions affect the performance of SPION-based biosensors. By exploring the magnetization dynamics of SPIONs in the presence of different buffer solutions, I seek to enhance the reliability and accuracy of biosensing applications, ultimately contributing to the advancement of diagnostic technologies.

4.2. Materials and Methods

4.2.1. Synthesis and characterization of SPIONs modified with citric acid

The synthesis of bare SPIONs was conducted utilizing a solvothermal approach. Initially, a precursor solution was prepared by dissolving 1.4 gram of iron (III) acetylacetonate (14024-18-1, Sigma-Aldrich, USA) in 40 mL of tetraethylene glycol (112-60-7, Sigma-Aldrich, USA). This solution was heated to 343 K to ensure complete dissolution of the precursor. The solution was then transferred into four 10 mL stainless steel pressure vessels. These vessels were then sealed and placed in an electric furnace, where they were subjected to a temperature of 523 K for 15 hours, facilitating the solvothermal reaction. The synthesized SPIONs were subjected to a series of washing steps after the completion of the response. Initially, the SPIONs were washed with acetone to remove any residual solvent, followed by centrifugation to collect the nanoparticles. This process was repeated three times, alternating between

deionized (DI) water and ethanol to ensure thorough cleaning. Finally, the bare SPIONs were redispersed in 20 mL of DI water, preparing them for further process.

The synthesized SPIONs were dispersed in an aqueous solution containing 2 grams of trisodium citrate (197-06025, Wako Chemicals, Japan) in 120 mL of deionized (DI) water. This was achieved using an ultrasonic homogenizer at 343 K to modify the surface with citric acid molecules. After surface modification, the SPIONs were washed three times with 1 mL of DI water and 3 mL of ethanol, then dispersed in 5 mL of DI water.

We introduced salt concentration, sodium, and potassium to induce particle aggregation. When the appropriate concentration of salts is introduced, SPIONs and their clusters tend to aggregate owing to reduced electric-double layer thickness, forming larger clusters that can significantly influence their magnetic and physical properties. However, it is crucial to carefully manage the salt concentration, as excessive amounts can lead to undesirable precipitation of SPIONs, rendering them unsuitable for further applications. As we studied in Chapter 2, we observed peak-shift behavior in the mixture of SPIONs with sodium and potassium. While the peak-shift behavior is absent in Chapter 3 when SPIONs are mixed with PBS solution, the contents of sodium ions are comparable to the case in which we observed peak-shift in Chapter 2. Therefore, we mixed the SPIONs with the buffer solutions at different concentrations to study the effect of the buffer solution on the magnetization dynamics of SPIONs. This time, we used a different buffer solution, the HEPES solution, to enrich our data. To meticulously control this aspect, the suspension's ionic concentration (sodium and potassium) for evaluations was systematically varied. Firstly, we prepared a suspension of SPIONs in HEPES buffer with different concentrations of HEPES buffer, ranging from 0 mM to 25 mM. After that, we mixed 50 µL of suspensions with 50 µL of ionic solutions with concentrations ranging from 0 mM to 100 mM. The final concentrations of salts in the specimens were 50 mM, 25 mM, 5 mM, 2.5 mM, and 0 mM.

The primary and hydrodynamic sizes of the nanoparticles were determined using transmission

electron microscopy (TEM, H-8100, Hitachi High-Tech Corporation, Japan) and dynamic light scattering measurements (DLS, SZ-100-V2, HORIBA, Japan), respectively. The frequency dependence of the AC magnetization in the range of 10–10,000 Hz was analyzed using a physical property measurement system (PPMS; Quantum Design Corp., USA) at a magnetic field strength of 0.8 kA/m at 300 K. The SPIONs concentration and volume of specimens for PPMS measurements were 3.5 mg/mL and 100 µL, respectively.

4.3. Results

4.3.1. Dependence of HEPES buffer solution on the dynamic behavior of CA SPIONs.

Figure 4.1 shows (a) the real part and (b) the imaginary part of the Dynamic Magnetic Susceptibility (DMS) signal of SPIONs under varying concentrations of HEPES buffer solutions. The labels indicate the final concentration of HEPES buffer in the suspensions. The DMS signal reveals that the dynamic magnetization of SPIONs remains stable up to a HEPES buffer concentration of 50 mM, as evidenced by the similarity in the DMS signal of SPIONs in both HEPES (50 mM) and water (0 mM). However, at a concentration of 250 mM HEPES, a slight decrease in magnetic susceptibility is observed, as shown by the purple graph in Figure 4.1. This effect becomes more pronounced at 500 mM HEPES, where the real part of the DMS signal decreases from 6.4 x 10^{-4} to 4.0 x 10^{-4}. Additionally, the imaginary part of the DMS signal drops significantly to 3.0 x 10^{-5} at 500 mM HEPES, compared to 1.2 x 10^{-4} in water.

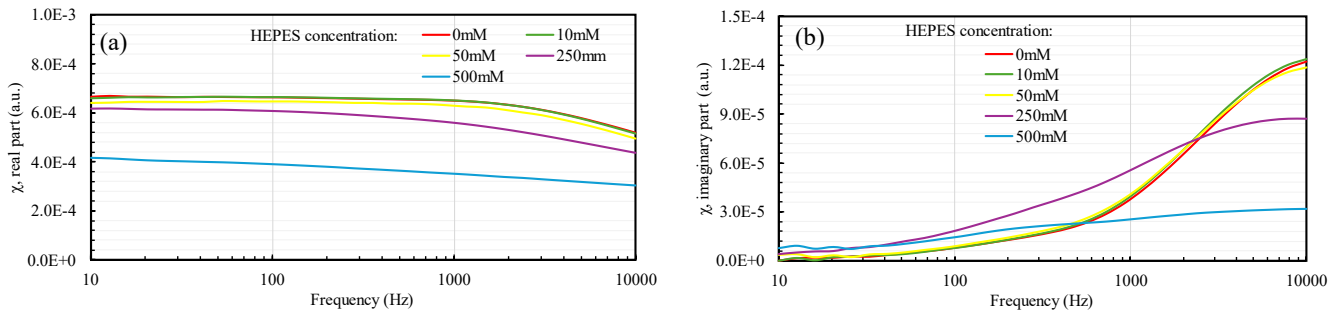

Figure 4.1. (a) real and (b) imaginary parts of the DMS signal of CA SPIONs in various concentrations of HEPES buffer.

Figure 4.2 shows the normalized imaginary part of the DMS signal of SPIONs under varying concentrations of HEPES buffer. In this experiment, suspensions were prepared with HEPES buffer concentrations ranging from 0 mM (SPIONs in water) to 500 mM. The results indicate that at low concentrations (0 - 50 mM), HEPES buffer does not affect the DMS signal of SPIONs. However, the DMS signal broadens at higher concentrations (250 mM - 500 mM), similar to observations made when SPIONs were mixed with sodium, potassium, or PBS buffer in previous chapters. It is important to note that the standard concentration of HEPES buffer used in most applications is around ten mM. Therefore, HEPES buffer at standard concentrations does not impact the dynamic magnetization of SPIONs.

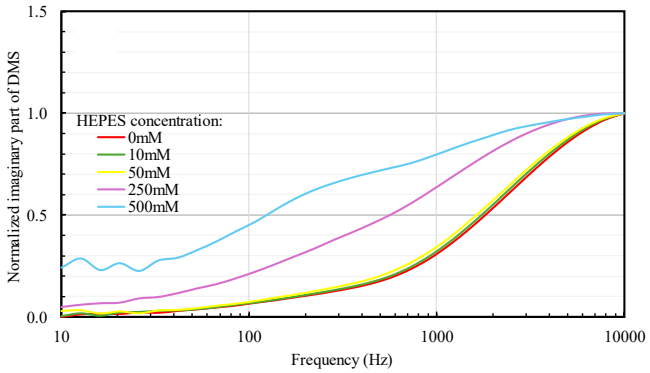

Figure 4.2. Normalized imaginary parts of the DMS signal of CA SPIONs in various concentrations of HEPES buffer.

4.3.2. Effect of HEPES buffer solution towards quasi-stable CA SPIONs

Figure 4.3. illustrates the (a) DMS signal and (b) the normalized imaginary part of SPIONs under varying concentrations of sodium ions. The DMS signal exhibits behavior similar to that discussed in Chapters 2 and 3, particularly in the dynamic magnetization of SPIONs, which changes in two distinct stages. Initially, the DMS signal broadens at lower sodium ion concentrations while maintaining a constant peak frequency. Subsequently, a noticeable peak shift is observed in the DMS signal at higher sodium ion concentrations (75 mM, highlighted with a red circle). This broadening effect and peak-shift behavior are also observed in SPIONs under the influence of potassium ions (Figure 4.3. c and d). Notably, the peak-shift behavior in SPIONs due to potassium ions occurs earlier than those under the

influence of sodium ions.

Several differences are evident when comparing these observations to the data presented in Chapter 2. The first difference lies in the concentration at which the peak-shift phenomenon is observed in sodium and potassium solutions. In Chapter 2, we noted peak shifts at 37.5 mM and 50 mM concentrations for potassium and sodium solutions, respectively. In contrast, in the current study, we observed peak shifts at slightly different concentrations: 50 mM and 75 mM for potassium and sodium ionic solutions, respectively. This discrepancy arises from using different batches of CA SPIONs. Due to insufficient samples identical to those used in Chapter 2, we opted to use a different batch of CA SPION samples. Samples from different batches can exhibit slight variations in stability, which is a regular occurrence in such experiments. Our observations demonstrate the repeatability of the peak shift and signal-broadening effects in CA SPIONs, confirming the consistency of these phenomena across different experimental conditions.

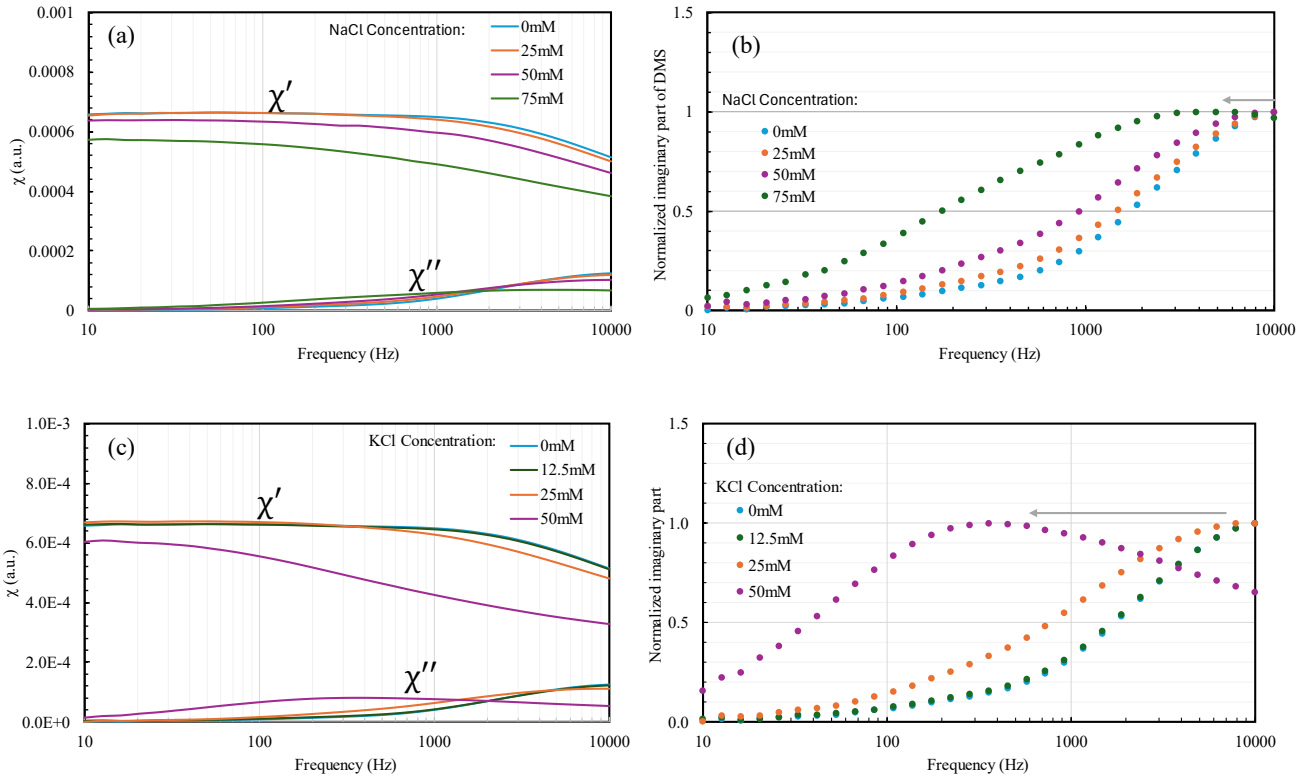

Figure 4.3. (a,c) DMS signal and (b,d) normalized imaginary parts of the DMS signal for CA SPIONs. The SPIONs were mixed with (a,b) sodium ions and (c,d) potassium ions to investigate the impact of

ionic solutions on their magnetization behavior.

Figure 4.4 illustrates the effect of HEPES buffer on SPIONs, influenced by the screening effect of potassium ionic solutions, as shown by the DMS signal (Figure 4.4a). The concentration of HEPES does not significantly change the dynamic magnetization of SPIONs, except at 25 mM HEPES, where a decrease in the real part of the DMS signal is observed. However, examining the normalized DMS signal, the peak-shift phenomenon becomes evident (Figure 4.4b). At 6.25 mM HEPES, the signal broadens without a significant shift in peak frequency. As the HEPES concentration increases, a peak shift occurs, as indicated by the arrow.

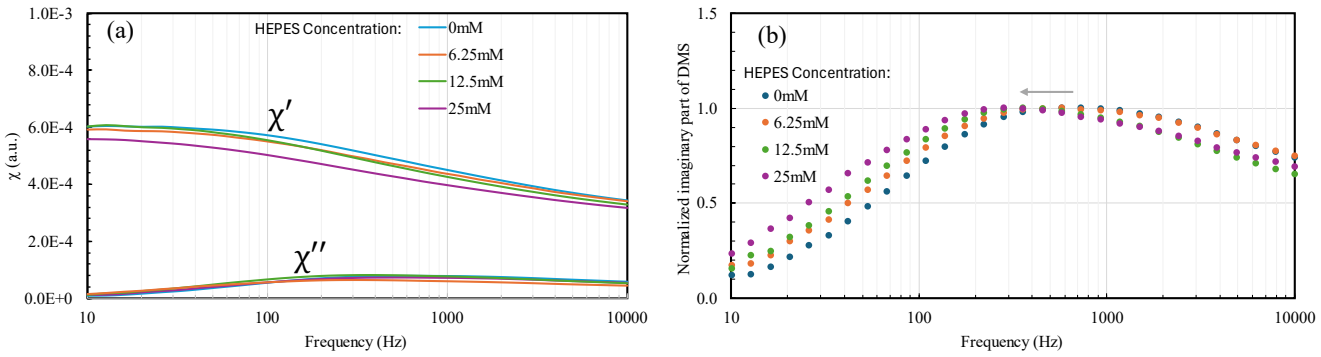

Figure 4.4. (a) DMS signal and (b) normalized imaginary parts of the DMS signal for CA SPIONs. The SPIONs were suspended in varying concentrations of HEPES buffer and then mixed with 50 mM of potassium ions to assess the impact of HEPES buffer on their magnetization behavior.

Figure 4.5 illustrates the effect of HEPES buffer on SPIONs, influenced by the screening effect of potassium ionic solutions, as shown by the DMS signal (Figure 4.5a). Across all HEPES concentrations, there is no significant change in the dynamic magnetization of SPIONs, as indicated by the stable magnetic susceptibility signal strength. However, examining the normalized DMS signal, the peak-shift and signal-broadening phenomenon become observable (Figure 4.5.b.). At 6.25 mM HEPES, the signal broadens without a significant shift in peak frequency. This broadening remains similar at 12.5 mM and 25 mM HEPES concentrations, indicating that higher concentrations do not further alter the signal.

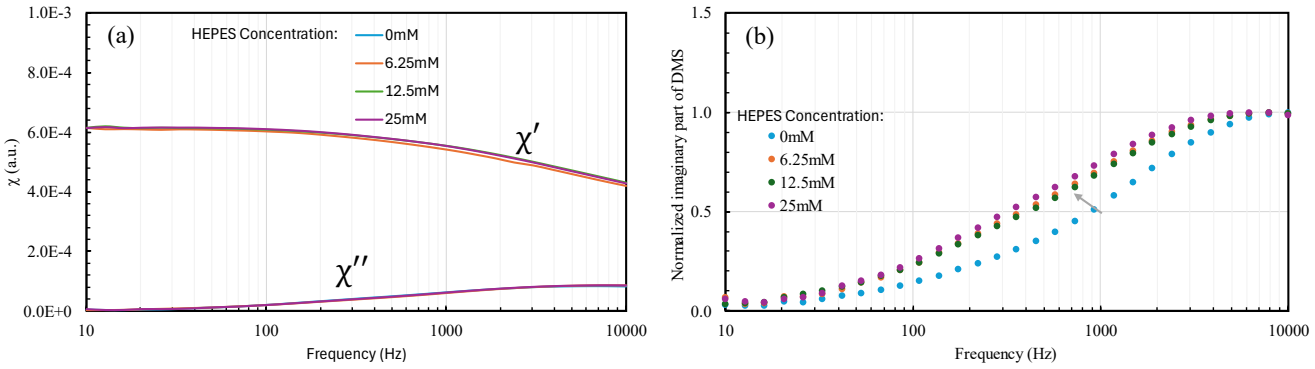

Figure 4.5. (a) DMS signal and (b) normalized imaginary parts of the DMS signal for CA SPIONs. The SPIONs were suspended in varying concentrations of HEPES buffer and then mixed with 50 mM of sodium ions to assess the impact of HEPES buffer on their magnetization behavior.

Figure 4.6 depicts the impact of HEPES buffer on SPIONs, highlighting the screening effect of potassium ionic solutions, as evidenced by the DMS signal (Figure 4.6a). The dynamic magnetization of SP and the consistent magnetic susceptibility signal strength indicate that IONs remain largely unaffected across varying HEPES concentrations. However, examining the normalized DMS signal, a peak-shift phenomenon becomes apparent (Figure 4.6b). Initially, at 0 mM HEPES, SPIONs in 75 mM sodium ions exhibit a signal peak frequency at 5000 Hz. Introducing 6.25 mM of HEPES buffer causes the signal peak frequency to shift slightly to 3000 Hz. This shift persists at 12.5 mM HEPES buffer. Upon increasing the HEPES concentration to 25 mM, a further peak shift to 1500 Hz is observed.

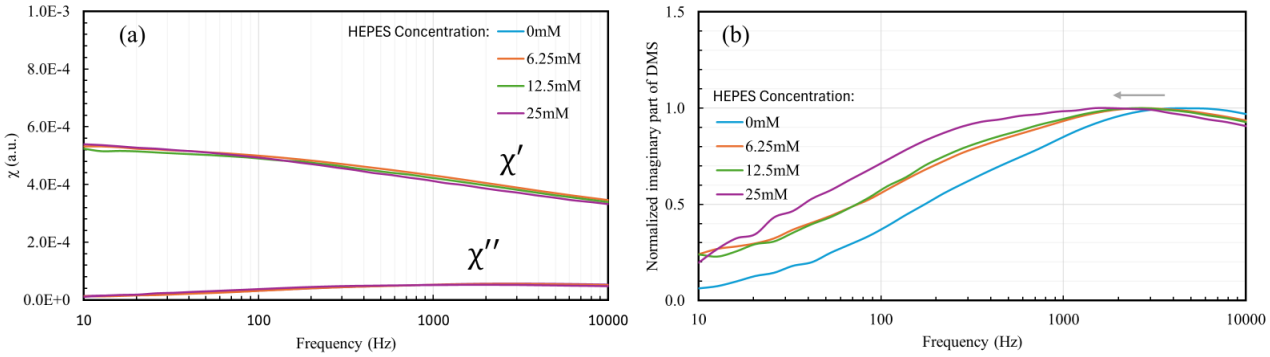

Figure 4.6. (a) DMS signal and (b) normalized imaginary parts of the DMS signal for CA SPIONs. The SPIONs were suspended in varying concentrations of HEPES buffer and then mixed with 75 mM of sodium ions to assess the impact of HEPES buffer on their magnetization behavior.

4.4. Discussion

The experimental data presented in Chapter 4 provides significant insights into the behavior of citric acid-coated superparamagnetic iron oxide nanoparticles (CA SPIONs) in various buffer solutions, specifically HEPES and phosphate-buffered saline (PBS). This discussion elaborates on the distinct effects of these buffers on the dynamic magnetization of CA SPIONs, supporting the proposed hypotheses.

Some may argue that the additional HEPES buffer caused the magnetic behavior of SPIONs due to the solution pH not being maintained constant. Therefore, we measured pH for all samples in Figures 4.4, 4.5, and 4.6, shown in Table 4.1. Table 4.1 shows the effect of HEPES molecules on the suspension's pH. We prepared a solution containing a mixed suspension of SPIONs with a concentration of 0.3 mg/mL with 50 mL of saline solutions. Specimen S1 in water has a pH of around 6.78. In a 50 mM NaCl solution, the initial pH is 6.16, which rises to 6.83 with 6.25 mM HEPES and 6.96 with 12.50 mM HEPES, stabilizing at 6.97 with 25.00 mM HEPES. Similarly, in a 75 mM NaCl solution, the pH starts at 6.00, increasing to 6.76 with 6.25 mM HEPES, reaching 6.91 with 12.50 mM, and slightly higher at 6.95 with 25.00 mM HEPES. In a 50 mM KCl solution, the pH at 6.07 rises to 6.93 with 6.25 mM HEPES. These observations indicate that HEPES buffer effectively elevates and stabilizes the pH of saline suspensions across different concentrations.

Table 4.1. Effect of HEPES molecules on suspension's pH.

Saline	Concentration of HEPES (mM)	pH
50 mM NaCl	0.00	6.16
	6.25	6.83
	12.50	6.96
	25.00	6.97
75 mM NaCl	0.00	6.00
	6.25	6.76
	12.50	6.91
	25.00	6.95
50mM KCl	0.00	6.07
	6.25	6.93

	12.50	6.95
	25.00	6.97

HEPES buffer, known for its zwitterionic properties, demonstrates a unique interaction with CA SPIONs. According to Khandelwal et al. [14], the behavior of HEPES buffer at a pH of around 7 reveals that it is not entirely neutral but carries a slight negative charge, as indicated in Figure 7 of their study. This characteristic is significant because it contradicts the common assumption that HEPES buffer is neutral at this pH level. The slight negativity of the HEPES buffer could potentially influence the electrostatic interactions with the nanoparticles, leading to altered stability. Khandelwal et al. further explored how this subtle negativity in HEPES affects the AC conductivity of ultra-dilute colloidal suspensions, highlighting that such buffers can influence the double layer of particles in suspension, thereby impacting their aggregation and overall stability. This is particularly relevant when considering the dynamic behavior of SPIONs in different buffer environments.

In order to study the magnetization dynamics of quasi-stable SPIONs under the influence of HEPES buffer solution, we prepared SPION (concentration of 0.3 mg/mL) containing 50 mM NaCl, 75 mM NaCl, or 50 mM KCl solutions then mixing them with HEPES buffer at various concentrations and sonicated the mixtures for several minutes. The hydrodynamic sizes of the samples were measured using DLS, and the results are presented in Figure 4.7. The image presents four graphs illustrating SPION’s hydrodynamic diameter distribution under different HEPES buffer concentrations and salt environments. The top left graph (a) shows that the hydrodynamic size of SPIONs remains stable across various HEPES buffer concentrations, with consistent peaks around 25 nm. The top right graph (b) indicates that in a 50 mM NaCl solution, HEPES buffer slightly shifts the SPIONs' size, with peaks around 25-35 nm. The bottom left graph (c) reveals similar slight changes in a 75 mM NaCl solution, with peaks around 30-55 nm. The bottom right graph (d) demonstrates that in a 50 mM KCl solution, HEPES buffer modifies the SPIONs' size more significantly, with peaks around 90-105 nm, and the size distribution broadens with increasing HEPES concentration. Overall, the graphs highlight that while SPIONs maintain stable sizes

in pure HEPES buffer, adding HEPES buffer in NaCl or KCl solutions leads to minor changes in their hydrodynamic size distribution.

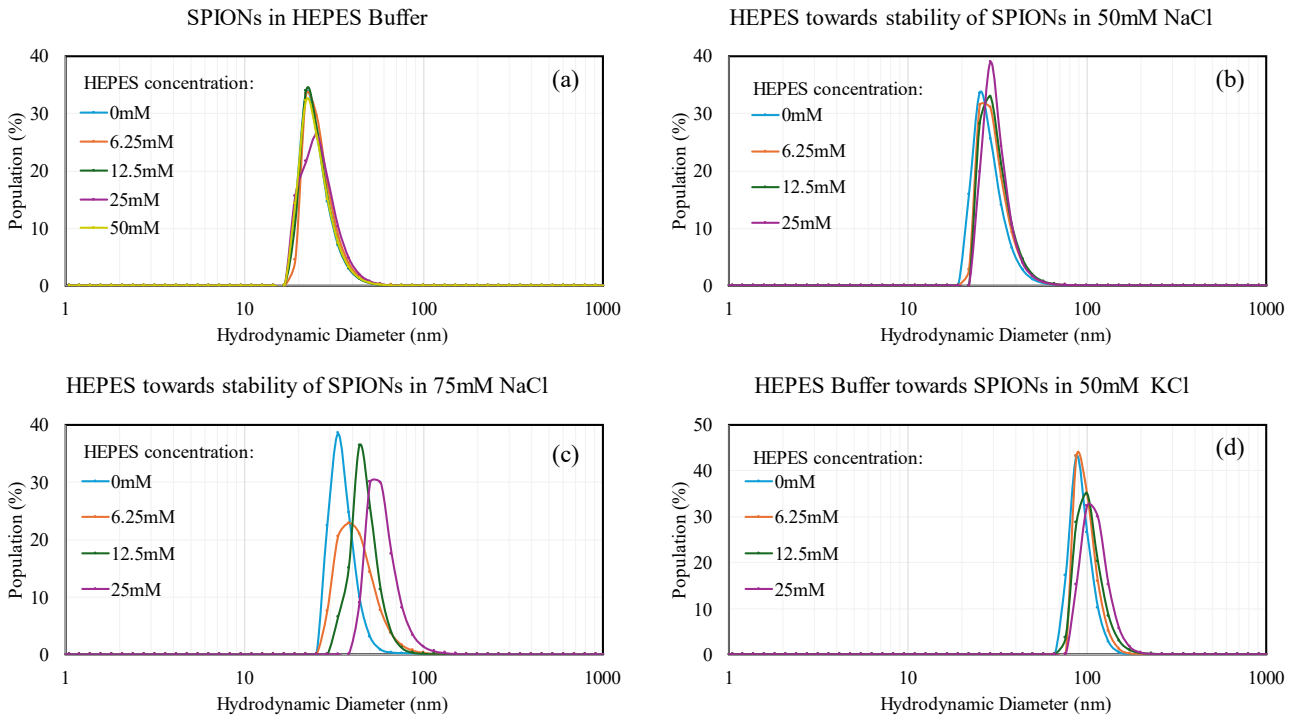

Figure 4.7 shows the hydrodynamic size changes from DLS measurements for SPIONs: (a) in buffer and (b-d) in saline solution. The pH value for all samples (b-d) was maintained by adding HEPES buffer.

The peak-frequency shift and broadening effect in the dynamic magnetic susceptibility (DMS) signal, as shown in Figures 4.4 to 4.6, indicate enhanced inter-cluster aggregation of SPIONs in the presence of HEPES buffer and potassium ionic solutions. In Figure 4.4, a decrease in the real part of the DMS signal at 25 mM HEPES and a peak shift at higher HEPES concentrations suggest initial aggregation. Figure 4.5 demonstrates that while the dynamic magnetization remains stable, signal broadening and peak shifting at 6.25 mM HEPES and higher concentrations indicate progressive aggregation. Similarly, Figure 4.6 shows that increasing HEPES concentrations shift the peak frequency from 5000 Hz at 0 mM HEPES to 1500 Hz at 25 mM HEPES, highlighting significant aggregation. Figure 4.7 further supports these findings by illustrating changes in the hydrodynamic diameter distribution of SPIONs under

different HEPES buffer concentrations and salt environments. SPIONs maintain a stable size of around 25 nm in pure HEPES buffer. However, in 50 mM NaCl, 75 mM NaCl, and 50 mM KCl solutions, HEPES buffer induces size shifts and broadening distributions, with more pronounced changes in the KCl solution, where peaks reach 90-105 nm. This correlation between DMS signal changes and hydrodynamic size distribution underscores the role of HEPES buffer while maintaining its pH; it may also promote further inter-cluster aggregation of SPIONs.

The peak-frequency shift and broadening effects observed in the dynamic magnetic susceptibility (DMS) signal, as shown in Figures 4.4 to 4.6, initially suggested that the introduction of HEPES buffer and potassium ionic solutions might enhance inter-cluster aggregation of SPIONs. However, it is important to note that the ionic strength of HEPES buffer, especially when compared to chloride or phosphate ions, is relatively weak and may not significantly destabilize the SPIONs. The subtle changes in magnetization behavior, such as the peak shift to lower frequencies, are likely not a direct result of interactions between the SPIONs and the HEPES buffer. Instead, these changes may be more reflective of the inherent properties of the SPIONs themselves, which could be in a quasi-stable state even in the absence of HEPES.

While it was initially hypothesized that adding HEPES buffer to a quasi-stable colloidal system would lead to significant aggregation of SPIONs, the experimental results show that only slight aggregation occurred at standard HEPES concentrations. This suggests that the role of HEPES in promoting aggregation is minimal. The observed effects are more likely due to interactions between SPIONs and other ions, such as potassium, sodium, chloride, or phosphate. Consequently, the influence of these ions on the DMS signal appears to follow the order of K > Na > PBS > HEPES.

4.5. Summary

The findings in this chapter clarify that the HEPES buffer does not significantly affect the stability and aggregation of citric acid-coated superparamagnetic iron oxide nanoparticles (CA SPIONs) under

standard conditions. Aggregation of SPIONs was only observed at extremely high concentrations of HEPES, far above the standard buffer concentration. Specifically, while standard HEPES buffer concentrations are typically between 10 - 20 mM, notable effects on SPION aggregation and dynamic magnetization were only detected at concentrations of 250 mM and higher.

Even at these elevated concentrations, the impact of HEPES on SPION aggregation was minimal, particularly when compared to the more pronounced effects of ionic buffers like PBS. Hydrodynamic size measurements further confirmed that HEPES, even at high concentrations, caused only minor changes in nanoparticle size distribution, particularly in saline environments. This underscores that the HEPES buffer does not significantly affect SPION aggregation under typical conditions.

In summary, under standard conditions, the HEPES buffer does not impact the stability and aggregation of SPIONs. The aggregation observed at high HEPES concentrations (250 mM and above) underscores that such effects are only relevant at higher levels than those typically used in biomedical applications. This insight is crucial for selecting appropriate buffer systems for SPION-based technologies, ensuring optimal performance and reliability across various environments.

References

(1) Reddy, L. H.; Arias, J. L.; Nicolas, J.; Couvreur, P. Magnetic Nanoparticles: Design and Characterization, Toxicity and Biocompatibility, Pharmaceutical and Biomedical Applications. Chemical Reviews 2012, 112 (11), 5818–5878. DOI:10.1021/cr300068p.

(2) Petri-Fink, A.; Hofmann, H. Superparamagnetic Iron Oxide Nanoparticles (SPIONs): From Synthesis to In Vivo Studies—A Summary of the Synthesis, Characterization, In Vitro, and In Vivo Investigations of SPIONs With Particular Focus on Surface and Colloidal Properties. IEEE Transactions on NanoBioscience 2007, 6 (4), 289–297. DOI:10.1109/tnb.2007.908987.

(3) Al Faraj, A.; Shaik, A. S.; Afzal, S.; Al-Muhsen, S.; Halwani, R. Specific Targeting and Noninvasive Magnetic Resonance Imaging of an Asthma Biomarker in the Lung Using Polyethylene Glycol Functionalized Magnetic Nanocarriers. Contrast Media & Molecular Imaging 2015, 11 (3), 172–183. DOI:10.1002/cmmi.1678.

(4) Xu, Y.; Zheng, H.; Schumacher, D.; Liehn, E. A.; Slabu, I.; Rusu, M. Recent Advancements of Specific Functionalized Surfaces of Magnetic Nano- and Microparticles as a Theranostics Source in Biomedicine. ACS Biomaterials Science & Engineering 2021, 7 (6), 1914–1932. DOI:10.1021/acsbiomaterials.0c01393.

(5) Gopalan, D.; Pandey, A.; Alex, A. T.; Kalthur, G.; Pandey, S.; Udupa, N.; Mutalik, S. Nanoconstructs as a Versatile Tool for Detection and Diagnosis of Alzheimer Biomarkers. Nanotechnology 2021, 32 (14), 142002. DOI:10.1088/1361-6528/abcdcb.

(6) Singh, B.; Ma, S.; Hara, T. O.; Singh, S. Nanomaterials-based Biosensors for the Detection of Prostate Cancer Biomarkers: Recent Trends and Future Perspective. Advanced Materials Technologies 2023, 8 (13). DOI:10.1002/admt.202201860.

(7) Peng, X.; Yang, Z.; Wang, J.; Fan, J.; He, Y.; Song, F.; Wang, B.; Sun, S.; Qu, J.; Qi, J.; Yan, M. Fluorescence Ratiometry and Fluorescence Lifetime Imaging: Using a Single Molecular Sensor for Dual Mode Imaging of Cellular Viscosity. Journal of the American Chemical Society 2011, 133 (17), 6626–6635. DOI:10.1021/ja1104014.

(8) Katiyar, A.; Dhar, P.; Das, S. K.; Nandi, T. Near-Field Magnetostatics and Néel–Brownian Interactions Mediated Magneto-Rheological Characteristics of Highly Stable Nano-Ferrocolloids. Soft Matter 2015, 11 (8), 1614–1627. DOI:10.1039/c4sm02458c.

(9) Moissl, U. M.; Wabel, P.; Chamney, P. W.; Bosaeus, I.; Levin, N. W.; Bosy-Westphal, A.; Korth, O.; Müller, M. J.; Ellegård, L.; Malmros, V.; Kaitwatcharachai, C.; Kuhlmann, M. K.; Zhu, F.; Fuller, N. J. Body Fluid Volume Determination via Body Composition Spectroscopy in Health and Disease. Physiological Measurement 2006, 27 (9), 921–933. DOI:10.1088/0967-3334/27/9/012.

(10) Pavani, P.; Kumar, K.; Rani, A.; Venkatesu, P.; Lee, M.-J. The Influence of Sodium Phosphate Buffer on the Stability of Various Proteins: Insights into Protein-Buffer Interactions. Journal of Molecular Liquids 2021, 331, 115753. DOI:10.1016/j.molliq.2021.115753.

(11) Yilmaz, B.; Pazarceviren, A. E.; Tezcaner, A.; Evis, Z. Historical Development of Simulated Body Fluids Used in Biomedical Applications: A Review. Microchemical Journal 2020, 155, 104713. DOI:10.1016/j.microc.2020.104713.

(12) Jörres, A.; Bender, T. O.; Finn, A.; Witowski, J.; Fröhlich, S.; Gahl, G. M.; Frei, U.; Keck, H.; Passlick-Deetjen, J. Biocompatibility and Buffers: Effect of Bicarbonate-Buffered Peritoneal Dialysis Fluids on Peritoneal Cell Function. Kidney International 1998, 54 (6), 2184–2193. DOI:10.1046/j.1523-1755.1998.00178.x.

(13) Amaral Silva, D.; Al-Gousous, J.; Davies, N. M.; Bou Chacra, N.; Webster, G. K.; Lipka, E.; Amidon, G.; Löbenberg, R. Simulated, Biorelevant, Clinically Relevant or Physiologically

Relevant Dissolution Media: The Hidden Role of Bicarbonate Buffer. European Journal of Pharmaceutics and Biopharmaceutics 2019, 142, 8–19. DOI:10.1016/j.ejpb.2019.06.006.
(14) Khandelwal, A. V.; Singh, A.; Pal, N.; Kumar, R.; Goel, G.; Gupta, S. AC Conductivity Measurements of Ultradilute Colloidal Suspensions in HEPES Buffer. Langmuir 2019, 35, 14725–14733. DOI: 10.1021/acs.langmuir.9b01464
(15) Liu, J.; Dai, C.; Hu, Y. Aqueous Aggregation Behavior of Citric Acid Coated Magnetite Nanoparticles: Effects of Ph, Cations, Anions, and Humic Acid. Environmental Research 2018, 161, 49–60. DOI: 10.1016/j.envres.2017.10.045

Chapter 5 – General Conclusions

This research comprehensively investigated the dynamic behavior of citric acid-coated superparamagnetic iron oxide nanoparticles (CA SPIONs) under various ionic conditions, focusing on their stability and magnetization dynamics. Through a series of experiments involving different ionic environments—sodium (Na+), potassium (K+), phosphate-buffered saline (PBS), and HEPES buffer—I sought to understand the interplay between ionic strength, electrostatic interactions, and nanoparticle clustering, all of which significantly influence the dynamic magnetic susceptibility (DMS) of CA SPIONs.

Summary of Findings

Our research began by exploring the impact of sodium and potassium ions on the magnetization dynamics of CA SPIONs. It was observed that both Na+ and K+ ions induced significant changes in the DMS spectra of the nanoparticles, with the extent of these changes being more pronounced in the presence of potassium ions. Specifically, K+ ions led to a peak shift in the DMS spectra at lower concentrations compared to Na+ ions, indicating a stronger influence on nanoparticle aggregation and magnetic behavior. This behavior is primarily attributed to the higher ionic strength of K+ ions, which more effectively screens the surface charges of the nanoparticles, thereby promoting aggregation and altering their rotational dynamics under an external magnetic field.

PBS, a more complex ionic environment, demonstrated a different effect on the CA SPIONs. While it also caused broadening in the DMS spectra, no significant peak shifts were observed, even at higher concentrations. This suggests that the phosphate ions present in PBS contribute to the stabilization of CA SPIONs, likely by forming a protective layer around the nanoparticles that prevents aggregation. The unique role of phosphate ions in maintaining nanoparticle stability underscores the importance of

considering the specific ionic composition of the environment when designing nanoparticle-based systems.

Finally, the effect of HEPES buffer on CA SPIONs was investigated. HEPES, known for its zwitterionic nature, exhibited the least influence on the DMS spectra compared to the other ionic environments studied. Although higher concentrations of HEPES led to some broadening and peak shifts in the DMS spectra, these effects were minimal, indicating that HEPES is less likely to destabilize CA SPIONs or significantly alter their magnetization dynamics.

Order of Influence on DMS

Through my comparative analysis, I established a clear hierarchy in the influence of different ionic environments on the DMS of CA SPIONs. The order of strength, from the most to least influential, is as follows:

1. **Potassium ions (K+) -** Exhibit the strongest influence on DMS, leading to significant peak shifts at lower concentrations, indicative of pronounced nanoparticle aggregation and changes in magnetization dynamics.
2. **Sodium ions (Na+) -** Also cause peak shifts and broadening in DMS spectra, but require higher concentrations compared to K+ ions to achieve similar effects.
3. **Phosphate-buffered saline (PBS) -** Primarily causes broadening in DMS spectra without significant peak shifts, suggesting a stabilizing effect due to the presence of phosphate ions.
4. **HEPES buffer** - Exhibits the weakest influence on DMS, with minimal broadening and peak shifts, indicating that it does not significantly destabilize CA SPIONs or alter their magnetization behavior.

Conclusion and Implications

The findings from this research highlight the critical role that ionic strength and specific ion types play in determining the stability and dynamic behavior of CA SPIONs. Understanding these interactions is crucial for optimizing the design and application of nanoparticle-based technologies in biomedical and

biosensing fields. By carefully selecting the appropriate ionic environment, we can enhance the stability and performance of SPIONs, ensuring their efficacy in various applications, from targeted drug delivery to magnetic resonance imaging (MRI) and beyond.

Future work should continue to explore the interactions between nanoparticles and a broader range of ionic environments, including multivalent ions and more complex biological fluids, to further refine our understanding of nanoparticle behavior in real-world applications. The insights gained from this research provide a solid foundation for advancing the development of SPION-based technologies and improving their integration into practical biomedical solutions.

Acknowledgments

I am deeply grateful to my supervisor, Professor Yoshitaka Kitamoto, who has inspired me, provided excellent guidance, and continuously supported me throughout my doctoral course. His wisdom, encouragement, and unwavering support have been instrumental in completing this dissertation.

I am also profoundly thankful to Assistant Professor Kyohei Okubo for his invaluable advice, insightful discussions, and steadfast support. His contributions have been crucial to the development of my research.

I wish to acknowledge Professor Masato Sone, Professor Takeharu Tuge, Professor Satoshi Okada, and Professor Hiroyuki Wada for examining my degree. Their expert evaluation and feedback have greatly enhanced the quality of my work.

I want to express my heartfelt gratitude to all members of the Kitamoto lab for their assistance, both academically and personally. Their active cooperation, courteous concerns, and warm support have made my time in the lab enjoyable and productive.

Finally, I wish to acknowledge my parents, wife, and family for their unwavering support and encouragement in all aspects of my student life. Their love and sacrifices have been a constant source of strength and motivation.

Wibias Muliawan

Accomplishment

PUBLICATIONS

- Muliawan, W., Okubo, K., Yoshitaka, K. Effect of interparticle and inter-cluster dipole-dipole interactions on the dynamic behavior of superparamagnetic iron oxide nanoparticles modified with citric acid. J. Appl. Phys. 2024. 136, 073903. DOI: 10.1063/5.0220689

.

CONFERENCE PRESENTATIONS

- **Muliawan W.**, Ye, C., Kyohei, O., Yoshitaka, K., Magnetization Dynamics of Interacting Iron Oxide Nanoparticles (IONPs) in Ionic Solutions. Oral presentation delivered at the IEEE International Magnetic Conference INTERMAG 2023, Sendai, Japan, May 2023
- **Muliawan, W.** and Yoshitaka, K., Dynamical Magnetic Response of Iron Oxide Nanoparticles (IONPs) Interact with Ionic Solution. Oral presentation delivered at the 11th International Conference on Fine Particles Magnetism, Yokohama, October 2022.
- **Muliawan, W.**, Kurashina, Y., Yoshitaka, K., Electrostatic Influence on Dynamic Magnetization Behaviors of Iron-oxide Nanoparticles in Hydrogels Using Charged Polymers. The poster presentation was delivered online at the Autumn meeting of the Japan Society of Powder and powder metallurgy 2021, November 2021.
- **Muliawan, W.**, Kurashina, Y., Yoshitaka, K., Influence of Polymers on Dynamic Magnetization Behaviors of Iron-oxide Nanoparticles in Ferrogels. Poster presentation delivered online at the Twelfth International Conference on the Science and Technology for Advanced Ceramics (STAC 12), July 2021.

CONFERENCE PRESENTATIONS

- Intermediate Presentation 中間発表 2020, Excellent Presentation Awards